bioRxiv preprint doi: https://doi.org/10.1101/2020.06.12.148254; this version posted November 30, 2020. The copyright holder for this preprint (which was not certified by peer review) is the author/funder, who has granted bioRxiv a license to display the preprint in perpetuity. It is made available under aCC-BY-NC 4.0 International license.

BUB-1 targets PP2A:B56 to regulate chromosome congression during meiosis I in *C. elegans* oocytes

Laura Bel Borja[1], Flavie Soubigou[1], Samuel J.P. Taylor[1], Conchita Fraguas Bringas[1], Jacqueline Budrewicz[2,3], Pablo Lara-Gonzalez[2,3], Christopher G. Sorensen Turpin[4], Joshua N. Bembenek[5], Dhanya K. Cheerambathur[6], and Federico Pelisch[1,*]

[1] Centre for Gene Regulation and Expression, Sir James Black Centre, School of Life Sciences, University of Dundee. Dundee, DD1 5EH, UK

[2] Ludwig Institute for Cancer Research, San Diego, California, 92093, USA

[3] Department of Cellular and Molecular Medicine, University of California at San Diego, La Jolla, California, 92093, USA

[4] Department of Biochemistry, Cellular and Molecular Biology, University of Tennessee, C211 Walters Life Sciences Building, 1414 Cumberland Avenue, Knoxville, TN 37996, USA

[5] Department of Molecular, Cellular, and Developmental Biology, University of Michigan. 1105 North University Ave., Ann Arbor, MI 48109-1085, USA

[6] Wellcome Centre for Cell Biology & Institute of Cell Biology, School of Biological Sciences, The University of Edinburgh, Edinburgh, EH9 3BF, UK

* Corresponding author: Federico Pelisch (f.pelisch@dundee.ac.uk)

bioRxiv preprint doi: https://doi.org/10.1101/2020.06.12.148254; this version posted November 30, 2020. The copyright holder for this preprint (which was not certified by peer review) is the author/funder, who has granted bioRxiv a license to display the preprint in perpetuity. It is made available under aCC-BY-NC 4.0 International license.

ABSTRACT

Protein Phosphatase 2A (PP2A) is an heterotrimer composed of scaffolding (A), catalytic (C), and regulatory (B) subunits with various key roles during cell division. While A and C subunits form the core enzyme, the diversity generated by interchangeable B subunits dictates substrate specificity. Within the B subunits, B56-type subunits play important roles during meiosis in yeast and mice by protecting centromeric cohesion and stabilising the kinetochore-microtubule attachments. These functions are achieved through targeting of B56 subunits to centromere and kinetochore by Shugoshin and BUBR1. In the nematode *Caenorhabditis elegans* (*C. elegans)* the closest BUBR1 ortholog lacks the B56 interaction domain and the Shugoshin orthologue is not required for normal segregation during oocyte meiosis. Therefore, the role of PP2A in *C. elegans* female meiosis is not known. Here, we report that PP2A is essential for meiotic spindle assembly and chromosome dynamics during *C. elegans* female meiosis. Specifically, B56 subunits PPTR-1 and PPTR-2 associate with chromosomes during prometaphase I and regulate chromosome congression. The chromosome localization of B56 subunits does not require shugoshin orthologue SGO-1. Instead we have identified the kinase BUB-1 as the key B56 targeting factor to the chromosomes during meiosis. PP2A BUB-1 recruits PP2A:B56 to the chromosomes via dual mechanism: 1) PPTR-1/2 interacts with the newly identified LxxIxE short linear motif (SLiM) within a disordered region in BUB-1 in a phosphorylation-dependent manner; and 2) PPTR-2 can also be recruited to chromosomes in a BUB-1 kinase domain-dependent manner. Our results highlight a novel, BUB-1-dependent mechanism for B56 recruitment, essential for recruiting a pool of PP2A required for proper chromosome congression during meiosis I.

bioRxiv preprint doi: https://doi.org/10.1101/2020.06.12.148254; this version posted November 30, 2020. The copyright holder for this preprint (which was not certified by peer review) is the author/funder, who has granted bioRxiv a license to display the preprint in perpetuity. It is made available under aCC-BY-NC 4.0 International license.

INTRODUCTION

Formation of a diploid embryo requires that sperm and egg contribute exactly one copy of each chromosome. The cell division in charge of reducing ploidy of the genome is meiosis, which involves two chromosome segregation steps after a single round of DNA replication (Marston and Amon, 2004; Ohkura, 2015). Female meiosis is particularly error-prone (Hassold and Hunt, 2001) which can lead to chromosomally abnormal embryos. Therefore, understanding the molecular events that guarantee proper chromosome segregation during female meiosis is of paramount importance. Cell division is under tight control of post-translational modifications (PTMs), of which phosphorylation is the most studied. The balance between kinase and phosphatase activities play a central role but we still lack a clear picture of how this is achieved during meiosis, especially when compared to mitosis (Gelens et al., 2018; Novak et al., 2010).

Protein Phosphatase 2A (PP2A) is a heterotrimeric serine/threonine phosphatase composed of a catalytic subunit C (PPP2C), a scaffolding subunit A (PPP2R1) and a regulatory subunit B (PPP2R2-PPP2R5) (Cho and Xu, 2007; Xu et al., 2008; Xu et al., 2006). While the core enzyme (A and C subunits) is invariant, diversity in PP2A holoenzyme composition arises from the different regulatory B subunits. Four families of B subunits have been characterised: B55 (B), B56 (B′), PR72 (B″), and Striatin (B‴) (Moura and Conde, 2019; Seshacharyulu et al., 2013; Shi, 2009). In mammals and yeast, PP2A:B56 regulates the spindle assembly checkpoint (SAC) (Espert et al., 2014; Hayward et al., 2019; Qian et al., 2017; Vallardi et al., 2019), chromosome congression (Xu et al., 2013; Xu et al., 2014), and centromeric cohesion (Kitajima et al., 2006; Riedel et al., 2006; Tang et al., 2006).

bioRxiv preprint doi: https://doi.org/10.1101/2020.06.12.148254; this version posted November 30, 2020. The copyright holder for this preprint (which was not certified by peer review) is the author/funder, who has granted bioRxiv a license to display the preprint in perpetuity. It is made available under aCC-BY-NC 4.0 International license.

PP2A:B56 can be targeted to distinct sites by different proteins and two mechanisms have been characterised at the structural level. While an N-terminal coiled coil domain in Shugoshin/MEI-S332 binds PP2A:B56 (Xu et al., 2009), other substrates and/or regulatory proteins contain short linear motifs (SLiMs) following the consensus LxxIxE, which interact directly with B56 subunits (Hertz et al., 2016; Van Roey and Davey, 2015; Wang et al., 2016). BubR1 is one of the most widely studied LxxIxE-containing proteins, and has been well characterised during mitosis, where it plays a role in targeting PP2A:B56 to kinetochores (Foley et al., 2011; Kruse et al., 2013; Suijkerbuijk et al., 2012). BubR1 is also required during mouse meiosis (Homer et al., 2009; Touati et al., 2015; Yoshida et al., 2015) where kinetochore-microtubule attachments are stabilized through kinetochore dephosphorylation by PP2A:B56 (Yoshida et al., 2015).

In *C. elegans*, the meiotic role of PP2A remains unexplored. The core components of the PP2A holoenzyme in *C. elegans* are LET-92 (catalytic C subunit) and PAA-1 (scaffolding A subunit), and the regulatory B subunits are $B55^{SUR-6}$ (Sieburth et al., 1999), $B56^{PPTR-1}$ and $B56^{PPTR-2}$ (Padmanabhan et al., 2009), $B72^{RSA-1}$ (Schlaitz et al., 2007), and CASH-1/Striatin (Pal et al., 2017). PP2A complexes containing $B55^{SUR-6}$ and $B72^{RSA-1}$ play important roles during mitosis (Kitagawa et al., 2011; Schlaitz et al., 2007; Song et al., 2011), and, while PP2A likely plays a role during meiosis (Schlaitz et al., 2007), this has not been studied. Interestingly, the closest *C. elegans* BubR1 orthologue $Mad3^{SAN-1}$, does not localise to unattached kinetochores (Essex et al., 2009) and lacks the domain responsible for PP2A:B56 targeting. Additionally, the *C. elegans* Shugoshin orthologue, SGO-1, is dispensable for protection of cohesion in meiosis I (de Carvalho et al., 2008) and for counteracting Aurora B-targeting histone H3T3 phosphorylation (Ferrandiz et al., 2018). These observations suggest the existence of additional unknown mechanisms of PP2A regulation.

bioRxiv preprint doi: https://doi.org/10.1101/2020.06.12.148254; this version posted November 30, 2020. The copyright holder for this preprint (which was not certified by peer review) is the author/funder, who has granted bioRxiv a license to display the preprint in perpetuity. It is made available under aCC-BY-NC 4.0 International license.

In the present work, we used *C. elegans* oocytes to establish the role and regulation of PP2A during female meiosis. We found that PP2A is essential for female meiosis and its recruitment to meiotic chromosomes and spindle is mediated by the B56 regulatory subunits PPTR-1 and PPTR-2. Targeting of the B56 subunits is mediated by the kinase BUB-1 through a canonical B56 LxxIxE motif which targets both PPTR-1 and PPTR-2 to the chromosomes and central-spindle during meiosis. Overall, we provide evidence for a novel, BUB-1-regulated role for PP2A:B56 in chromosome congression during female meiosis.

bioRxiv preprint doi: https://doi.org/10.1101/2020.06.12.148254; this version posted November 30, 2020. The copyright holder for this preprint (which was not certified by peer review) is the author/funder, who has granted bioRxiv a license to display the preprint in perpetuity. It is made available under aCC-BY-NC 4.0 International license.

RESULTS

Protein Phosphatase 2A is essential for spindle assembly and chromosome segregation during meiosis I

We used dissected *C. elegans* oocytes to assess the role and regulation of PP2A (see Figure 1A for schematic) during female meiosis by following spindle and chromosome dynamics using GFP-tagged tubulin and mCherry-tagged histone. During meiosis I, six pairs of homologous chromosomes (bivalents) are captured by an acentrosomal spindle. Chromosomes then align and segregate. For our analysis, we defined Metaphase I (t = 0) as the frame before we detected chromosome separation (Figure 1B). In wild type oocytes, chromosome segregation is associated with dramatic changes in microtubule organisation as anaphase progresses, with microtubule density decreasing in poles and the bulk of GFP::tubulin is detected in the central-spindle (Figure 1C; Supp. Movie 1). In contrast, depletion of the PP2A catalytic subunit LET-92 drastically affects meiosis I with chromosomes failing to align in 84% of the oocytes (Figure 1C, cyan arrow; Figure 1D; P<0.0001, Fisher's exact test). During anaphase, chromosomes collapse into a small area where, in some cases, two chromosome masses were visible (Figure 1C, yellow arrow). Interestingly, severe chromosome segregation defects do not necessarily lead to polar body extrusion (PBE) defects (Schlientz and Bowerman, 2020). In the absence of PP2Ac only 15% of oocytes achieved polar body extrusion (Figure 1E, P<0.0001, Fisher's exact test). Similar defects were observed by depleting the sole PP2A scaffolding subunit, PAA-1 (Figure S1A-C). In *let-92(RNAi)* and *paa-1(RNAi)* oocytes microtubules do not organise into a bipolar structure (Figure 1B and Figure S1A, magenta arrows), as assessed by localisation of the spindle pole protein GFP::ASPM-1 (Connolly et al., 2014). GFP::ASPM-1 displays two focused poles in 100% of wild type oocytes (Figure 1F,G, cyan arrows). In contrast,

bioRxiv preprint doi: https://doi.org/10.1101/2020.06.12.148254; this version posted November 30, 2020. The copyright holder for this preprint (which was not certified by peer review) is the author/funder, who has granted bioRxiv a license to display the preprint in perpetuity. It is made available under aCC-BY-NC 4.0 International license.

GFP::ASPM-1 foci fail to coalesce in 95% of *let-92(RNAi)* oocytes, displaying a cluster of small foci (Figure 1F, orange arrows; Figure 1G; Supp. Movie 2).

We then sought to determine whether the lack of chromosome segregation was due to a defect in meiosis I progression. We measured endogenously GFP-tagged Securin^{IFY-1} levels as a readout for Anaphase Promoting Complex/Cyclosome (APC/C) activity (i.e. anaphase progression). Cytoplasmic Securin^{IFY-1} degradation proceeded at similar rates in wild type and LET-92-depleted oocytes (Figure 1H,I; Supp. Movie 3), indicating that APC/C activity is largely unperturbed in the absence of PP2A. Given the similarity of this phenotype to the depletion of CLASP orthologue CLS-2 I (Dumont et al., 2010; Laband et al., 2017; Schlientz and Bowerman, 2020), we analysed the localisation of CLS-2 and detected no changes in CLS-2 levels throughout meiosis (Figure S2; Supp Movie 4).

Taken together, we have found that PP2A is required for spindle assembly, chromosome alignment, and polar body extrusion during meiosis I. Additionally, APC activity is unperturbed by PP2A depletion, but we cannot rule out an impact on other pathways acting redundantly with APC (Sonneville and Gonczy, 2004; Wang et al., 2013).

PP2A:B56 localises to meiotic chromosomes and spindle

To assess the localisation of the core PP2A enzyme (A and C subunits) in vivo we attempted to tag endogenous LET-92 with GFP but were unsuccessful, presumably due to disruption of its native structure, in agreement with a recent report (Magescas et al., 2019). We generated a GFP-tagged version of the sole *C. elegans* PP2A scaffold subunit, PAA-1, and used this to assess the localisation of the core enzyme during meiosis I (Figure 2A; Supp Movie 5). The fusion protein localised in centrosomes and P-granules during the early embryonic mitotic divisions (Figure S3A), in agreement with previous immunofluorescence data (Lange et al., 2013). During meiosis I, GFP::PAA-1 localises to spindle poles (Figure 2A, cyan arrows) and

bioRxiv preprint doi: https://doi.org/10.1101/2020.06.12.148254; this version posted November 30, 2020. The copyright holder for this preprint (which was not certified by peer review) is the author/funder, who has granted bioRxiv a license to display the preprint in perpetuity. It is made available under aCC-BY-NC 4.0 International license.

chromosomes (Figure 2A, magenta arrows). The chromosomal signal is a combination of midbivalent and kinetochore populations, visible when analysing single Z-planes in the time-lapses (Figure S3B, magenta and yellow arrows). As meiosis I progresses, GFP::PAA-1 signal concentrates in the central-spindle between the segregating chromosomes (Figure 2A, magenta arrowhead), finally disappearing by late anaphase I. This pattern differs substantially from that of Protein Phosphatase 1 (PP1) which localises in the characteristic cup-shaped kinetochores (Hattersley et al., 2016).

To address which regulatory subunits are involved in targeting PP2A to the meiotic spindle and chromosomes, we first assessed the localisation of the two *C. elegans* B56 orthologues, PPTR-1 and PPTR-2 and the single B55 orthologue, SUR-6 (Figure S4A). Live imaging of endogenous, GFP-tagged regulatory subunits revealed that both B56 orthologues, PPTR-1 and PPTR-2, localised strongly and dynamically within the meiotic spindle whereas no spindle or chromosome localisation of $B55^{SUR-6}$ could be detected (Figure S4B). PPTR-1 has the highest sequence identity with human B56α2 (68.3%) and ε3 (71.87%) whereas PPTR-2 displays the highest sequence identity with human B56δ3 (66.19%) and B56γ1 (68.97%) (Table 1 and Supp. Table 1). Closer analysis of the C-terminal sequence in B56 which plays a key role in specifying centromere versus kinetochore localisation (Vallardi et al., 2019), further confirmed that PPTR-1 displays the highest sequence identity with the centromeric B56s, α and ε (93.75% and 87.5% respectively), while PPTR-2 displays the highest sequence identity with the kinetochore-localised B56, γ and δ (93.75% and 100%) (Figure S4C). We will henceforth refer to PPTR-1 as $B56\alpha^{PPTR-1}$ and to PPTR-2 as $B56\gamma^{PPTR-2}$. We used endogenous GFP-tagged versions of $B56\alpha^{PPTR-1}$ and $B56\gamma^{PPTR-2}$ (Kim et al., 2017) and analysed their dynamic localisation pattern in greater spatial and temporal detail. $B56\alpha^{PPTR-1}$ localises mainly to the region between homologous chromosomes (midbivalent) during

bioRxiv preprint doi: https://doi.org/10.1101/2020.06.12.148254; this version posted November 30, 2020. The copyright holder for this preprint (which was not certified by peer review) is the author/funder, who has granted bioRxiv a license to display the preprint in perpetuity. It is made available under aCC-BY-NC 4.0 International license.

153 metaphase of meiosis I (Figure 2B, magenta arrow; Supp. Movie 6) and faintly in
154 kinetochores (Figure 2B, yellow arrows). During anaphase I, B56α^{PPTR-1} is present
155 exclusively on the central spindle (Figure 2B, magenta arrowhead; Supp. Movie 6). B56γ^{PPTR-}
156 ^{2} localises mainly in the midbivalent during metaphase of meiosis I (Figure 2C, magenta
157 arrow; Supp. Movie 7) and faintly in kinetochores (Figure 2C, yellow arrow). A difference
158 between the two paralogs arises during anaphase: B56γ^{PPTR2} is present in the central spindle
159 and on chromosomes (Figure 2C, magenta and yellow arrowheads; Supp. Movie 7). In spite
160 of this difference, the levels of B56α^{PPTR-1} and B56γ^{PPTR-2} within the meiotic spindle follow
161 similar dynamics (Figure S5A-C).
162 These results show that *C. elegans* B56 subunits, like their mammalian counterparts, display a
163 similar but not identical localisation pattern: while both B56α^{PPTR-1} and B56γ^{PPTR-2} are present
164 in the midbivalent and central spindle, B56γ^{PPTR-2} is also associated with chromosomes during
165 anaphase.
166
167 **Depletion of B56α^{PPTR-1} and B56γ^{PPTR-2} leads to chromosome congression defects**
168 To address the role of the *C. elegans* B56 subunits during meiosis I, we combined a B56γ^{PPTR-}
169 ^{2} deletion allele (*ok1467*, '*pptr-2Δ*') with RNAi-mediated depletion of B56α^{PPTR-1} ('*pptr-*
170 *1(RNAi)*'), which we will refer to hereafter as 'PPTR-1/2 depletion'. While there was no
171 significant change in GFP::PAA-1 localisation upon depletion of B56α^{PPTR-1} or deletion of
172 B56γ^{PPTR-2}, no PAA-1 signal is detected associated with chromosomes upon double PPTR-1/2
173 depletion (Figure 2D, magenta arrow; Supp. Movie 8). Of note, PP2A targeting to poles was
174 still detected (Figure 2D, cyan arrows), indicating that B56 subunits target PP2A complex to
175 chromosomes but are not necessary for spindle pole targeting (Figure 2D; Supp. Movie 8).
176 We noticed that chromosomes failed to align upon PPTR-1/2 depletion (Figure 2D, yellow
177 arrow) and in order to quantify this phenotype, we measured the angle between the bivalent

bioRxiv preprint doi: https://doi.org/10.1101/2020.06.12.148254; this version posted November 30, 2020. The copyright holder for this preprint (which was not certified by peer review) is the author/funder, who has granted bioRxiv a license to display the preprint in perpetuity. It is made available under aCC-BY-NC 4.0 International license.

long axis and the spindle axis ('θ', Figure 2F, Figure S6) and the distance between the centre of the midbivalent and the metaphase plate, defined as the line in the middle of the spindle ('d', Figure 2G, Figure S6). We chose a time of 80 seconds prior to metaphase I for the analysis since most chromosomes are aligned by this stage (Figure S6) in agreement with previous data (Hattersley et al., 2016). Both the angle (θ) and the distance (d) increased significantly upon PPTR-1/2 double depletion (Figure 2F,G).Taken together, these results indicate that B56 subunits are involved in chromosomal and central spindle targeting PP2A and play a role in chromosome congression prior to anaphase. The PAA-1 localisation and chromosome alignment defects observed upon PPTR-1/2 depletion suggest that the subunits are at least partially redundant.

Shugoshin^{SGO-1} and BUBR1/Mad3^{SAN-1} are not essential for B56 subunit targeting

We next sought to identify the protein(s) involved in targeting PP2A:B56 to meiotic chromosomes. Two of the most studied proteins involved in B56 targeting are Shugoshin and BubR1. The BubR1 orthologue, Mad3^{SAN-1} is not detected in meiotic chromosomes or spindle (Figure S7A) and Mad3^{SAN-1} depletion by RNAi or a Mad3^{SAN-1} deletion allele (*ok1580*) does not inhibit B56 localisation (Figure S7B,C). We therefore tested the role of the Shugoshin ortholog, SGO-1. We used a *sgo-1* deletion allele generated by CRISPR (Ferrandiz et al., 2018; Figure S7A) and observed no change in B56α^{PPTR-1} levels (Figure S8B,C) and a slight reduction in B56γ^{PPTR-2} levels (Figure S8D,E). The PPTR-2 signal decreased between 20-40% in the *sgo-1Δ* mutant (Figure S8E, shaded area) and this reduction correlated with the timing of the congression defect in XX depletion (prior to metaphase I). Hence, Mad3^{SAN-1} and Shugoshin^{SGO-1} are not essential in PP2A:B56 targeting during meiosis in *C. elegans* oocytes.

bioRxiv preprint doi: https://doi.org/10.1101/2020.06.12.148254; this version posted November 30, 2020. The copyright holder for this preprint (which was not certified by peer review) is the author/funder, who has granted bioRxiv a license to display the preprint in perpetuity. It is made available under aCC-BY-NC 4.0 International license.

BUB-1 targets B56 subunits through a conserved LxxIxE motif

C. elegans B56 subunits display a dynamic localisation pattern similar to that of the kinase BUB-1 throughout meiosis I (Dumont et al., 2010; Monen et al., 2005; Pelisch et al., 2019; Pelisch et al., 2017) and interestingly, BUB-1 depletion by RNAi or using an auxin-inducible degradation system leads to alignment and segregation defects during meiosis (Dumont et al., 2010; Pelisch et al., 2019). We therefore tested whether BUB-1 is involved in B56 subunits recruitment to meiotic chromosomes. RNAi-mediated depletion of BUB-1 abolished meiotic chromosome localisation of B56α^{PPTR-1} (Figure 3A,B; Supp. Movie 9) and B56γ^{PPTR-2} (Figure 3C,D; Supp. Movie 10). GFP::PAA-1 localisation on chromosomes was also abolished by BUB-1 depletion (Figure 3E; Supp Movie 11). While we could not address the intensity on spindle poles due to the strong spindle defect in the absence of BUB-1, we could detect GFP::PAA-1 in extrachromosomal regions (Figure 3E, cyan arrows), indicating that BUB-1 specifically regulates PP2A:B56 chromosomal targeting. Consistent with this idea, BUB-1 depletion does not affect the localisation of the catalytic subunit of another major phosphatase, PP1^{GSP-2} (Figure S9; Supp. Movie 12). In agreement with published data (Dumont et al., 2010), BUB-1 depletion causes severe defects in chromosome alignment (Figure 3F).

C. elegans BUB-1 contains a conserved N-terminal tetratricopeptide repeat (TPR) domain, a C-terminal kinase domain, and regions mediating its interaction with Cdc20 and BUB3 (ABBA and GLEBS motifs, respectively) (Figure 4A; Kim et al., 2017; Kim et al., 2015; Moyle et al., 2014). Sequence analysis of *C. elegans* BUB-1 revealed the presence of a putative B56 LxxIxE motif in residues 282-287 (Figure 4A). When compared with two well-characterised LxxIxE motifs, in BubR1 and RepoMan, there is a high degree of conservation in the key residues making contacts with the B56 hydrophobic pockets (Figure 4A). In addition, the SLiM-binding hydrophobic pocket in B56 subunits is very well conserved in *C.*

bioRxiv preprint doi: https://doi.org/10.1101/2020.06.12.148254; this version posted November 30, 2020. The copyright holder for this preprint (which was not certified by peer review) is the author/funder, who has granted bioRxiv a license to display the preprint in perpetuity. It is made available under aCC-BY-NC 4.0 International license.

elegans (Figure S10). The putative LxxIxE motif lies within a region predicted to be disordered (Figure 4B) with serine 283 fitting a Cdk1 Ser/Thr-Pro motif.

Using a fluorescence polarisation-based assay, we confirmed that the LxxIxE motif of BUB-1 binds to purified recombinant PPTR-2, and this binding is abolished by the L282A,V285A mutations (Figure 4C). While localisation of BUB-1^{L282A,V285A} was indistinguishable from that of wild type BUB-1 during metaphase I (Figure S11A), localisation of B56α^{PPTR-1} to the midbivalent and central spindle was almost completely lost in the BUB-1^{L282A,V285A} mutant (Figure 4D-F; Supp. Movie 13). B56γ^{PPTR-2} midbivalent localisation leading to metaphase I and central-spindle localisation during anaphase were also dependent on the BUB-1 LxxIxE motif (Figure 4G, magenta arrows, and 4H; Supp. Movie 14). In contrast, chromosome-associated B56γ^{PPTR-2} was less affected in the BUB-1^{L282A,V285A} mutant (Figure 4G, yellow arrows). Importantly, the LxxIxE motif mutations BUB-1^{L282A,V285A} abrogates GFP::PAA-1 localisation in the midbivalent and central spindle (Figure 4I, magenta arrows; Supp Movie 15) without affecting the spindle pole PAA-1 localisation (Figure 4I, cyan arrows; Supp Movie 15). Some GFP::PAA-1 signal was still detected in anaphase chromosomes, consistent with the remaining B56γ^{PPTR-2} on chromosomes (Figure 4I,J, yellow arrows). This LxxIxE motif-dependent regulation is specific for B56 subunits because the localisation of the spindle assembly checkpoint component Mad1^{MDF-1}, a known BUB-1 interactor (Moyle et al., 2014), is not disrupted after mutating the BUB-1 LxxIxE motif (Figure S11B). Mutation of the BUB-1 LxxIxE motif not only impairs B56 chromosomal targeting but also leads to alignment/congression defects (Figure 4K,L), indicating that the BUB-1 LxxIxE motif recruits PP2A:B56 and plays an important role in chromosome congression. Lagging chromosomes were detected in 36% of oocytes in the BUB-1^{L282A,V285A} mutant, versus 10% in wild type oocytes (P=0.0125, Fisher's exact test), but segregation was achieved in 100% of the cases with no polar body extrusion defects were detected. Interestingly, the newly

bioRxiv preprint doi: https://doi.org/10.1101/2020.06.12.148254; this version posted November 30, 2020. The copyright holder for this preprint (which was not certified by peer review) is the author/funder, who has granted bioRxiv a license to display the preprint in perpetuity. It is made available under aCC-BY-NC 4.0 International license.

identified LxxIxE motif specifically recruits PP2A:B56 to metaphase chromosomes and anaphase central spindle, but not anaphase chromosomes.

Phosphorylation of BUB-1 LxxIxE is important for PP2A:B56 chromosome targeting

Since phosphorylation of LxxIxE motifs can increase affinity for B56 by ~10-fold (Wang et al., 2016), we sought to determine if Ser 283 within BUB-1 LxxIxE motif is phosphorylated in vivo. To this end, we immunoprecipitated endogenous, GFP-tagged BUB-1 from embryo lysates using a GFP nanobody. Immunoprecipitated material was digested with trypsin, peptides analysed by mass spectrometry and searches conducted for peptides containing phosphorylated adducts. As expected GFP-tagged, but not untagged, BUB-1 was pulled down by the GFP nanobody (Figure S12A) along with the BUB-1 partner, BUB-3 (Figure 5A, blue arrow). We found four phospho-sites clustered within a disordered region, one of which is Ser 283, within the LxxIxE motif (Figure 5B; see also representative MS spectra for Ser 283 in Figure S12B). We expressed a BUB-1 fragment containing the LxxIxE motif (Figure 5C) and performed Cdk1 kinase assays, which showed that Cdk1 can phosphorylate the 259-332 BUB-1 fragment (Figure 5D). Western blot analysis using a phospho-specific antibody revealed that Cdk1 can phosphorylate Ser 283 in vitro (Figure 5E). Importantly, LxxIxE motif peptides with phosphorylated Ser 283 bound recombinant B56γ^{PPTR-2} with higher affinity than non-phosphorylated LxxIxE peptide (Figure 5F). During meiosis, while BUB-1 phosphorylated in Ser 283 is detected in midbivalent and kinetochore, it is preferentially enriched in the midbivalent (Figure 5G,H).

Mutating the Ser 283 to Ala in endogenous BUB-1 ('BUB-1^{S283A}') had a similar effect to that of the BUB-1^{L282A,V285A} mutant: it significantly reduced B56α^{PPTR-1} localisation (Figure 6A,B; Supp. Movie S16) and in the case of B56γ^{PPTR-2}, it significantly reduced its midbivalent and central spindle localisation (Figure 6C,D; Supp. Movie S17). In line with these results and

bioRxiv preprint doi: https://doi.org/10.1101/2020.06.12.148254; this version posted November 30, 2020. The copyright holder for this preprint (which was not certified by peer review) is the author/funder, who has granted bioRxiv a license to display the preprint in perpetuity. It is made available under aCC-BY-NC 4.0 International license.

consistent with a B56-dependent chromatin recruitment of PP2A, GFP::PAA-1 was not detected on chromosomes during prometaphase/metaphase in the BUB-1^{S283A} mutant (Figure 6E,F; Supp. Movie S18). BUB-1^{S283A} mutation not only impairs PP2A/B56 chromosomal targeting but also leads to alignment/congression defects (Figure 6G,H), indicating that phosphorylation of Ser 283 within the BUB-1 LxxIxE motif recruits PP2A/B56 and plays an important role in chromosome congression.

Anaphase chromosomal recruitment of PP2A:B56γ^{PPTR-2} depends on BUB-1 C-terminal kinase domain

Since not all of B56γ^{PPTR-2} is targeted by the BUB-1 LxxIxE motif, we turned our attention to BUB-1 kinase domain. In *C. elegans* BUB-1 kinase domain regulates its interaction with binding partners such as Mad1^{MDF-1}. The K718R/D847N double mutation (equivalent to positions K821 and D917 in human Bub1) destabilizes the kinase domain and prevents its interaction with Mad1^{MDF-1} (Moyle et al., 2014). We generated endogenous BUB-1^{K718R,D847N} (Figure 7A) and confirmed that these mutations abolish recruitment of Mad1^{MDF-1} (Figure S11B). B56α^{PPTR-1}::GFP localisation and dynamics remained largely unaltered in the mutant BUB-1^{K718R,D847N} (Figure S13; Supp. Movie 19). The B56γ^{PPTR-2}::GFP pool most affected by the K718R,D847N mutant was the chromosomal one (Figure 7B, yellow arrows; Supp. Movie 20) with the central-spindle pool reduced but still present (Figure 7B, magenta arrow; Supp. Movie 20). We therefore combined the K718R,D847N with the L282A,V285A mutations to generate 'BUB-1 $^{L282A,V285A;K718R,D847N}$' observed a significant decrease in both chromosomal and central spindle B56γ^{PPTR-2}::GFP (Figure 7B; Supp. Movie 20). Line profiles highlighting these localisation differences in the mutants are shown in Figure 7C. We then analysed GFP::PAA-1 was not found associated with chromosomes during prometaphase I in the BUB-1$^{L282A,V285A;K718R,D847N}$ mutant (Figure 7E, magenta arrow; Supp. Movie 21). Of note, a

bioRxiv preprint doi: https://doi.org/10.1101/2020.06.12.148254; this version posted November 30, 2020. The copyright holder for this preprint (which was not certified by peer review) is the author/funder, who has granted bioRxiv a license to display the preprint in perpetuity. It is made available under aCC-BY-NC 4.0 International license.

significant population of GFP::PAA-1 remained associated with spindles poles (Figure 7D, cyan arrows) and surrounding the spindle area during anaphase (Figure 7D, yellow arrows). These results show that the BUB-1 kinase domain is important for recruitment of B56γ^{PPTR-2} but not of B56α^{PPTR-1}. Thus, BUB-1 is a key factor for the recruitment of PP2A:B56 but could also provide the basis for establishing (probably together with other proteins) the two pools of B56γ^{PPTR-2}.

bioRxiv preprint doi: https://doi.org/10.1101/2020.06.12.148254; this version posted November 30, 2020. The copyright holder for this preprint (which was not certified by peer review) is the author/funder, who has granted bioRxiv a license to display the preprint in perpetuity. It is made available under aCC-BY-NC 4.0 International license.

DISCUSSION

In the present manuscript, we have uncovered new roles for PP2A during oocyte meiosis in *C. elegans.* PP2A is essential for meiosis I: depletion of the catalytic or scaffold subunits lead to severe spindle assembly defects, lack of chromosome segregation, and failure to achieve polar body extrusion. These effects are a likely brought about by a combination of different PP2A subcomplexes with varying regulatory B subunits. PP2A:B56 regulates chromosome dynamics prior to segregation, since depletion of the two B56 orthologues, PPTR-1 and PPTR-2 lead to alignment defects. We have uncovered a new phospho-regulated B56 LxxIxE motif in *C. elegans* BUB-1 that recruits PP2A:B56 and is important for chromosome alignment during meiosis I.

Dissecting the role of PP2A during oocyte meiosis

Depletion of the sole catalytic or scaffold PP2A subunits lead to massive meiotic failure and embryonic lethality. The earliest effect we could see in our experimental setup is a failure to assemble a bipolar spindle. This will of course have a direct impact on any process that should occur after spindle assembly, including chromosome alignment and segregation, followed by polar body extrusion. However, BUB-1 depletion leads to a severe spindle assembly defect, followed by alignment defects. Then, in the majority of cases chromosomes segregate (with visible errors – lagging chromosomes) and polar bodies do extrude. Hence, lack of a proper bipolar metaphase spindle is not sufficient to result in lack of segregation or polar body extrusion. Along this line, PP2A complexes harbouring the B56 subunits PPTR-1 and PPTR-2 are important to target the phosphatase to chromosomes to regulate chromosome alignment in metaphase I. Furthermore, this chromosomal B56 pool is recruited by BUB-1 through its LxxIxE SLiM motif. Mutation of this motif that abolish binding to B56 subunits leads to alignment defects. B56 subunits however are not involved in spindle pole targeting of

bioRxiv preprint doi: https://doi.org/10.1101/2020.06.12.148254; this version posted November 30, 2020. The copyright holder for this preprint (which was not certified by peer review) is the author/funder, who has granted bioRxiv a license to display the preprint in perpetuity. It is made available under aCC-BY-NC 4.0 International license.

PP2A, suggesting that it is this spindle pole pool the one relevant for spindle assembly. Our attempts to address a possible role for other B subunits where focused on RSA-1 and SUR-6 given their reported centrosomal roles during mitosis (Enos et al., 2018; Kitagawa et al., 2011; Schlaitz et al., 2007; Song et al., 2011). However, neither RSA-1 nor SUR-6 were required for meiotic spindle assembly. It is likely that the role of PP2A on spindle assembly is achieved by a combination of B subunits and that could also include uncharacterised B subunits (Bye-A-Jee et al., 2020).

B56 targeting during different stages of meiosis I

Chromosomal PPTR-1 and PPTR-2 and the ensuing PP2A targeting prior to chromosome segregation depends on the BUB-1 LxxIxE motif. Interestingly, this dependency changes during anaphase, where PPTR-2 chromosomal targeting is BUB-1-dependent but LxxIxE motif-independent and depends on the kinase domain. The regulation of protein localisation during meiosis I in *C. elegans* oocytes is highly dynamic and differences have been observed between metaphase and anaphase. For example, while kinetochore localisation of the CLASP orthologue CLS-2 during metaphase depends on BUB-1, a pool of CLS-2 is able localise in the anaphase central spindle in a BUB-1-independent manner (Laband et al., 2017). In this line, since its role during meiosis was first described (Dumont et al., 2010), there has been no clear explanation as to the cause of the alignment and segregation defects upon BUB-1 depletion. Our results provide a plausible explanation for the role of BUB-1 in chromosome alignment during oocyte meiosis in *C. elegans* through the recruitment of PP2A/B56.

Possible function of chromosome-associated PP2A

As mentioned above, the PP2A complexes are likely playing a number of important roles during meiosis. Our work uncovers a function during chromosome congression involving

bioRxiv preprint doi: https://doi.org/10.1101/2020.06.12.148254; this version posted November 30, 2020. The copyright holder for this preprint (which was not certified by peer review) is the author/funder, who has granted bioRxiv a license to display the preprint in perpetuity. It is made available under aCC-BY-NC 4.0 International license.

B56 subunits targeted by BUB-1. Similar to mice and yeast, it is therefore likely that PP2A complexes at the chromosome control proper chromosome-spindle attachments. The alignment defects we observed upon PPTR-1/2 depletion (or in the LxxIxE motif mutant) resemble those reported in the absence of kinetochore proteins (Danlasky et al., 2020; Dumont et al., 2010). Interestingly, PP2A:B56 complexes containing PPTR-1 and PPTR-2 are present at the meiotic kinetochore, and it is therefore possible that PP2A/B56 works in parallel to and/or regulates kinetochore protein(s). Furthermore, we detected GFP::PAA-1 on anaphase chromosomes, similar to kinetochore proteins (Danlasky et al., 2020; Dumont et al., 2010; Hattersley et al., 2016).

During meiosis in *C. elegans*, the Aurora B orthologue, AIR-2, concentrates in the interface between homologous chromosomes (i.e. the midbivalent (Kaitna et al., 2002; Rogers et al., 2002; Schumacher et al., 1998) and its activity is counteracted by PP1, which is recruited by the protein LAB-1 (Tzur et al., 2012). PP1 counteracts Aurora B^{AIR-2} during meiosis by antagonising Haspin-mediated H3T3 phosphorylation in the long arm of the bivalent (Ferrandiz et al., 2018). Consistent with this, PP1 depletion leads to loss of sister chromatid cohesion during meiosis I (Kaitna et al., 2002; Rogers et al., 2002). During prometaphase and metaphase I, Aurora B^{AIR-2} is retained in the bivalent whereas PP1 resides mainly in kinetochores (Hattersley et al., 2016) and it is therefore likely that another phosphatase(s) will be involved in controlling Aurora B-mediated phosphorylation events during metaphase I. Since PP2A:B56 is concentrated in the midbivalent during meiosis I, we hypothesise that it could be the phosphatase balancing AIR-2 activity during meiosis. In this respect, we found that serine 612 in BUB-1 is phosphorylated and this serine is embedded in a sequence (RRL<u>S</u>I) closely resembling the consensus for PP2A:B56 reported in (Kruse et al., 2020). Furthermore, the sequence also fits into the loosely defined Aurora B consensus RRxSφ

bioRxiv preprint doi: https://doi.org/10.1101/2020.06.12.148254; this version posted November 30, 2020. The copyright holder for this preprint (which was not certified by peer review) is the author/funder, who has granted bioRxiv a license to display the preprint in perpetuity. It is made available under aCC-BY-NC 4.0 International license.

(where φ is a hydrophobic aa) (Cheeseman et al., 2002; Deretic et al., 2019; Kettenbach et al., 2011). Therefore, BUB-1 itself could be subject to an Aurora B-PP2A:B56 balance and it will be very interesting to address if BUB-1 and other meiotic proteins are regulated by the balance between Aurora B and PP2A:B56.

In summary, we provide evidence for a novel, BUB-1-regulated role for PP2A:B56 during female meiosis in *C. elegans.* It will be interesting to test in the future our hypothesis that PP2A is the main phosphatase counteracting Aurora B-mediated phosphorylation to achieve proper phosphorylation levels during meiosis I.

bioRxiv preprint doi: https://doi.org/10.1101/2020.06.12.148254; this version posted November 30, 2020. The copyright holder for this preprint (which was not certified by peer review) is the author/funder, who has granted bioRxiv a license to display the preprint in perpetuity. It is made available under aCC-BY-NC 4.0 International license.

ACKNOWLEDGEMENTS

We would like to thank Guy Benian, Needhi Bhalla, Bruce Bowerman, Arshad Desai, Tony Hyman, and Enrique Martinez-Perez for sharing *C. elegans* strains and antibodies. We would like to thank Egon Ogris for sharing unpublished data on the use of the PP2Ac monoclonal antibody. We thank Arshad Desai, Ron Hay, and Tomo Tanaka for comments on the manuscript. This work was supported by a Career Development Award from the Medical Research Council (grant MR/R008574/1) and an ISSF grant funded by the Wellcome Trust (105606/Z/14/Z). ST is funded by a Medical Research Council Doctoral Training Programme. D.K.C. is supported by a Sir Henry Dale Fellowship from the Wellcome Trust (208833). P.L-G. and J.B. were supported by NIH grant R01 GM074215, awarded to Arshad Desai. Work in the J.N.B. lab is supported by NIH grant R01 GM114471. We acknowledge the FingerPrints Proteomics Facility and the Dundee Imaging Facility, which are supported by a 'Wellcome Trust Technology Platform' award (097945/B/11/Z) and the Tissue Imaging Facility, funded by a Wellcome Trust award (101468/Z/13/Z). Some nematode strains were provided by the CGC, which is funded by NIH Office of Research Infrastructure Programs (P40 OD010440).

bioRxiv preprint doi: https://doi.org/10.1101/2020.06.12.148254; this version posted November 30, 2020. The copyright holder for this preprint (which was not certified by peer review) is the author/funder, who has granted bioRxiv a license to display the preprint in perpetuity. It is made available under aCC-BY-NC 4.0 International license.

AUTHOR CONTRIBUTIONS

L.B B. Investigation; formal analysis; writing – review and editing.

F.S. Investigation; Formal analysis; writing – review and editing.

S.J.P.T. Investigation; writing – review and editing.

C.F B. Investigation; writing – review and editing.

J.B. Investigation.

P.L-G. Investigation; writing – review and editing.

C.G.S.T. Investigation; writing – review and editing.

J.N.B. Investigation; writing – review and editing.

D.K.C. Investigation; writing – review and editing.

F.P. Funding acquisition; conceptualisation; project administration; investigation; methodology; supervision; formal analysis. writing – original draft. writing – review and editing.

bioRxiv preprint doi: https://doi.org/10.1101/2020.06.12.148254; this version posted November 30, 2020. The copyright holder for this preprint (which was not certified by peer review) is the author/funder, who has granted bioRxiv a license to display the preprint in perpetuity. It is made available under aCC-BY-NC 4.0 International license.

REFERENCES

Allan, C., Burel, J.M., Moore, J., Blackburn, C., Linkert, M., Loynton, S., Macdonald, D., Moore, W.J., Neves, C., Patterson, A., *et al.* (2012). OMERO: flexible, model-driven data management for experimental biology. Nat Methods *9*, 245-253.

Bye-A-Jee, H., Zaru, R., Magrane, M., Orchard, S., and Consortium, t.U. (2020). Caenorhabditis elegans phosphatase complexes in UniProtKB and Complex Portal. The FEBS Journal *287*, 2664-2684.

Cheeseman, I.M., Anderson, S., Jwa, M., Green, E.M., Kang, J., Yates, J.R., 3rd, Chan, C.S., Drubin, D.G., and Barnes, G. (2002). Phospho-regulation of kinetochore-microtubule attachments by the Aurora kinase Ipl1p. Cell *111*, 163-172.

Cho, U.S., and Xu, W. (2007). Crystal structure of a protein phosphatase 2A heterotrimeric holoenzyme. Nature *445*, 53-57.

Connolly, A.A., Osterberg, V., Christensen, S., Price, M., Lu, C., Chicas-Cruz, K., Lockery, S., Mains, P.E., and Bowerman, B. (2014). Caenorhabditis elegans oocyte meiotic spindle pole assembly requires microtubule severing and the calponin homology domain protein ASPM-1. Mol Biol Cell *25*, 1298-1311.

Danlasky, B.M., Panzica, M.T., McNally, K.P., Vargas, E., Bailey, C., Li, W., Gong, T., Fishman, E.S., Jiang, X., and McNally, F.J. (2020). Evidence for anaphase pulling forces during C. elegans meiosis. J Cell Biol *219*.

de Carvalho, C.E., Zaaijer, S., Smolikov, S., Gu, Y., Schumacher, J.M., and Colaiacovo, M.P. (2008). LAB-1 antagonizes the Aurora B kinase in C. elegans. Genes Dev *22*, 2869-2885.

Deretic, J., Kerr, A., and Welburn, J.P.I. (2019). A rapid computational approach identifies SPICE1 as an Aurora kinase substrate. Mol Biol Cell *30*, 312-323.

bioRxiv preprint doi: https://doi.org/10.1101/2020.06.12.148254; this version posted November 30, 2020. The copyright holder for this preprint (which was not certified by peer review) is the author/funder, who has granted bioRxiv a license to display the preprint in perpetuity. It is made available under aCC-BY-NC 4.0 International license.

Desai, A., Rybina, S., Müller-Reichert, T., Shevchenko, A., Shevchenko, A., Hyman, A., and Oegema, K. (2003). KNL-1 directs assembly of the microtubule-binding interface of the kinetochore in C. elegans. Genes & Development *17*, 2421-2435.

Dickinson, D.J., Pani, A.M., Heppert, J.K., Higgins, C.D., and Goldstein, B. (2015). Streamlined Genome Engineering with a Self-Excising Drug Selection Cassette. Genetics *200*, 1035-1049.

Dumont, J., Oegema, K., and Desai, A. (2010). A kinetochore-independent mechanism drives anaphase chromosome separation during acentrosomal meiosis. Nat Cell Biol *12*, 894-901.

Enos, S.J., Dressler, M., Gomes, B.F., Hyman, A.A., and Woodruff, J.B. (2018). Phosphatase PP2A and microtubule-mediated pulling forces disassemble centrosomes during mitotic exit. Biology Open *7*, bio029777.

Espert, A., Uluocak, P., Bastos, R.N., Mangat, D., Graab, P., and Gruneberg, U. (2014). PP2A-B56 opposes Mps1 phosphorylation of Knl1 and thereby promotes spindle assembly checkpoint silencing. The Journal of Cell Biology *206*, 833.

Essex, A., Dammermann, A., Lewellyn, L., Oegema, K., and Desai, A. (2009). Systematic analysis in Caenorhabditis elegans reveals that the spindle checkpoint is composed of two largely independent branches. Mol Biol Cell *20*, 1252-1267.

Ferrandiz, N., Barroso, C., Telecan, O., Shao, N., Kim, H.-M., Testori, S., Faull, P., Cutillas, P., Snijders, A.P., Colaiácovo, M.P., *et al.* (2018). Spatiotemporal regulation of Aurora B recruitment ensures release of cohesion during C. elegans oocyte meiosis. Nature Communications *9*, 834.

Foley, E.A., Maldonado, M., and Kapoor, T.M. (2011). Formation of stable attachments between kinetochores and microtubules depends on the B56-PP2A phosphatase. Nature Cell Biology *13*, 1265-1271.

bioRxiv preprint doi: https://doi.org/10.1101/2020.06.12.148254; this version posted November 30, 2020. The copyright holder for this preprint (which was not certified by peer review) is the author/funder, who has granted bioRxiv a license to display the preprint in perpetuity. It is made available under aCC-BY-NC 4.0 International license.

Gelens, L., Qian, J., Bollen, M., and Saurin, A.T. (2018). The Importance of Kinase-Phosphatase Integration: Lessons from Mitosis. Trends Cell Biol *28*, 6-21.

Hassold, T., and Hunt, P. (2001). To err (meiotically) is human: the genesis of human aneuploidy. Nat Rev Genet *2*, 280-291.

Hattersley, N., Cheerambathur, D., Moyle, M., Stefanutti, M., Richardson, A., Lee, K.Y., Dumont, J., Oegema, K., and Desai, A. (2016). A Nucleoporin Docks Protein Phosphatase 1 to Direct Meiotic Chromosome Segregation and Nuclear Assembly. Dev Cell *38*, 463-477.

Hayward, D., Bancroft, J., Mangat, D., Alfonso-Pérez, T., Dugdale, S., McCarthy, J., Barr, F.A., and Gruneberg, U. (2019). Checkpoint signaling and error correction require regulation of the MPS1 T-loop by PP2A-B56. The Journal of Cell Biology, jcb.201905026.

Hertz, E.P.T., Kruse, T., Davey, N.E., Lopez-Mendez, B., Sigurethsson, J.O., Montoya, G., Olsen, J.V., and Nilsson, J. (2016). A Conserved Motif Provides Binding Specificity to the PP2A-B56 Phosphatase. Molecular Cell *63*, 686-695.

Homer, H., Gui, L., and Carroll, J. (2009). A spindle assembly checkpoint protein functions in prophase I arrest and prometaphase progression. Science *326*, 991-994.

Kaitna, S., Pasierbek, P., Jantsch, M., Loidl, J., and Glotzer, M. (2002). The aurora B kinase AIR-2 regulates kinetochores during mitosis and is required for separation of homologous Chromosomes during meiosis. Curr Biol *12*, 798-812.

Kettenbach, A.N., Schweppe, D.K., Faherty, B.K., Pechenick, D., Pletnev, A.A., and Gerber, S.A. (2011). Quantitative phosphoproteomics identifies substrates and functional modules of Aurora and Polo-like kinase activities in mitotic cells. Sci Signal *4*, rs5.

Kim, T., Lara-Gonzalez, P., Prevo, B., Meitinger, F., Cheerambathur, D.K., Oegema, K., and Desai, A. (2017). Kinetochores accelerate or delay APC/C activation by directing Cdc20 to opposing fates. Genes Dev *31*, 1089-1094.

bioRxiv preprint doi: https://doi.org/10.1101/2020.06.12.148254; this version posted November 30, 2020. The copyright holder for this preprint (which was not certified by peer review) is the author/funder, who has granted bioRxiv a license to display the preprint in perpetuity. It is made available under aCC-BY-NC 4.0 International license.

Kim, T., Moyle, M.W., Lara-Gonzalez, P., De Groot, C., Oegema, K., and Desai, A. (2015). Kinetochore-localized BUB-1/BUB-3 complex promotes anaphase onset in C. elegans. J Cell Biol *209*, 507-517.

Kitagawa, D., Fluckiger, I., Polanowska, J., Keller, D., Reboul, J., and Gonczy, P. (2011). PP2A phosphatase acts upon SAS-5 to ensure centriole formation in C. elegans embryos. Dev Cell *20*, 550-562.

Kitajima, T.S., Sakuno, T., Ishiguro, K.-i., Iemura, S.-i., Natsume, T., Kawashima, S.A., and Watanabe, Y. (2006). Shugoshin collaborates with protein phosphatase 2A to protect cohesin. Nature *441*, 46-52.

Kruse, T., Gnosa, S.P., Nasa, I., Garvanska, D.H., Hein, J.B., Nguyen, H., Samsoe-Petersen, J., Lopez-Mendez, B., Hertz, E.P.T., Schwarz, J.*, et al.* (2020). Mechanisms of site-specific dephosphorylation and kinase opposition imposed by PP2A regulatory subunits. EMBO J, e103695.

Kruse, T., Zhang, G., Larsen, M.S., Lischetti, T., Streicher, W., Kragh Nielsen, T., Bjorn, S.P., and Nilsson, J. (2013). Direct binding between BubR1 and B56-PP2A phosphatase complexes regulate mitotic progression. Journal of Cell Science *126*, 1086-1092.

Laband, K., Lacroix, B., Edwards, F., Canman, J.C., and Dumont, J. (2018). Methods in Cell Biology, Vol 145.

Laband, K., Le Borgne, R., Edwards, F., Stefanutti, M., Canman, J.C., Verbavatz, J.M., and Dumont, J. (2017). Chromosome segregation occurs by microtubule pushing in oocytes. Nat Commun *8*, 1499.

Lange, K.I., Heinrichs, J., Cheung, K., and Srayko, M. (2013). Suppressor mutations identify amino acids in PAA-1/PR65 that facilitate regulatory RSA-1/B″ subunit targeting of PP2A to centrosomes in C. elegans. Biology open *2*, 88-94.

bioRxiv preprint doi: https://doi.org/10.1101/2020.06.12.148254; this version posted November 30, 2020. The copyright holder for this preprint (which was not certified by peer review) is the author/funder, who has granted bioRxiv a license to display the preprint in perpetuity. It is made available under aCC-BY-NC 4.0 International license.

Magescas, J., Zonka, J.C., and Feldman, J.L. (2019). A two-step mechanism for the inactivation of microtubule organizing center function at the centrosome. eLife *8*, e47867.

Marston, A.L., and Amon, A. (2004). Meiosis: cell-cycle controls shuffle and deal. Nat Rev Mol Cell Biol *5*, 983-997.

Monen, J., Maddox, P.S., Hyndman, F., Oegema, K., and Desai, A. (2005). Differential role of CENP-A in the segregation of holocentric C. elegans chromosomes during meiosis and mitosis. Nature Cell Biology *7*, 1248.

Moura, M., and Conde, C. (2019). Phosphatases in Mitosis: Roles and Regulation. Biomolecules *9*.

Moyle, M.W., Kim, T., Hattersley, N., Espeut, J., Cheerambathur, D.K., Oegema, K., and Desai, A. (2014). A Bub1-Mad1 interaction targets the Mad1-Mad2 complex to unattached kinetochores to initiate the spindle checkpoint. J Cell Biol *204*, 647-657.

Novak, B., Kapuy, O., Domingo-Sananes, M.R., and Tyson, J.J. (2010). Regulated protein kinases and phosphatases in cell cycle decisions. Curr Opin Cell Biol *22*, 801-808.

Ohkura, H. (2015). Meiosis: an overview of key differences from mitosis. Cold Spring Harb Perspect Biol *7*.

Padmanabhan, S., Mukhopadhyay, A., Narasimhan, S.D., Tesz, G., Czech, M.P., and Tissenbaum, H.A. (2009). A PP2A regulatory subunit regulates C. elegans insulin/IGF-1 signaling by modulating AKT-1 phosphorylation. Cell *136*, 939-951.

Pal, S., Lant, B., Yu, B., Tian, R., Tong, J., Krieger, J.R., Moran, M.F., Gingras, A.C., and Derry, W.B. (2017). CCM-3 Promotes C. elegans Germline Development by Regulating Vesicle Trafficking Cytokinesis and Polarity. Curr Biol *27*, 868-876.

Pelisch, F., Bel Borja, L., Jaffray, E.G., and Hay, R.T. (2019). Sumoylation regulates protein dynamics during meiotic chromosome segregation in *C. elegans* oocytes. Journal of Cell Science *132*, jcs232330.

bioRxiv preprint doi: https://doi.org/10.1101/2020.06.12.148254; this version posted November 30, 2020. The copyright holder for this preprint (which was not certified by peer review) is the author/funder, who has granted bioRxiv a license to display the preprint in perpetuity. It is made available under aCC-BY-NC 4.0 International license.

Pelisch, F., Tammsalu, T., Wang, B., Jaffray, E.G., Gartner, A., and Hay, R.T. (2017). A SUMO-Dependent Protein Network Regulates Chromosome Congression during Oocyte Meiosis. Mol Cell *65*, 66-77.

Qian, J., Garcia-Gimeno, M.A., Beullens, M., Manzione, M.G., Van der Hoeven, G., Igual, J.C., Heredia, M., Sanz, P., Gelens, L., and Bollen, M. (2017). An Attachment-Independent Biochemical Timer of the Spindle Assembly Checkpoint. Mol Cell *68*, 715-730 e715.

Riedel, C.G., Katis, V.L., Katou, Y., Mori, S., Itoh, T., Helmhart, W., Gálová, M., Petronczki, M., Gregan, J., Cetin, B.*, et al.* (2006). Protein phosphatase 2A protects centromeric sister chromatid cohesion during meiosis I. Nature *441*, 53-61.

Rogers, E., Bishop, J.D., Waddle, J.A., Schumacher, J.M., and Lin, R. (2002). The aurora kinase AIR-2 functions in the release of chromosome cohesion in Caenorhabditis elegans meiosis. J Cell Biol *157*, 219-229.

Schindelin, J., Arganda-Carreras, I., Frise, E., Kaynig, V., Longair, M., Pietzsch, T., Preibisch, S., Rueden, C., Saalfeld, S., Schmid, B.*, et al.* (2012). Fiji: an open-source platform for biological-image analysis. Nat Methods *9*, 676-682.

Schlaitz, A.-L., Srayko, M., Dammermann, A., Quintin, S., Wielsch, N., MacLeod, I., de Robillard, Q., Zinke, A., Yates, J.R., Müller-Reichert, T.*, et al.* (2007). The C. elegans RSA Complex Localizes Protein Phosphatase 2A to Centrosomes and Regulates Mitotic Spindle Assembly. Cell *128*, 115-127.

Schlientz, A.J., and Bowerman, B. (2020). C. elegans CLASP/CLS-2 negatively regulates membrane ingression throughout the oocyte cortex and is required for polar body extrusion. PLoS Genet *16*, e1008751.

Schumacher, J.M., Golden, A., and Donovan, P.J. (1998). AIR-2: An Aurora/Ipl1-related protein kinase associated with chromosomes and midbody microtubules is required for polar

bioRxiv preprint doi: https://doi.org/10.1101/2020.06.12.148254; this version posted November 30, 2020. The copyright holder for this preprint (which was not certified by peer review) is the author/funder, who has granted bioRxiv a license to display the preprint in perpetuity. It is made available under aCC-BY-NC 4.0 International license.

body extrusion and cytokinesis in Caenorhabditis elegans embryos. J Cell Biol *143*, 1635-1646.

Seshacharyulu, P., Pandey, P., Datta, K., and Batra, S.K. (2013). Phosphatase: PP2A structural importance, regulation and its aberrant expression in cancer. Cancer Letters *335*, 9-18.

Shi, Y. (2009). Serine/threonine phosphatases: mechanism through structure. Cell *139*, 468-484.

Sieburth, D.S., Sundaram, M., Howard, R.M., and Han, M. (1999). A PP2A regulatory subunit positively regulates Ras-mediated signaling during Caenorhabditis elegans vulval induction. Genes Dev *13*, 2562-2569.

Sievers, F., Wilm, A., Dineen, D., Gibson, T.J., Karplus, K., Li, W., Lopez, R., McWilliam, H., Remmert, M., Soding, J.*, et al.* (2011). Fast, scalable generation of high-quality protein multiple sequence alignments using Clustal Omega. Mol Syst Biol *7*, 539.

Song, M.H., Liu, Y., Anderson, D.E., Jahng, W.J., and O'Connell, K.F. (2011). Protein phosphatase 2A-SUR-6/B55 regulates centriole duplication in C. elegans by controlling the levels of centriole assembly factors. Dev Cell *20*, 563-571.

Sonneville, R., and Gonczy, P. (2004). Zyg-11 and cul-2 regulate progression through meiosis II and polarity establishment in C. elegans. Development *131*, 3527-3543.

Suijkerbuijk, S.J., Vleugel, M., Teixeira, A., and Kops, G.J. (2012). Integration of kinase and phosphatase activities by BUBR1 ensures formation of stable kinetochore-microtubule attachments. Dev Cell *23*, 745-755.

Tang, Z., Shu, H., Qi, W., Mahmood, N.A., Mumby, M.C., and Yu, H. (2006). PP2A Is Required for Centromeric Localization of Sgo1 and Proper Chromosome Segregation. Developmental Cell *10*, 575-585.

bioRxiv preprint doi: https://doi.org/10.1101/2020.06.12.148254; this version posted November 30, 2020. The copyright holder for this preprint (which was not certified by peer review) is the author/funder, who has granted bioRxiv a license to display the preprint in perpetuity. It is made available under aCC-BY-NC 4.0 International license.

Timmons, L., Court, D.L., and Fire, A. (2001). Ingestion of bacterially expressed dsRNAs can produce specific and potent genetic interference in Caenorhabditis elegans. Gene *263*, 103-112.

Timmons, L., and Fire, A. (1998). Specific interference by ingested dsRNA. Nature *395*, 854.

Touati, S.A., Buffin, E., Cladiere, D., Hached, K., Rachez, C., van Deursen, J.M., and Wassmann, K. (2015). Mouse oocytes depend on BubR1 for proper chromosome segregation but not for prophase I arrest. Nat Commun *6*, 6946.

Tzur, Y.B., Egydio de Carvalho, C., Nadarajan, S., Van Bostelen, I., Gu, Y., Chu, D.S., Cheeseman, I.M., and Colaiacovo, M.P. (2012). LAB-1 targets PP1 and restricts Aurora B kinase upon entrance into meiosis to promote sister chromatid cohesion. PLoS Biol *10*, e1001378.

UniProt, C. (2019). UniProt: a worldwide hub of protein knowledge. Nucleic Acids Res *47*, D506-D515.

Vallardi, G., Allan, L.A., Crozier, L., and Saurin, A.T. (2019). Division of labour between PP2A-B56 isoforms at the centromere and kinetochore. eLife *8*, e42619.

Van Roey, K., and Davey, N.E. (2015). Motif co-regulation and co-operativity are common mechanisms in transcriptional, post-transcriptional and post-translational regulation. Cell Communication and Signaling *13*, 45.

Wang, R., Kaul, Z., Ambardekar, C., Yamamoto, T.G., Kavdia, K., Kodali, K., High, A.A., and Kitagawa, R. (2013). HECT-E3 ligase ETC-1 regulates securin and cyclin B1 cytoplasmic abundance to promote timely anaphase during meiosis in C. elegans. Development *140*, 2149-2159.

Wang, S., Wu, D., Quintin, S., Green, R.A., Cheerambathur, D.K., Ochoa, S.D., Desai, A., and Oegema, K. (2015). NOCA-1 functions with gamma-tubulin and in parallel to Patronin to assemble non-centrosomal microtubule arrays in C. elegans. Elife *4*, e08649.

bioRxiv preprint doi: https://doi.org/10.1101/2020.06.12.148254; this version posted November 30, 2020. The copyright holder for this preprint (which was not certified by peer review) is the author/funder, who has granted bioRxiv a license to display the preprint in perpetuity. It is made available under aCC-BY-NC 4.0 International license.

Wang, X., Bajaj, R., Bollen, M., Peti, W., and Page, R. (2016). Expanding the PP2A Interactome by Defining a B56-Specific SLiM. Structure *24*, 2174-2181.

Waterhouse, A.M., Procter, J.B., Martin, D.M., Clamp, M., and Barton, G.J. (2009). Jalview Version 2--a multiple sequence alignment editor and analysis workbench. Bioinformatics *25*, 1189-1191.

Xu, P., Raetz, E.A., Kitagawa, M., Virshup, D.M., and Lee, S.H. (2013). BUBR1 recruits PP2A via the B56 family of targeting subunits to promote chromosome congression. Biology Open *2*, 479.

Xu, P., Virshup, D.M., and Lee, S.H. (2014). B56-PP2A regulates motor dynamics for mitotic chromosome alignment. Journal of Cell Science *127*, 4567.

Xu, Y., Chen, Y., Zhang, P., Jeffrey, P.D., and Shi, Y. (2008). Structure of a Protein Phosphatase 2A Holoenzyme: Insights into B55-Mediated Tau Dephosphorylation. Molecular Cell *31*, 873-885.

Xu, Y., Xing, Y., Chen, Y., Chao, Y., Lin, Z., Fan, E., Yu, J.W., Strack, S., Jeffrey, P.D., and Shi, Y. (2006). Structure of the Protein Phosphatase 2A Holoenzyme. Cell *127*, 1239-1251.

Xu, Z., Cetin, B., Anger, M., Cho, U.S., Helmhart, W., Nasmyth, K., and Xu, W. (2009). Structure and Function of the PP2A-Shugoshin Interaction. Molecular Cell *35*, 426-441.

Yoshida, S., Kaido, M., and Kitajima, T.S. (2015). Inherent Instability of Correct Kinetochore-Microtubule Attachments during Meiosis I in Oocytes. Dev Cell *33*, 589-602.

bioRxiv preprint doi: https://doi.org/10.1101/2020.06.12.148254; this version posted November 30, 2020. The copyright holder for this preprint (which was not certified by peer review) is the author/funder, who has granted bioRxiv a license to display the preprint in perpetuity. It is made available under aCC-BY-NC 4.0 International license.

METHODS

C. elegans strains

Strains used in this study were maintained at 20 degrees unless indicated otherwise. For a complete list of strains, please refer to Supplementary Table 2. Requests for strains not deposited in the CGC should be done through the FP lab's website (https://pelischlab.co.uk/reagents/).

RNAi

For RNAi experiments, we cloned the different sequences in the L4440 RNAi feeding vector (Timmons and Fire, 1998).

All sequences were inserted into L4440 using the NEBuilder HiFi DNA Assembly Master Mix (New England Biolabs) and transformed into DH5a bacteria. The purified plasmids were then transformed into HT115(DE3) bacteria (Timmons et al., 2001). RNAi clones were picked and grown overnight at 37°C in LB with 100 µg/ml ampicillin. Saturated cultures were diluted 1:100 and allowed to grow until reaching an OD_{600} of 0.6–0.8. IPTG (isopropyl-β-d-thiogalactopyranoside) was added to a final concentration of 1 mM and cultures were incubated overnight at 20°C. Bacteria were then seeded onto NGM plates made with agarose and allowed to dry. L4 worms were then plated on RNAi plates and grown to adulthood at 20°C for 24 hs in the case of *let-92(RNAi)*, *bub-1(RNAi)*, and *paa-1(RNAi)*, and 48 hs in all other cases.

CRISPR strains

GFP::SUR-6

For the generation of in situ-tagged GFP::SUR-6, we used the Self-Excising Cassette method (Dickinson et al., 2015). In brief, N2 adults were injected with a plasmid mix containing Cas9, a sgRNA targeting the N-terminus of sur-6 and a repairing template to insert the GFP sequence, along with a LoxP-flanked cassette that encoded for a hygromycin resistance gene,

bioRxiv preprint doi: https://doi.org/10.1101/2020.06.12.148254; this version posted November 30, 2020. The copyright holder for this preprint (which was not certified by peer review) is the author/funder, who has granted bioRxiv a license to display the preprint in perpetuity. It is made available under aCC-BY-NC 4.0 International license.

a sqt-1 mutant to confer a dominant roller phenotype, and heat-shocked-induced Cre recombinase. After selection in hygromycin, positive integrants (evidenced by their roller phenotype) were heat-shocked to express Cre and remove the cassette.

The strains AID::GFP::GSP-2, GFP::PAA-1, BUB-1^{K718R,D847N}, and BUB-1^{L282A,V285A} were generated by Sunybiotech.

<u>AID::GFP::GSP-2</u>

(AID in purple, GFP in green, synonimous mutations in cyan)

ATGCCTAAAGATCCAGCCAAACCTCCGGCCAAGGCACAAGTTGTGGGATGGCCA
CCGGTGAGATCATACCGGAAGAACGTGATGGTTTCCTGCCAAAAATCAAGCGGT
GGCCCGGAGGCGGCGGCGTTCGTGAAGAGTAAAGGAGAAGAACTTTTCACTGGA
GTTGTCCCAATTCTTGTTGAATTAGATGGTGATGTTAATGGGCACAAATTTTCTGT
CAGTGGAGAGGGTGAAGGTGATGCAACATACGGAAAACTTACCCTTAAATTTATT
TGCACTACTGGAAAACTACCTGTTCCATGGgtaagtttaaacatatatatactaactaaccctgattatttaaat
tttcagCCAACACTTGTCACTACTTTCTgTTATGGTGTTCAATGCTTcTCgAGATACCCA
GATCATATGAAACgGCATGACTTTTTCAAGAGTGCCATGCCCGAAGGTTATGTAC
AGGAAAGAACTATATTTTTCAAAGATGACGGGAACTACAAGACACgtaagtttaaacagtt
cggtactaactaaccatacatatttaaattttcagGTGCTGAAGTCAAGTTTGAAGGTGATACCCTTGTT
AATAGAATCGAGTTAAAAGGTATTGATTTTAAAGAAGATGGAAACATTCTTGGAC
ACAAATTGGAATACAACTATAACTCACACAATGTATACATCATGGCAGACAAAC
AAAAGAATGGAATCAAAGTTgtaagtttaaacatgattttactaactaactaatctgatttaaattttcagAACTTC
AAAATTAGACACAACATTGAAGATGGAAGCGTTCAACTAGCAGACCATTATCAA
CAAAATACTCCAATTGGCGATGGCCCTGTCCTTTTACCAGACAACCATTACCTGT
CCACACAATCTGCCCTTTCGAAAGATCCCAACGAAAAGAGAGACCACATGGTCCT

bioRxiv preprint doi: https://doi.org/10.1101/2020.06.12.148254; this version posted November 30, 2020. The copyright holder for this preprint (which was not certified by peer review) is the author/funder, who has granted bioRxiv a license to display the preprint in perpetuity. It is made available under aCC-BY-NC 4.0 International license.

TCTTGAGTTTGTAACAGCTGCTGGGATTACACATGGCATGGATGAACTATACAAA

GACGTAGAAAAGCTTAATCTCGACAATATCATCTCCAGATTATTGGAAG.

GFP::PAA-1

(GFP in green, synonimous mutations in cyan)

ATGAGTAAAGGAGAAGAACTTTTCACTGGAGTTGTCCCAATTCTTGTTGAATTAG

ATGGTGATGTTAATGGGCACAAATTTTCTGTCAGTGGAGAGGGTGAAGGTGATGC

AACATACGGAAAACTTACCCTTAAATTTATTTGCACTACTGGAAAACTACCTGTT

CCATGGgtaagtttaaacatatatatactaactaaccctgattatttaaattttcagCCAACACTTGTCACTACTTTC

TgTTATGGTGTTCAATGCTTcTCgAGATACCCAGATCATATGAAACgGCATGACTTT

TTCAAGAGTGCCATGCCCGAAGGTTATGTACAGGAAAGAACTATATTTTTCAAAG

ATGACGGGAACTACAAGACACgtaagtttaaacagttcggtactaactaaccatacatatttaaattttcagGTGC

TGAAGTCAAGTTTGAAGGTGATACCCTTGTTAATAGAATCGAGTTAAAAGGTATT

GATTTTAAAGAAGATGGAAACATTCTTGGACACAAATTGGAATACAACTATAACT

CACACAATGTATACATCATGGCAGACAAACAAAAGAATGGAATCAAAGTTgtaagttt

aaacatgattttactaactaactaatctgatttaaattttcagAACTTCAAAATTAGACACAACATTGAAGATG

GAAGCGTTCAACTAGCAGACCATTATCAACAAAATACTCCAATTGGCGATGGCCC

TGTCCTTTTACCAGACAACCATTACCTGTCCACACAATCTGCCCTTTCGAAAGATC

CCAACGAAAAGAGAGACCACATGGTCCTTCTTGAGTTTGTAACAGCTGCTGGGAT

TACACATGGCATGGATGAACTATACAAAGGAGGTGGATCCGGTGGTGGATCCTC

GGTTGTCGAAGAAGCTACTGACGACGCG.

bub-1^{K718R,D847N}

The wild type sequence:

bioRxiv preprint doi: https://doi.org/10.1101/2020.06.12.148254; this version posted November 30, 2020. The copyright holder for this preprint (which was not certified by peer review) is the author/funder, who has granted bioRxiv a license to display the preprint in perpetuity. It is made available under aCC-BY-NC 4.0 International license.

GTAACCGATGATCAAAGGACAGTAGCTGTGAAGTACGAGGTGCCATCATGTTCGT
GGGAAGTGTACATTTGCGACCAAATGCGGAATCGCCTGAAAGATCGAGGTTTGG
AGCTGATGGCCAAATGTTGCATTATGGAAGTGATGGATGCTTATGTTTATTCAAC
TGCTTCGCTTCTTGTTAATCAGTACCACGAATATGGAACGCTGCTTGAATATGCG
AATAACATGAAGGATCCGAATTGGCACATAACCTGCTTCTTGATTACCCAAATGG
CCCGAGTTGTGAAGGAAGTCCATGCCTCTAAAATTATTCATGGAGATATCAAACC
GGATAATTTTATGATCACCAGAAAgtatgggaaaacatttgttaattttagacgttatctttttcagGATCGA
TGATAAATGGGGCAAAGATGCTCTGATGAGTAACGACAGCTTTGTCATCAAGATT
ATCGACTGGGGACGTGCCATTGACATGATGCCACTGAAGAACCAGCGT

was mutated to:

GTAACCGATGATCAAAGGACAGTAGCTGTGCGCTACGAGGTGCCATCATGTTCGT
GGGAAGTGTACATTTGCGACCAAATGCGGAATCGCCTGAAAGATCGAGGTTTGG
AGCTGATGGCCAAATGTTGCATTATGGAAGTGATGGATGCTTATGTTTATTCAAC
TGCTTCGCTTCTTGTTAATCAGTACCACGAATATGGAACGCTGCTTGAATATGCG
AATAACATGAAGGATCCGAATTGGCACATAACCTGCTTCTTGATTACCCAAATGG
CCCGAGTTGTGAAGGAAGTCCATGCCTCTAAAATTATTCATGGAGATATCAAACC
GGATAATTTTATGATCACCAGAAAgtatgggaaaacatttgttaattttagacgttatctttttcagGATCGA
TGATAAATGGGGCAAAGATGCTCTGATGAGTAACGACAGCTTTGTCATCAAGATT
ATCAATTGGGGACGTGCGATTGACATGATGCCACTGAAGAACCAGCGT

The introduced changes are shown in red and synonymous mutations are shown in cyan.

bub-1^{L282A,V285A}

The wild type sequence:

AACGCCAATCTAAATCCTAGAAGACGTCATCTTTCACCAGTCAGTGAGAAAACGG
TTGATGATGAGGAGGAAAAG

bioRxiv preprint doi: https://doi.org/10.1101/2020.06.12.148254; this version posted November 30, 2020. The copyright holder for this preprint (which was not certified by peer review) is the author/funder, who has granted bioRxiv a license to display the preprint in perpetuity. It is made available under aCC-BY-NC 4.0 International license.

was mutated to:

AACGCCAATCTAAATCCTAGAAGACGTCATGCATCACCAGCTAGCGAGAAAACG GTTGATGATGAGGAGGAAAAG

The introduced changes are shown in red and synonymous mutations are shown in cyan. See Supplementary Table 3 for the primer sequences used for genotyping.

Live imaging of oocytes

A detailed protocol for live imaging of *C. elegans* oocytes was used with minor modifications (Laband et al., 2018). Fertilized oocytes were dissected and mounted in 5 µl of L-15 blastomere culture medium (0.5 mg/mL Inulin; 25 mM HEPES, pH 7.5 in 60% Leibowitz L-15 medium and 20% heat-Inactivated FBS) on 24×40 mm #1.5 coverslips. Once dissection was performed and early oocytes identified using a stereomicroscope, a circle of Vaseline was laid around the sample, and a custom-made 24×40 mm plastic holder (with a centred window) was placed on top. The sample was imaged immediately. Live imaging was done using a 60X/NA 1.4 oil objective on a spinning disk confocal microscope (MAG Biosystems) mounted on a microscope (IX81; Olympus), an EMCCD Cascade II camera (Photometrics), spinning-disk head (CSU-X1; Yokogawa Electric Corporation). Acquisition parameters were controlled by MetaMorph 7 software (Molecular Devices). Images were acquired every 20 seconds (with the exception of Figures 1B, 3C, and S1A, where a 30-second interval was used). For all live imaging experiments, partial max-intensity projections are presented in the figures and full max-intensity projections are presented in the supplementary movies. All files were stored, classified, and managed using OMERO (Allan et al., 2012). Figures were prepared using OMERO.figure and assembled using Adobe Illustrator. Representative movies shown in Supplementary material were assembled using custom-made macros in Fiji/ImageJ (Schindelin et al., 2012).

bioRxiv preprint doi: https://doi.org/10.1101/2020.06.12.148254; this version posted November 30, 2020. The copyright holder for this preprint (which was not certified by peer review) is the author/funder, who has granted bioRxiv a license to display the preprint in perpetuity. It is made available under aCC-BY-NC 4.0 International license.

Generation of phospho-Ser 283 BUB-1 antibody.

The antibody was generated by Moravian Biotec by immunising rabbits with the following peptide: RRRHL(pS)PVSEKTC. Serum was adsorbed with a non-phosphorylated peptide (RRRHLSPVSEKTC) followed by affinity purification with the antigenic, phosphorylated peptide. Different fractions were tested in immunofluorescence by incubating different dilutions (1:1,000 & 1:10,000) with 1 µM and 10 µM of either non-phosphorylated or phosphorylated peptide. Only the phosphorylated peptide compited out the signal. Additionally, we used the BUB-1^{S283A} strain and no antibody signal was detected.

Immunofluorescence

Worms were placed on 4 µl of M9 worm buffer in a poly-D-lysine (Sigma, P1024)-coated slide and a 24×24-cm coverslip was gently laid on top. Once the worms extruded the embryos, slides were placed on a metal block on dry ice for >10 min. The coverslip was then flicked off with a scalpel blade, and the samples were fixed in methanol at 20°C for 30 min. After blocking in PBS buffer plus 3% BSA and 0.1% Triton X-100 (AbDil), samples were incubated overnight at 4°C with anti-BUB-1 (Desai et al., 2003) and anti-tubulin (1/400, clone DM1α, Sigma Aldrich) in AbDil. After three washes with PBS plus 0.1% Tween, secondary antibodies were added at 1/1000 (goat anti-mouse and goat anti-rabbit conjugated to Alexa Fluor™ 488, Alexa Fluor™ 594, Thermo Scientific). After two hours at room temperature and three washes with PBS plus 0.1% Tween, embryos were mounted in ProLong Diamond antifade mountant with DAPI (Thermo Scientific).

For the comparisson of total versus phospho-Ser 283 BUB-1, a total BUB-1 antibody was labelled with Alexa-488 while phospho-Ser 283 BUB-1 was labelled with Alexa 647, using the APEX™ Alexa Fluor™ Antibody Labelling kits (Thermo). We used the strain HY604, which is a temperature-sensitive allele of the the APC component MAT-1, that arrests in meiosis I prior to spindle rotation when moved to the restrictive temperature.

bioRxiv preprint doi: https://doi.org/10.1101/2020.06.12.148254; this version posted November 30, 2020. The copyright holder for this preprint (which was not certified by peer review) is the author/funder, who has granted bioRxiv a license to display the preprint in perpetuity. It is made available under aCC-BY-NC 4.0 International license.

GFP immunoprecipitation

For GFP immunoprecipitations, we followed a published protocol (Sonneville et al., 2017) with minor modifications (Pelisch et al., 2019). Approximately 1000 worms expressing GFP-tagged endogenous BUB-1 were grown for two generations at 20°C in large 15-cm NGM plates with concentrated HT115 bacteria. Worms were bleached and embryos were laid in new 15-cm NGM plates with concentrated HT115 bacteria. Once >80% of the worm population was at the L3/L4 stage, worms were washed and placed on 15-cm agarose plates containing concentrated HT115 bacteria. After 24 hs, worms were bleached and the embryos were resuspended in a lysis buffer containing 100 mM HEPES-KOH pH 7.9, 50 mM potassium acetate, 10 mM magnesium acetate, 2 mM EDTA, 1X Protease inhibitor ULTRA (Roche), 2X PhosSTOP (Roche), and 1 mM DTT. The solution was added drop-wise to liquid nitrogen to generate beads that were later grinded using a SPEX SamplePrep 6780 Freezer/Mill. After thawing, we added one-quarter volume of buffer containing lysis buffer supplemented with 50% glycerol, 300 mM potassium acetate, 0.5% NP40, plus DTT, protease and phosphatase inhibitors as above. DNA was digested with 1,600U of Pierce Universal Nuclease for 30 min on ice. Extracts were centrifuged at 25,000 g for 30 min and then at 100,000 g for 1 h. The extract was then incubated for 60 min with 30 µl of a GFP nanobody covalently coupled to magnetic beads. The beads were washed ten times with 1 ml of wash buffer (100 mM HEPES-KOH pH 7.9, 300 mM potassium acetate, 10 mM magnesium acetate, 2 mM EDTA, 0.1% NP40, plus protease and phosphatase inhibitors) at 4°C (cold room). Bound proteins were eluted twice using two rounds of 50 µl LDS sample buffer (Thermo Scientific) at 70°C for 15 min and stored at −80°C.

Sample preparation for mass spectrometry

bioRxiv preprint doi: https://doi.org/10.1101/2020.06.12.148254; this version posted November 30, 2020. The copyright holder for this preprint (which was not certified by peer review) is the author/funder, who has granted bioRxiv a license to display the preprint in perpetuity. It is made available under aCC-BY-NC 4.0 International license.

IP samples were run onm 4-12% Bis-Tris SDS gels with MOPS running buffer and the gel was stained using Quick Coomassie Stain (Generon). Bands of interest were cut and washed with water:acetonitrile (50:50), followed by a wash with 100 mM ammonium bicarbonate. The gel pieces were then washed with 100 mM ammonium bicarbonate:acetonitrile (50:50), followed by a final wash with acetonitrile. Gel pieces were dried using a SpeedVac. Samples were reduced with 10mM DTT in 20 mM ammonium bicarbonate and alkilated With 50 mM IAA in 20 mM ammonium bicarbonate. Samples were then washed sequentially with 100 mM ammonium bicarbonate, 100 mM ammonium bicarbonate:Acetonitrile (50:50), and acetonitrile. Gel pieces were dried using a SpeedVac.

Trypsin solution (12.5 µg/ml stock in 20 mM ammonium bicarbonate) was added to cover the gel pieces and and incubated for 30 mins on a shaking platform and incubated sample overnight at 30ºC on a shaker. Peptides were extracted by standard procedures and reconstituted in 10 µl of 5% formic acid/10% acetonitrile. After vortexing for 1 min, water was added to 50 µl.

Mass Spectrometry analysis

Samples were run on an Ultimate 3000 RSLCnano system (ThermoFisher Scientific) coupled to a Q-Exactive Plus Mass Spectrometer (Thermo Fisher Scientific). Peptides initially trapped on an Acclaim PepMap 100 (Thermo Fisher Scientific) and then separated on an Easy-Spray PepMap RSLC C18 column (Thermo Fisher Scientific). Sample was transferred to mass spectrometer via an Easy-Spray source with temperature set at 50˚C and a source voltage of 2.1 kV. The mass spectrometer was operated on in data dependent acquisition mode (top 15 method). MS resolution was 70,000 with a mass range of 350 to 1600. MS/MS resolution was 17,500.

bioRxiv preprint doi: https://doi.org/10.1101/2020.06.12.148254; this version posted November 30, 2020. The copyright holder for this preprint (which was not certified by peer review) is the author/funder, who has granted bioRxiv a license to display the preprint in perpetuity. It is made available under aCC-BY-NC 4.0 International license.

.RAW data files were extracted and converted to mascot generic files (.mgf) using MSC Convert. Extracted data then searched against *Caenorhabditis elegans* proteome and BUB-1 specifically, using the Mascot Search Engine (Mascot Daemon Version 2.3.2). Type of search used was MS/MS Ion Search, using Trypsin/P. Carbamidomethyl (C) was set as a fixed modification and variable modifications were as follows: acetyl (N-term), dioxidation (M), Gln to pyro-Glu (N-term Q), Oxidation (M), Deamidation (NQ), and Phosphorylation (STY). Peptide Mass Tolerance was ± 10 ppm (# 13C = 2) with a Fragment Mass Tolerance of ± 0.6 Da. Maximum number of missed cleavages was 2.

Sequence Alignment

All sequence alignments were performed using Clustal Omega (Sievers et al., 2011), version 1.2.4. Full-length mammalian B56α (UniProtKB Q15172), β (UniProtKB Q15173), γ (UniProtKB Q13362), δ (UniProtKB Q14738) and ε (UniProtKB Q16537) alongside their alternative splicing isoforms were retrieved from UniProt (Bateman et.al., 2017) and aligned with full-length *C. elegans* PPTR-1 (UniProtKB O18178) and PPTR-2 (UniProtKB A9UJN4-1). A guide tree was calculated from the distance matrix generated from sequence pairwise scores.

The C-terminal regions of mammalian isoforms B56γ (S378-A393), δ (S454-A469), β (S409-V424), α (S403-V418), ε (S395-V410) and *C. elegans* PPTR-1 (S420-V435) and PPTR-2 (S449-A464) were used for the alignment. The canonical sequences of each B56 isoform were retrieved from UniProt (UniProt, 2019).

The short linear motifs (SLiMs) of *C. elegans* BUB-1 (R279-D292;UniProtKB Q21776), human BubR1 (I666-A679;UniProtKB O60566-1) and RepoMan (K587-P600; UniProtKB

bioRxiv preprint doi: https://doi.org/10.1101/2020.06.12.148254; this version posted November 30, 2020. The copyright holder for this preprint (which was not certified by peer review) is the author/funder, who has granted bioRxiv a license to display the preprint in perpetuity. It is made available under aCC-BY-NC 4.0 International license.

Q69YH5-1) were aligned with Clustal Omega (Sievers et al., 2011) and visualised with Jalview (Waterhouse et al., 2009).

Kinase assays

Forty µl reactions were set up containing 40 mM Tris-HCl pH 7.5, 100 µM ATP, 10 mM $MgCl_2$, and 2 µg of either BUB-1 (259-332) or H1. At t=0, 15 ng/µl Cdk1/Cyclin B was added, before incubation at 30ºC for 30 min. Aliquots were taken immediately after Cdk1/CyclinB addition at t=0 and then again after the 30 min incubation. All samples were then incubated at 70ºC for 15 mins in a final concentration of 1X LDS buffer. SDS-PAGE was then conducted on a NuPage 4-12% Bis-Tris gel (Thermo) with MES buffer before being stained with ProQ Diamond (Thermo) and imaged using Bio-Rad ChemiDoc. Once fluorescence was recorded, Coomassie staining was performed. For the western blot, SDS-PAGE was conducted as above with 67 ng of substrate protein per well before the western was conducted using a nitrocellulose membrane (GE healthcare) and 1X NuPage transfer buffer (Thermo). The membrane was blocked using Intercept PBS blocking buffer (LI-COR), the primary antibodies used were anti-GST at 1:1,000 (made in sheep), and anti- phospho-Ser 283 1:20,000 (made in rabbit). Secondary antibodies were anti-sheep IRDye 680RD anti-rabbit 800CW (LI-COR),both at 1:50,000. The membrane was then imaged using LI-COR Odyssey CLx.

Expression and purification of PPTR-2

PPTR-2 was expressed from pHISTEV30a vector as a 6xHis- and Strep-tagged protein (plasmid fgp_445) in E. coli strain BL21 (DE3) and the bacterial culture was incubated overnight at 37ºC with shaking at 220 rpm. Bacteria were grown in TB medium at 37°C with shaking at 220 rpm until OD600 reached ~0.6 -0.8 and induced with 150 µM IPTG. Induction

bioRxiv preprint doi: https://doi.org/10.1101/2020.06.12.148254; this version posted November 30, 2020. The copyright holder for this preprint (which was not certified by peer review) is the author/funder, who has granted bioRxiv a license to display the preprint in perpetuity. It is made available under aCC-BY-NC 4.0 International license.

was performed at 18°C with shaking at 220 rpm for ~16 hours. Cells were pelleted and lysed by sonication in 50 mM NaP, 300 mM NaCl, 10 mM imidazole, 10% Glycerol, 0.5 mM TCEP, and protease inhibitors. After binding to a Ni-NTA column, protein was washed with 20 mM imidazole and then eluted with 350 mM imidazole. The tag was cleaved with 6xHis-tagged TEV protease overnight at 4°C and the tag and protease were removed from the sample by binding to Ni-NTA. PPTR-2 was concentrated and further purified using a HiLoad 16/600 Superdex 200 pg size exclusion column.

Fluorescence Polarisation

The following peptides were synthesised by peptides&elephants GmbH: BUB-1 FITC-Ahx-NPRRRHLSPVSEKTVDDEEE, pBUB-1 FITC-Ahx-NPRRRHLphSPVSEKTVDDEEE, and LAVA FITC-Ahx-NPRRRHASPASEKTVDDEEE. Reactions (35 µl) were set up in FP buffer (50 mM NaP pH 7.5, 150 mM NaCl, 0.5 mM TCEP) containing peptide concentrations of 1 µM. These were then used to create a 1:2 serial dilution series using FP buffer containing the same peptide concentrations as above as well as ~208 µM PPTR-2. The reactions were left for 30 min before triplicates of each dilution were aliquoted into a black 384-well plate, centrifuged (2 min, 2000 rpm), and analysed using the PheraStar FS.

Image analysis and Statistics

For time-dependent analysis, metaphase I was taken as time = 0 seconds. This frame was chosen as the previous frame where the first indication of chromosome separation was visible. All image analysis was done in Fiji (Schindelin et al., 2012). For total intensity measurements within the meiotic spindle, images were thresholded and binary images were generated using the ReinyEntropy method and used to automatically generate the regions of interest (ROIs) for each slice (z) and time point (t) or in the sum-projected image. Going through all the slices

bioRxiv preprint doi: https://doi.org/10.1101/2020.06.12.148254; this version posted November 30, 2020. The copyright holder for this preprint (which was not certified by peer review) is the author/funder, who has granted bioRxiv a license to display the preprint in perpetuity. It is made available under aCC-BY-NC 4.0 International license.

was particularly necessary when measuring protein intensity associated with a specific structure/location, since the angle of the spindle can lead to erroneous analysis. All ROIs were recorded and, in order to get background measurements, the ROIs were automatically placed on a different oocyte region, away from the spindle. Background-substracted intensity values were then normalised to the maximum intensity value of the control movie using Graphpad Prism 7.0 and are presented as mean ± s.e.m.

Central spindle to chromosome ratio for PPTR-2::GFP (Figure 4G) were obtained as follows. Images were selected at early anaphase (t = 40 sec) and to obtain the chromosome ROIs, we used the mCherry::histone channel to create a mask. These ROIs were transferred to the PPTR-2::GFP channel and the intensity was measured as above. The region between the chromosomes was selected intensities were measured to obtain the central spindle intensity. Background corrected values were used to obtain the ratio central spindle/chromosome. Results are shown as median with interquartile range and differences were analysed using an unpaired two-tailed t-test with Welch's correction.

For the alignment/congression analysis, we selected movies in which the spindles were contained in a single Z-plane at -80 sec. There, we established the spindle axes with a line extending from pole to pole and the 'metaphase plate' with a perpendicular line in the middle of the spindle (See Figure S5). A line was drawn on the long axes of the bivalents and the angle between this line and the spindle axis was measured ('θ'). Additionally, for each bivalent, the distance ('d') between the center of the bivalent and the metaphase plate was measured.

bioRxiv preprint doi: https://doi.org/10.1101/2020.06.12.148254; this version posted November 30, 2020. The copyright holder for this preprint (which was not certified by peer review) is the author/funder, who has granted bioRxiv a license to display the preprint in perpetuity. It is made available under aCC-BY-NC 4.0 International license.

Contingency tables were analysed using the Fisher's exact test (two-tailed) and the P values are presented in the figures and/or in the text.

Generation of Supplementary movies

The 4D TIFF files were converted to movie (.avi) files using a custom-made macro that uses the StackReg Fiji plugin for image registration. Movies were assembled using max intensity projections hence the movies might not match a specific panel within the main figures, which are single slices or partial projections in order to highlight specific characteristics.

Bel Borja et al. Figure 1

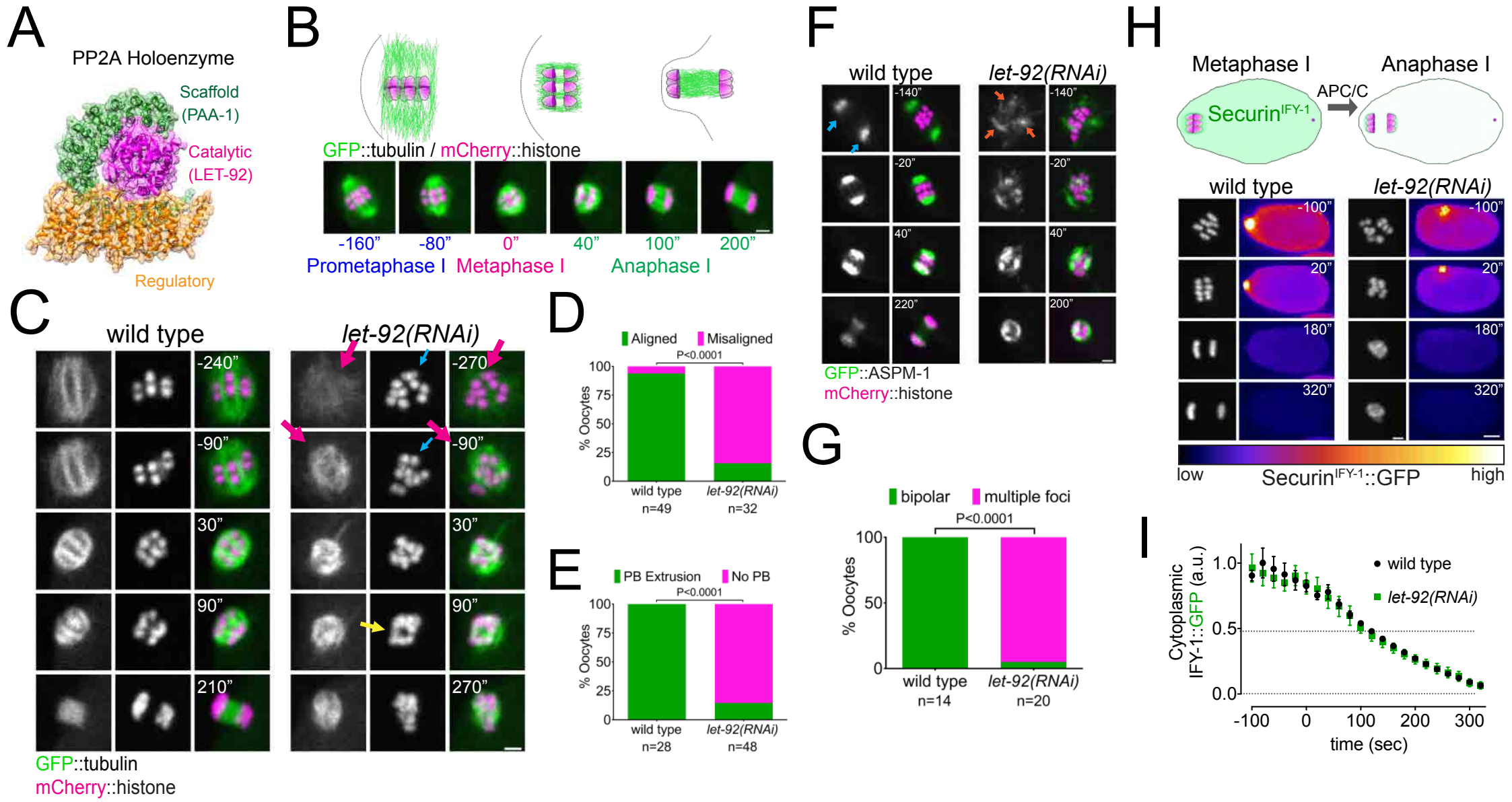

bioRxiv preprint doi: https://doi.org/10.1101/2020.06.12.148254; this version posted November 30, 2020. The copyright holder for this preprint (which was not certified by peer review) is the author/funder, who has granted bioRxiv a license to display the preprint in perpetuity. It is made available under aCC-BY-NC 4.0 International license.

Figure 1. PP2A is essential for Meiosis I in *C. elegans* oocytes.

A. Schematic of the PP2A heterotrimer highlighting the single catalytic and scaffold subunits in *C. elegans* (LET-92 and PAA-1, respectively). The schematic was generated from the PDB structure 2npp (Xu et al., 2006).

B. Schematic of the timescales used throughout the paper. Metaphase I was defined as time zero and chosen as the frame prior to the one where chromosome separation was detected.

C. Microtubule and chromosome dynamics were followed in wild type and *let-92(RNAi)* oocytes expressing GFP::tubulin and mCherry::histone. Magenta arrows point to defective spindle structure; the cyan arrow points to misaligned chromosomes; the yellow arrow shows an apparent separation between chromosome masses. Inset numbers represent the time relative to metaphaseI in seconds. Scale bar, 2 µm. See Supp. Movie 1.

D. The number of oocytes with misaligned chromosomes in metaphase I was compared between wild type and *let-92(RNAi)* oocytes and the percentage is represented ($P<0.0001$, Fisher's exact test). The number of oocytes analysed (n) is shown.

E. The number of oocytes with an extruded polar body (PB) after meiosis I in wild type and *let-92(RNAi)* oocytes was analysed and the percentage is represented ($P<0.0001$, Fisher's exact test). The number of oocytes analysed (n) is shown.

F. ASPM-1 and chromosome dynamics were followed in wild type and *let-92 (RNAi)* oocytes expressing GFP::ASPM-1 and mCherry::histone. Inset numbers represent the time relative to metaphase I in seconds. Cyan arrows point to spindle poles whereas orange arrows highlight the unfocused ASPM-1 cumuli. Scale bar, 2 µm. See Supp. Movie 2.

G. The number of oocytes with defective spindle at prometaphase I in wild type and *let-92(RNAi)* oocytes was analysed and the percentage is represented ($P<0.0001$, Fisher's exact test). The number of oocytes analysed (n) is shown.

bioRxiv preprint doi: https://doi.org/10.1101/2020.06.12.148254; this version posted November 30, 2020. The copyright holder for this preprint (which was not certified by peer review) is the author/funder, who has granted bioRxiv a license to display the preprint in perpetuity. It is made available under aCC-BY-NC 4.0 International license.

H. Securin^{IFY-1} degradation was used as a proxy for anaphase progression and followed in wild type and *let-92(RNAi)* oocytes. Greyscale images of the chromosomes are shown as well as whole oocyte images using the 'fire' LUT. The intensity scale is shown in the bottom. Inset numbers represent the time relative to metaphaseI in seconds. Scale bar, 2 µm. See Supp. Movie 3.

I. Cytoplasmic Securin^{IFY-1} levels were measured throughout meiosis I and the mean ± s.e.m is shown in the graph.

Bel Borja et al. Figure 2

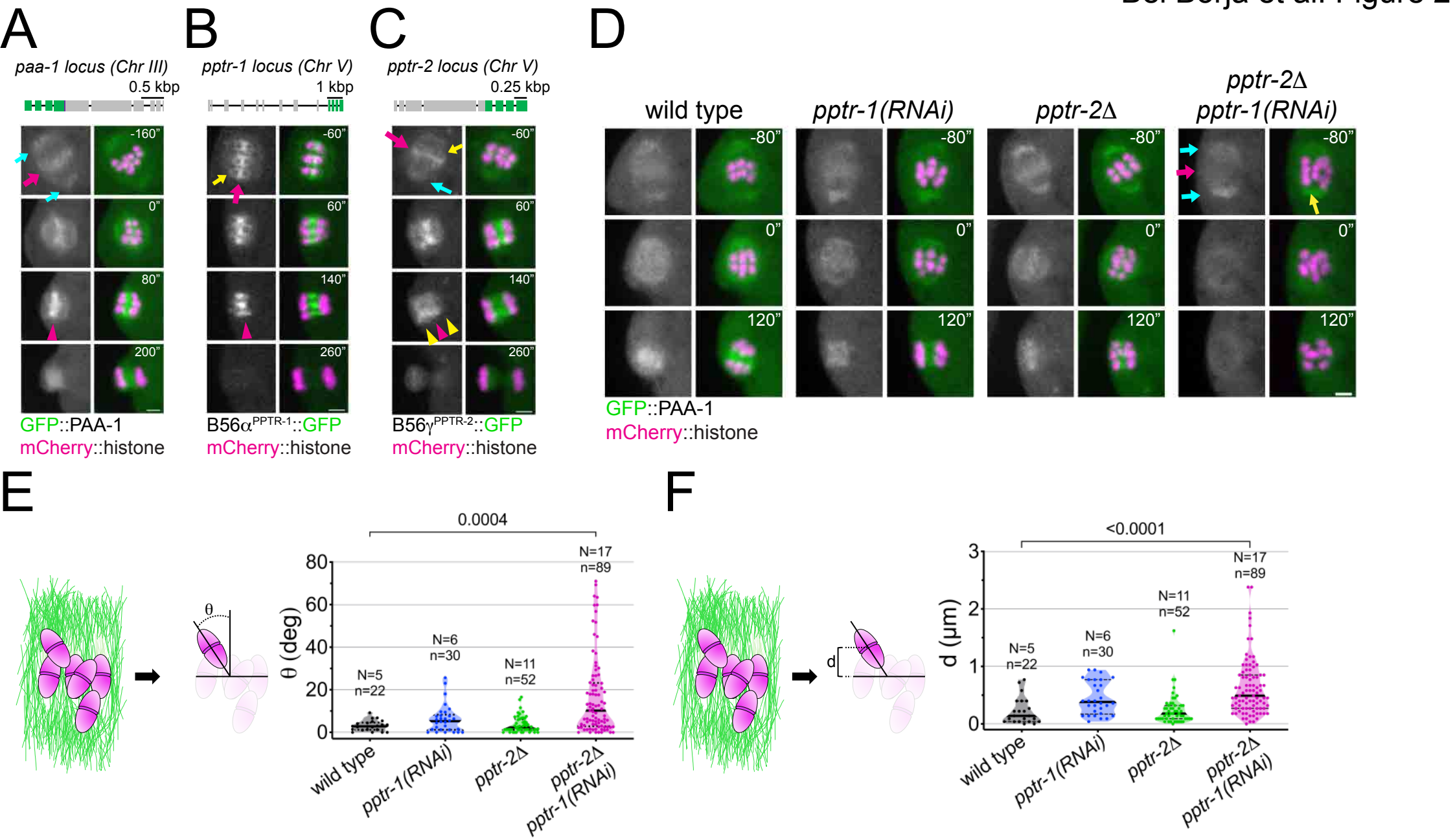

bioRxiv preprint doi: https://doi.org/10.1101/2020.06.12.148254; this version posted November 30, 2020. The copyright holder for this preprint (which was not certified by peer review) is the author/funder, who has granted bioRxiv a license to display the preprint in perpetuity. It is made available under aCC-BY-NC 4.0 International license.

Figure 2. *C. elegans* B56 regulatory subunits PPTR-1 and PPTR-2 are required for normal Meiosis I.

A. Top**,** Schematic of the *paa-1* gene structure and its tagging with *gfp*. Bottom, the PP2A scaffold subunit GFP::PAA-1 was followed throughout meiosis I in a dissected oocyte. Magenta arrows point to the midbivalent; cyan arrows point to spindle poles and magenta arrowhead highlights the central-spindle localisation. Inset numbers represent the time relative to metaphaseI in seconds. Scale bar, 2 µm. See Supp. Movie 5.

B. Top, Schematic of the *pptr-1* gene structure and its tagging with *gfp*. Bottom, PPTR-1 and chromosome dynamics were followed in oocytes expressing PPTR-1::GFP and mCherry::histone. The magenta arrow points to the midbivalent and the yellow arrow points to the kinetochore. Magenta arrowhead highlights the central-spindle localisation. Inset numbers represent the time relative to metaphaseI in seconds. Scale bar, 2 µm. See Supp. Movie 6.

C. Top, Schematic of the *pptr-2* gene structure and its tagging with *gfp*. Bottom, PPTR-2 and chromosome dynamics were followed in oocytes expressing PPTR-2::GFP and mCherry::histone. The magenta arrow points to the midbivalent, the yellow arrow points to the kinetochore, and the cyan arrow to the spindle pole. Inset numbers represent the time relative to metaphaseI in seconds. Scale bar, 2 µm. Magenta arrowhead highlights the central-spindle localisation and yellow arrowhead highlights the chromosome-associated signal. See Supp. Movie 7.

D. PAA-1 and chromosome dynamics were followed in wild type, *pptr-1(RNAi)*, *pptr-2Δ,* and *pptr-2Δ+pptr-1(RNAi)* oocytes expressing GFP::PAA-1 and mCherry::histone. Magenta arrows point to the absence of GFP signal on prometaphase chromosomes and the cyan arrows point to spindle poles. The yellow arrows highlights one misaligned bivalent. Inset

bioRxiv preprint doi: https://doi.org/10.1101/2020.06.12.148254; this version posted November 30, 2020. The copyright holder for this preprint (which was not certified by peer review) is the author/funder, who has granted bioRxiv a license to display the preprint in perpetuity. It is made available under aCC-BY-NC 4.0 International license.

numbers represent the time relative to metaphaseI in seconds. Scale bar, 2 µm. See Supp. Movie 8.

E. On the left, the schematic depicts how angles were measured relative to the spindle pole-to-pole axis. On the right, the angle of bivalents at 80 seconds before metaphase I in wild type, *pptr-1(RNAi)*, *pptr-2Δ* and *pptr-2Δ+pptr-1(RNAi)* oocytes. Violin plot includes each data point (chromosome), the median (straight black line), and the interquartile range (dashed black lines). N respresents number of oocytes and n number of bivalents measured. P values shown in the figure were obtained using a Kruskal-Wallis test.

F. On the left, the schematic depicts how distances were measured relative to the centre of the spindle. On the right, the distance of bivalents 80 seconds before metaphase I was measured in wild type, *pptr-1(RNAi)*, *pptr-2Δ* and *pptr-2Δ+pptr-1(RNAi)* oocytes. Violin plot includes each data point (chromosome), the median (straight black line), and the interquartile range (dashed black lines). N respresents number of oocytes and n number of bivalents measured. P values shown in the figure were obtained using a Kruskal-Wallis test.

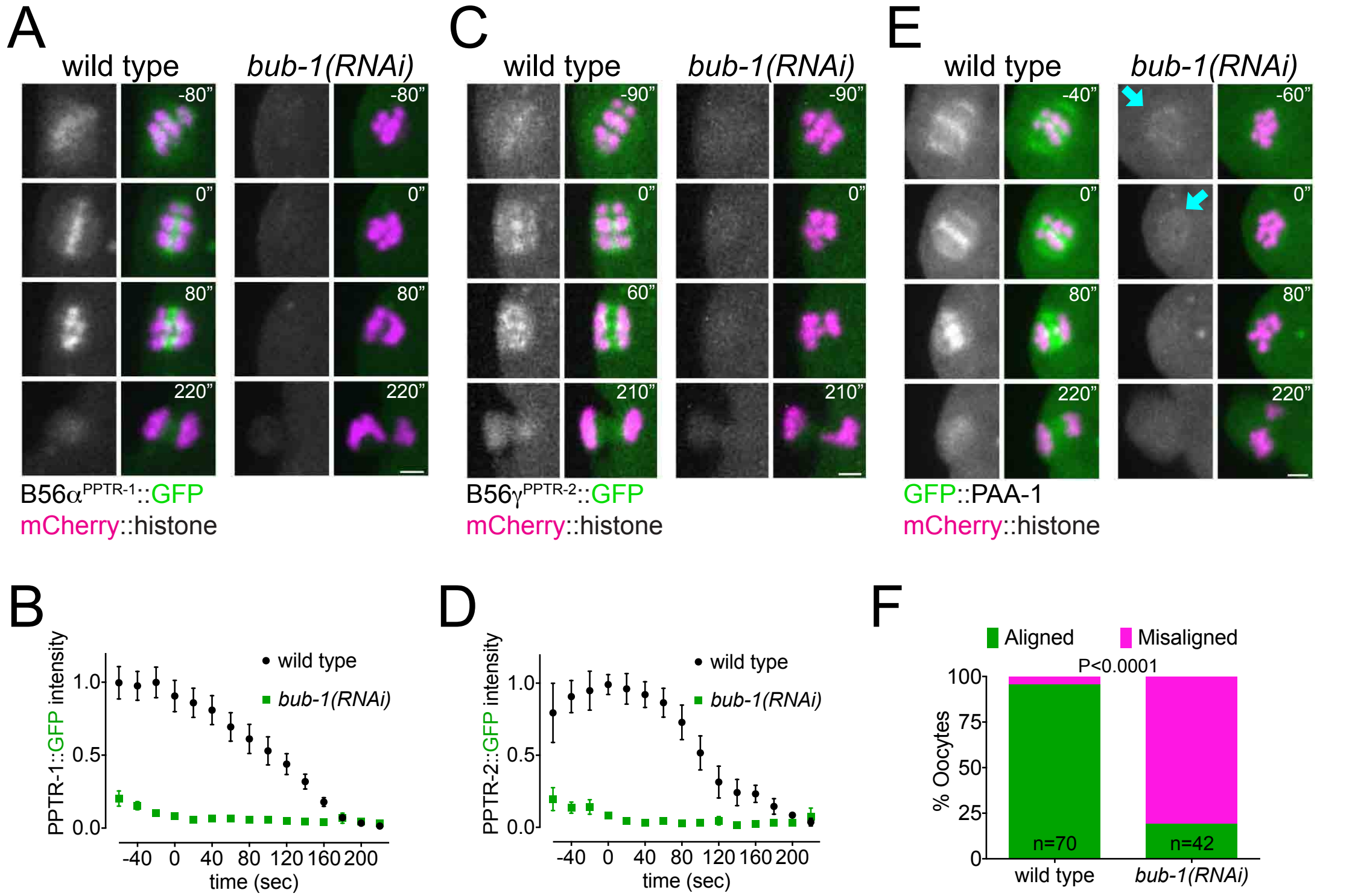
A
wild type
bub-1(RNAi)
-80”
0”
80”
220”
B56αPPTR-1::GFP
mCherry::histone
C
wild type
bub-1(RNAi)
-90”
0”
60”
210”
B56γPPTR-2::GFP
mCherry::histone
E
wild type
bub-1(RNAi)
-40”
-60”
0”
80”
220”
GFP::PAA-1
mCherry::histone
B
PPTR-1::GFP intensity
1.0
0.5
0.0
wild type
bub-1(RNAi)
-40 0 40 80 120 160 200
time (sec)
D
PPTR-2::GFP intensity
1.0
0.5
0.0
wild type
bub-1(RNAi)
-40 0 40 80 120 160 200
time (sec)
F
Aligned
Misaligned
P<0.0001
% Oocytes
100
75
50
25
0
n=70
n=42
wild type
bub-1(RNAi)

bioRxiv preprint doi: https://doi.org/10.1101/2020.06.12.148254; this version posted November 30, 2020. The copyright holder for this preprint (which was not certified by peer review) is the author/funder, who has granted bioRxiv a license to display the preprint in perpetuity. It is made available under aCC-BY-NC 4.0 International license.

Figure 3. BUB-1 recruits B56α^{PPTR-1} and B56γ^{PPTR-2} during oocyte meiosis.

A. B56α^{PPTR-1} and chromosome dynamics were followed in wild type and *bub-1(RNAi)* oocytes expressing PPTR-1::GFP and mCherry::histone. Scale bar, 2 µm. See Supp. Movie 9.

B. PPTR-1::GFP levels were measured in wild type and *bub-1(RNAi)* oocytes throughout meiosis I and the mean ± s.e.m is shown in the graph.

C. B56γ^{PPTR-2} and chromosome dynamics were followed in wild type and *bub-1(RNAi)* oocytes expressing PPTR-2::GFP and mCherry::histone. Scale bar, 2 µm. See Supp. Movie 10.

D. PPTR-2::GFP levels were measured in wild type and *bub-1(RNAi)* oocytes throughout meiosis I and the mean ± s.e.m is shown in the graph.

E. Scaffold subunit PAA-1 and chromosome dynamics were followed in wild type and *bub-1(RNAi)* oocytes expressing GFP::PAA-1 and mCherry::histone. cyan arrows highlight the GFP::PAA-1 remaining in *bub-1(RNAi)* oocytes. Scale bar, 2 µm. See Supp. Movie 11.

F. The number of oocytes with misaligned chromosomes at metaphaseI in wild type and *bub-1(RNAi)* oocytes was analysed and the percentage is represented ($P<0.0001$, Fisher's exact test).

Bel Borja et al. Figure 4

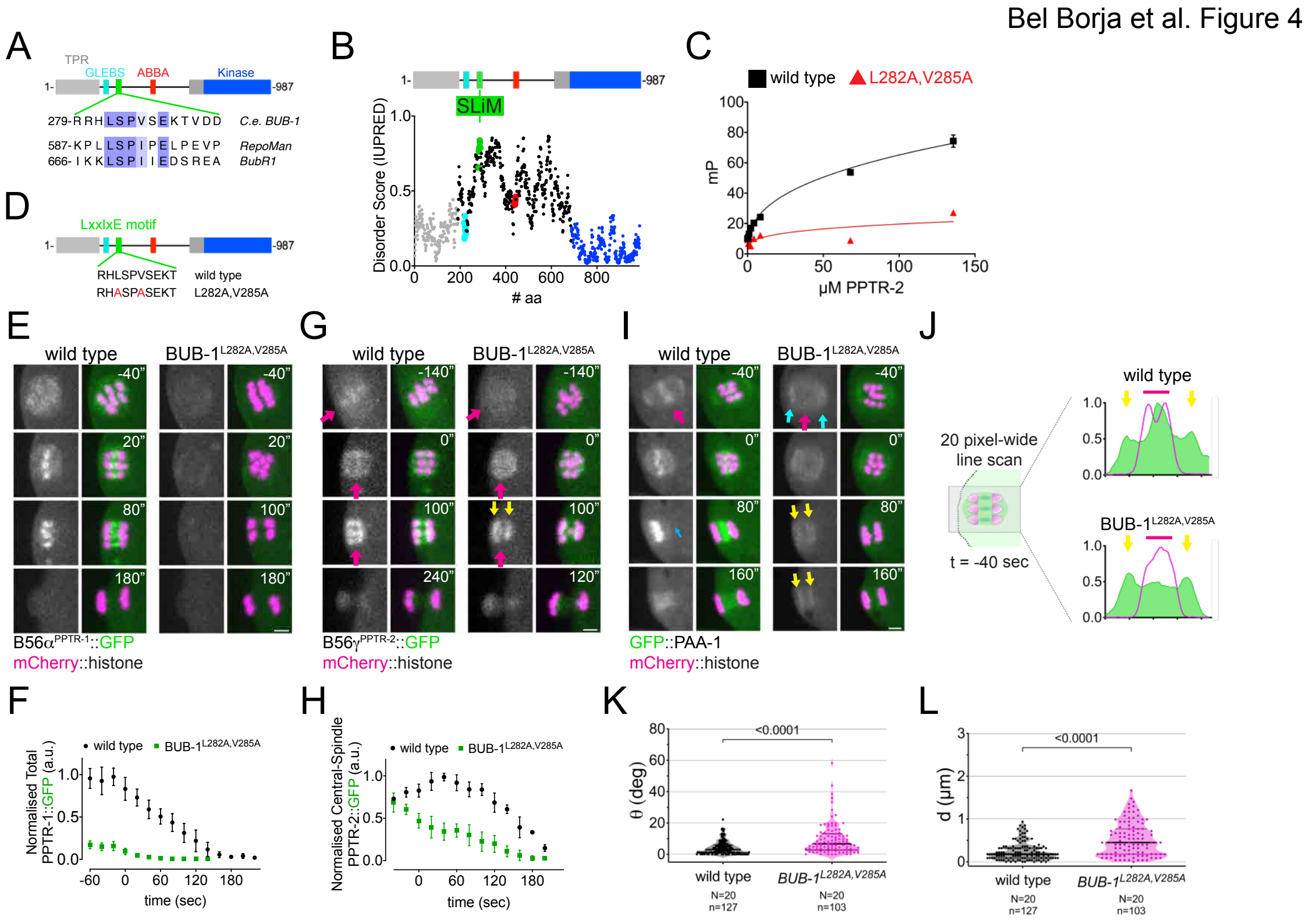

bioRxiv preprint doi: https://doi.org/10.1101/2020.06.12.148254; this version posted November 30, 2020. The copyright holder for this preprint (which was not certified by peer review) is the author/funder, who has granted bioRxiv a license to display the preprint in perpetuity. It is made available under aCC-BY-NC 4.0 International license.

Figure 4. B56α^{PPTR-1} and B56γ^{PPTR-2} are targeted through a LxxIxE motif in BUB-1.

A. *C. elegans* BUB-1 LxxIxE SLiM is shown aligned with BubR1 and Repoman SLiMs. The only change within the LxxIxE sequence itself is the presence of a valine instead of isoleucine, which still fits within the consensus (Wang et al., 2016). The alignment was performed using Clustal Omega and visualised with Jalview (Waterhouse et al., 2009).

B. Disorder prediction of full-length BUB-1 was done using IUPRED2A (Erdős and Dosztányi, 2020). All prevuously characterised BUB-1 domains fall within ordered regions <0.5). The putative SLiM is in a disordered region (IUPRED score ~0.8).

C. PPTR-2 interaction with a LxxIxE motif-containing synthetic peptide was assessed using fluorescence polarisation. Increasing amounts of purified recombinant PPTR-2 were incubated with FITC-labelled wild type or L282A,V285A mutant peptide. The graph was taken from a representative experiment and shows the mean ± s.d. of technical triplicates.

D. Schematic showing the LxxIxE motif in BUB-1 and the BUB-1^{L282A,V285A} mutant.

E. B56α^{PPTR-1} and chromosome dynamics were followed in wild type and in BUB-1^{L282A,V285A} oocytes expressing PPTR-1::GFP and mCherry::histone. Scale bar, 2 µm. See Supp. Movie 13.

F. PPTR-1::GFP levels were measured in wild type and BUB-1^{L282A,V285A} oocytes throughout meiosis I and the mean ± s.e.m is shown in the graph.

G. B56γ^{PPTR-2} and chromosome dynamics were followed in wild type and in BUB-1^{L282A,V285A} oocytes expressing PPTR-2::GFP and mCherry::histone. Magenta arrows point towards prometaphase chromosomes and anaphase central-spindle whereas yellow arrows point towards the chromosome-associated anaphase signal. Scale bar, 2 µm. See Supp. Movie 14.

H. Midbivalent/Central spindle PPTR-2::GFP levels were measured in wild type and BUB-1^{L282A,V285A} oocytes throughout meiosis I and the mean ± s.e.m is shown in the graph.

bioRxiv preprint doi: https://doi.org/10.1101/2020.06.12.148254; this version posted November 30, 2020. The copyright holder for this preprint (which was not certified by peer review) is the author/funder, who has granted bioRxiv a license to display the preprint in perpetuity. It is made available under aCC-BY-NC 4.0 International license.

I. GFP::PAA-1 is present on chromosomes in the BUB-1^{L282A,V285A} mutant. PAA-1 and chromosome dynamics were followed in wild type and in BUB-1^{L282A,V285A} oocytes expressing GFP::PAA-1 and mCherry::histone. Magenta arrows point towards prometaphase chromosomes and anaphase central-spindle whereas yellow arrows point towards the chromosome-associated anaphase signal. Cyan arrows point towards spindle poles. Scale bar, 2 µm. See Supp. Movie 15.

J. Representative, spindle-wide (20 pixels) line profiles are shown for wild type (top) and BUB-1^{L282A,V285A} mutant (bottom) measured in prometaphase I (40 seconds before metaphase I). Green arrows point to the PAA-1 pole signal and blue line to the chromosome associated population.

K. The angle of bivalents 80 seconds before segregation in meiosis I relative to the average angle of the spindle was measured in wild type and in BUB-1^{L282A,V285A} oocytes. Violin plot includes each data point (chromosome), the median (straight black line), and the interquartile range (dashed black lines). N respresents number of oocytes and n number of bivalents measured. P value shown in the figure was obtained using a Mann-Whitney test.

L. Distance of bivalents 80 seconds before segregation in meiosis I relative to the center of the spindle was measured in wild type and in BUB-1^{L282A,V285A} oocytes. Violin plot includes each data point (chromosome), the median (straight black line), and the interquartile range (dashed black lines). N respresents number of oocytes and n number of bivalents measured. P value shown in the figure was obtained using a Mann-Whitney test.

bioRxiv preprint doi: https://doi.org/10.1101/2020.06.12.148254; this version posted November 30, 2020. The copyright holder for this preprint (which was not certified by peer review) is the author/funder, who has granted bioRxiv a license to display the preprint in perpetuity. It is made available under aCC-BY-NC 4.0 International license.

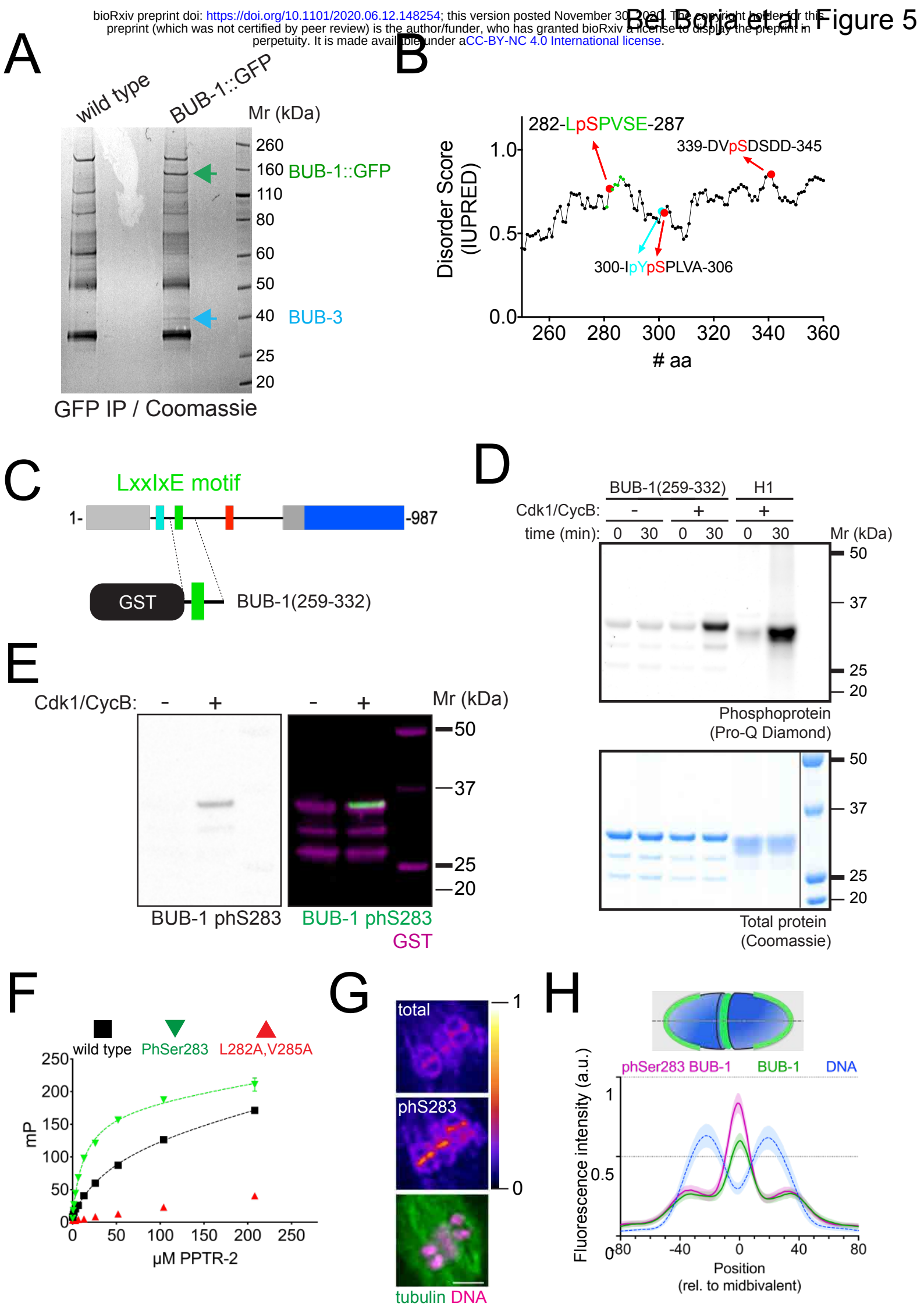

bioRxiv preprint doi: https://doi.org/10.1101/2020.06.12.148254; this version posted November 30, 2020. The copyright holder for this preprint (which was not certified by peer review) is the author/funder, who has granted bioRxiv a license to display the preprint in perpetuity. It is made available under aCC-BY-NC 4.0 International license.

Figure 5. Phosphorylation of Ser 283 within the LxxIxE motif regulates B56 subunit binding.

A. BUB-1::GFP was immunoprecipitated and the eluted proteins were run on SDS-PAGE followed by coomassie staining. The position of BUB-1::GFP and BUB-3 are highlighted with green and blue arrows, respectively. The band corresponding to BUB-1::GFP was further analysed by mass spectrometry to look for phospho-modified peptides.

B. Serine 283 is phosphorylated in vivo. In addition, three other phosphorylation sites were identified within this disordered region.

C. A fragment of BUB-1 (259-332) containing the LxxIxE motif (282-287) was expressed in bacteria fused to a GST tag.

D. GST-BUB-1(259-332) was phosphorylated in vitro using Cdk1/CyclinB ('Cdk1/CycB'). Histone H1 was used as a positive control. Reactions were run on 4-12% SDS-PAGE and subject to phosphoprotein staining (top) followed by total protein staining (bottom).

E. GST-BUB-1(259-332) was phosphorylated in vitro using Cdk1/CyclinB ('Cdk1/CycB') and subject to western blotting using a specific antibody against phosphorylated Serine 283. Anti-GST served as a loading control for the substrate.

F. PPTR-2 interaction with a LxxIxE motif-containing synthetic peptide was assessed using fluorescence polarisation. Increasing amounts of purified recombinant PPTR-2 were incubated with FITC-labelled wild type, Serine 283 phosphorylated, or L282A,V285A mutant peptide. The graph was taken from a representative experiment and shows the mean ± s.d. of technical triplicates.

G. Fixed oocytes were subject to immunofluorescence using labelled BUB-1 ('total'), phospho-Ser283-BUB-1 ('phS283'), and tubulin. Single-channel images for BUB-1 and phospho-Ser283-BUB-1 are shown in 'fire' LUT and the bottom panel shows tubulin (green) and DNA (magenta).

bioRxiv preprint doi: https://doi.org/10.1101/2020.06.12.148254; this version posted November 30, 2020. The copyright holder for this preprint (which was not certified by peer review) is the author/funder, who has granted bioRxiv a license to display the preprint in perpetuity. It is made available under aCC-BY-NC 4.0 International license.

H. Line profile analysis was performed in samples co stained with labelled BUB-1 (Alexa488) and phospho-Ser283-BUB-1 (Alexa647) as described in the methods section. The lines represent the mean and the shaded area represents the s.d. of the indicated number of bivalents.

Bel Borja et al. Figure 6

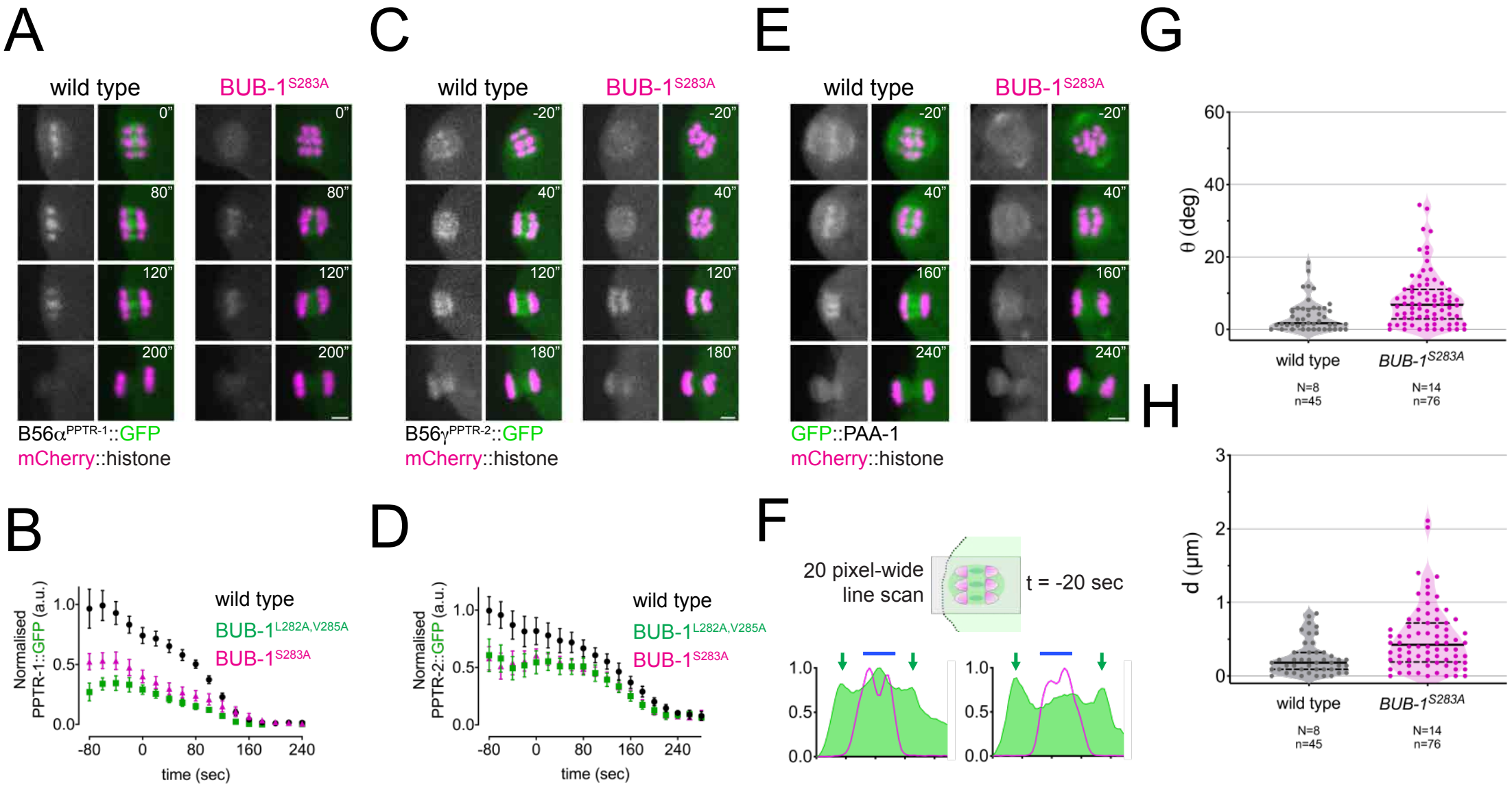

bioRxiv preprint doi: https://doi.org/10.1101/2020.06.12.148254; this version posted November 30, 2020. The copyright holder for this preprint (which was not certified by peer review) is the author/funder, who has granted bioRxiv a license to display the preprint in perpetuity. It is made available under aCC-BY-NC 4.0 International license.

Figure 6. LxxIxE motif phosphorylation regulates the recruitment of B56s subunits in vivo.

A. B56α^{PPTR-1} and chromosome dynamics were followed in wild type and in BUB-1^{S283A} oocytes expressing PPTR-1::GFP and mCherry::histone. Scale bar, 2 µm. See Supp. Movie 16.

B. PPTR-1::GFP levels were measured in wild type, BUB-1^{L282A,V285A} and in BUB-1^{S283A} oocytes throughout meiosis I and the mean ± s.e.m. is shown in the graph.

C. B56γ^{PPTR-2} and chromosome dynamics were followed in wild type and in BUB-1^{S283A} oocytes expressing PPTR-2::GFP and mCherry::histone. Scale bar, 2 µm. See Supp. Movie 17.

D. PPTR-2::GFP levels were measured in wild type, BUB-1^{L282A,V285A} and in BUB-1^{S283A} oocytes throughout meiosis I and the mean ± s.e.m is shown in the graph.

E. GFP::PAA-1 is present on chromosomes in the BUB-1^{S283A} mutant. PAA-1 and chromosome dynamics were followed in wild type and in BUB-1^{S283A} oocytes expressing GFP::PAA-1 and mCherry::histone. Yellow dotted line shows that chromosome associated PAA-1 is lost in the BUB-1^{S283A} mutant. Scale bar, 2 µm. See Supp. Movie 18.

F. Representative, spindle-wide (20 pixels) line profiles are shown for wild type (left) and BUB-1^{S283A} mutant (right) measured in prometaphase I (20 seconds before metaphase I). Green arrows point to the PAA-1 pole signal and blue line to the chromosome associated population.

G. Angle of bivalents 80 seconds before segregation in meiosis I relative to the average angle of the spindle was measured in wild type and in BUB-1^{S283A} oocytes. Violin plot includes each data point (chromosome), the median (straight black line), and the interquartile range (dashed black lines). N respresents number of oocytes and n number of bivalents measured. P value shown in the figure was obtained using a Mann-Whitney test.

bioRxiv preprint doi: https://doi.org/10.1101/2020.06.12.148254; this version posted November 30, 2020. The copyright holder for this preprint (which was not certified by peer review) is the author/funder, who has granted bioRxiv a license to display the preprint in perpetuity. It is made available under aCC-BY-NC 4.0 International license.

I. Distance of bivalents 80 seconds before segregation in meiosis I relative to the center of the spindle was measured in wild type and in BUB-1^{S283A} oocytes. Violin plot includes each data point (chromosome), the median (straight black line), and the interquartile range (dashed black lines). N respresents number of oocytes and n number of bivalents measured. P value shown in the figure was obtained using a Mann-Whitney test.

Bel Borja et al. Figure 7

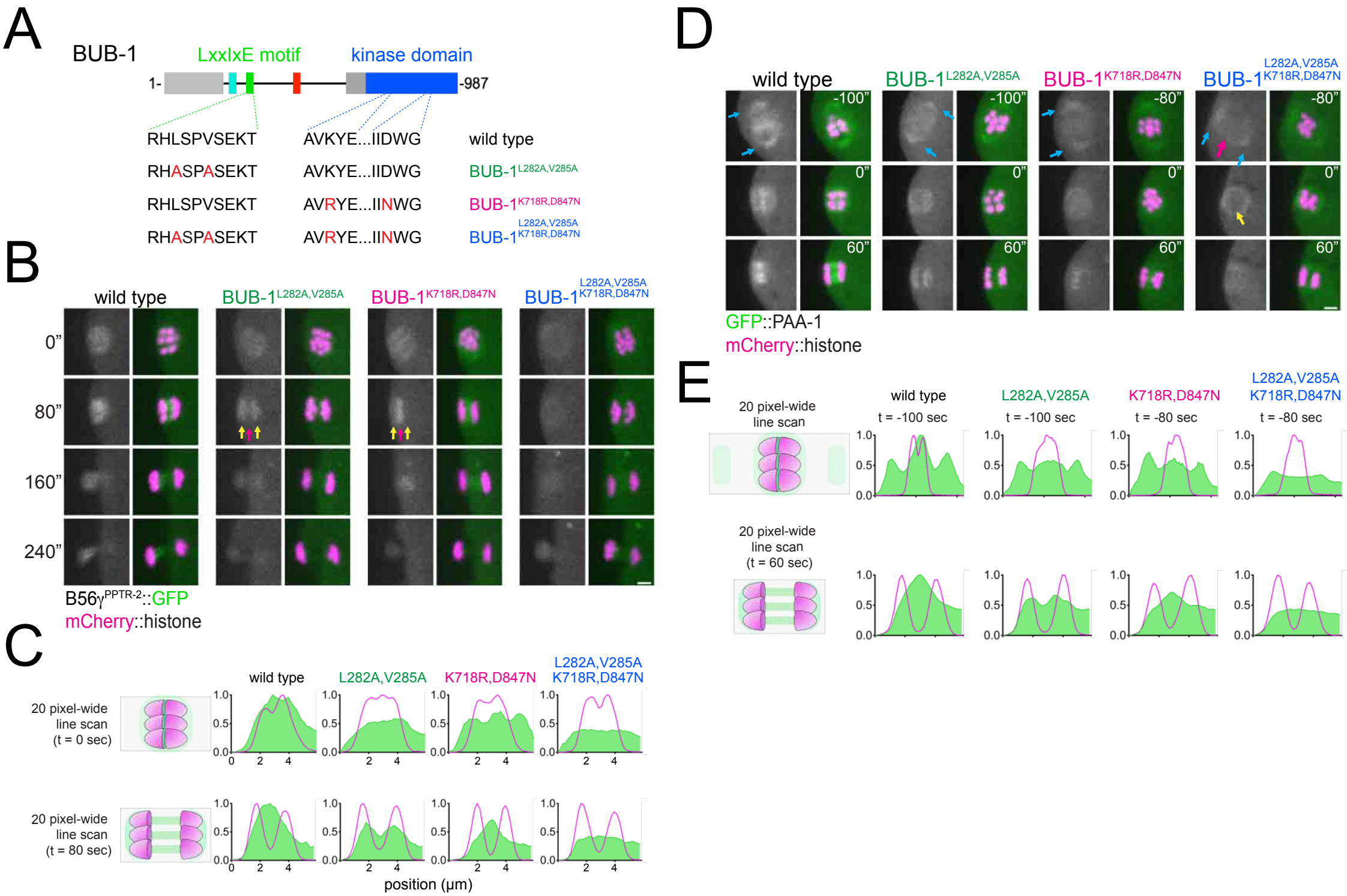

bioRxiv preprint doi: https://doi.org/10.1101/2020.06.12.148254; this version posted November 30, 2020. The copyright holder for this preprint (which was not certified by peer review) is the author/funder, who has granted bioRxiv a license to display the preprint in perpetuity. It is made available under aCC-BY-NC 4.0 International license.

Figure 7. Role of BUB-1 kinase domain in B56γ^{PPTR-2} chromosomal targeting

A. Schematic showing the LxxIxE motif and the kinase domain in BUB-1 of the wild type, the BUB-1^{L282A,V285A}, BUB-1^{K718R,D847N}, and BUB-1$^{L282A,V285A,\ K718R,D847N}$ mutant.

B. B56γ^{PPTR-2} and chromosome dynamics were followed in wild type, the BUB-1^{L282A,V285A}, BUB-1^{K718R,D847N}, and BUB-1$^{L282A,V285A,\ K718R,D847N}$ oocytes expressing PPTR-2::GFP and mCherry::histone. Magenta arrows point towards the central spindle and yellow arrows towards chromosomes. Scale bar, 2 µm. See also Supp. Movie 20.

C. Representative, spindle-wide (20 pixels) line profiles are shown for wild type, the BUB-1^{L282A,V285A}, BUB-1^{K718R,D847N}, and BUB-1$^{L282A,V285A,\ K718R,D847N}$. On top profiles of metaphase plate just in anaphase onset, on the bottom profiles 80 seconds after segregation to show central spindle levels.

D. Scaffolding subunit PAA-1 and chromosome dynamics were followed in wild type, the BUB-1^{L282A,V285A}, BUB-1^{K718R,D847N}, and BUB-1$^{L282A,V285A,\ K718R,D847N}$ oocytes expressing GFP::PAA-1 and mCherry::histone. Cyan arrows point to pole population of PAA-1, magenta arrow signals chromosomes, and yellow arrow highlight the levels of PAA-1 in anaphase onset. Scale bar, 2 µm. See also Supp. Movie 21.

E. Representative, spindle-wide (20 pixels) line profiles are shown for wild type, the BUB-1^{L282A,V285A}, BUB-1^{K718R,D847N}, and BUB-1$^{L282A,V285A,\ K718R,D847N}$. On top profiles before segregation starts (different time points matching the first pannel on Figure 7D) to highlight the PAA-1 in the poles, on the bottom profiles 60 seconds after segregation to show central spindle levels.

	PPTR-1	B56β1	B56ε3	B56α2	PPTR-2	B56δ3	B56γ1
PPTR-1		60.12	71.87	68.30	52.26	60.17	64.48
PPTR-2	52.26	56.36	63.94	60.84		66.19	68.97

Table 1. Sequence identity between full-length mammalian B56 isoforms and *C.elegans* orthologues PPTR-1 and PPTR-2. Table was created using Clustal Omega version 2.1. See Supplementary Table 1 for full Percent Identity Matrix.

Bel Borja et al. Supp. Figure 1

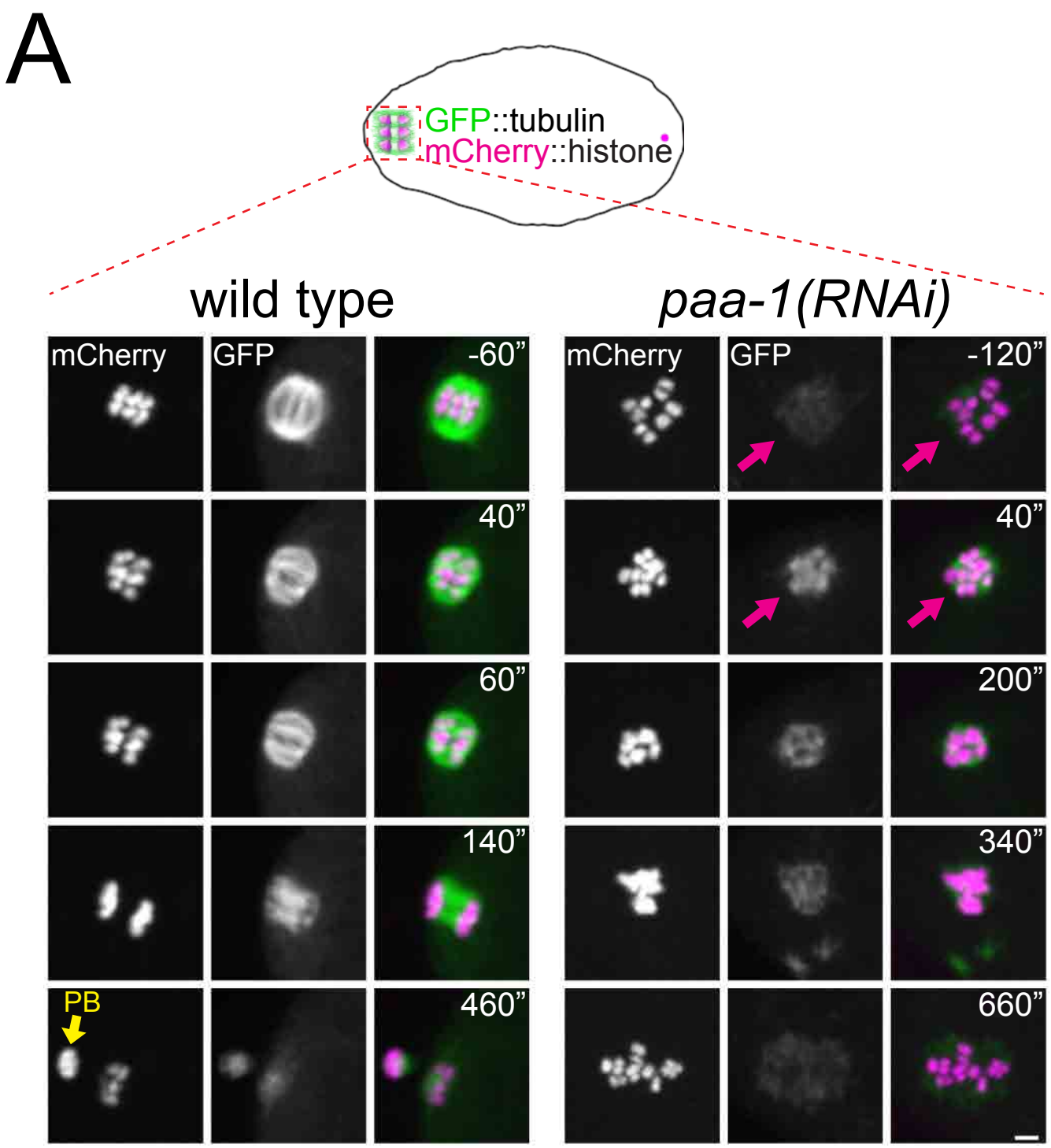

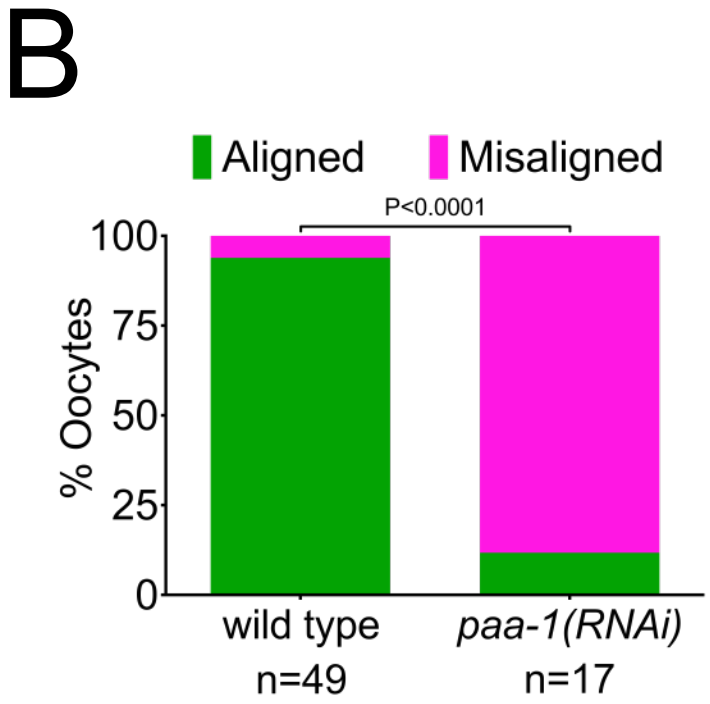

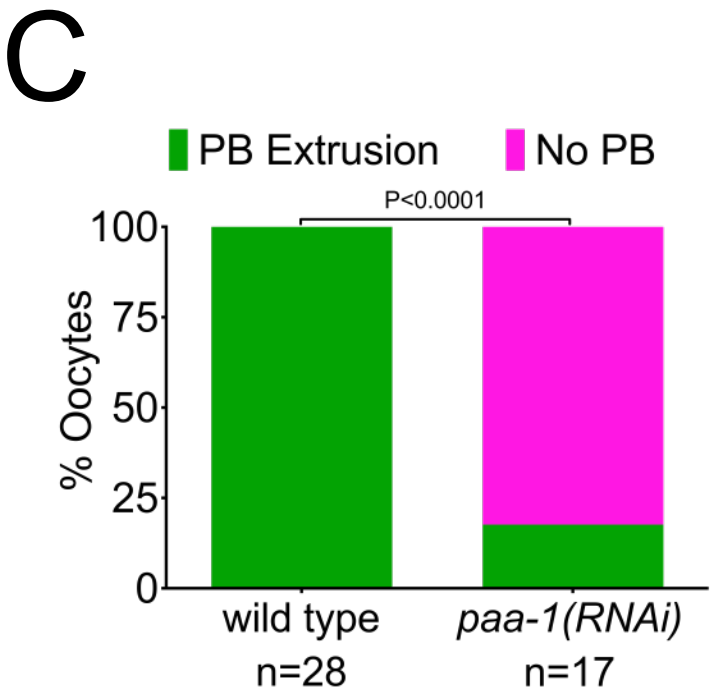

bioRxiv preprint doi: https://doi.org/10.1101/2020.06.12.148254; this version posted November 30, 2020. The copyright holder for this preprint (which was not certified by peer review) is the author/funder, who has granted bioRxiv a license to display the preprint in perpetuity. It is made available under aCC-BY-NC 4.0 International license.

Supplementary Figure 1. PP2A is essential for Meiosis I in *C. elegans* oocytes.

A. Microtubule and chromosome dynamics were followed in wild type and *paa-1(RNAi)* oocytes expressing GFP::tubulin and mCherry::histone. Yellow arrow shows polar body (PB) and magenta arrows point to the lack of a bipolar spindle in *paa-1(RNAi)* oocytes. Inset numbers represent the time relative to metaphase I in seconds. Scale bar, 2 µm.

B. The number of oocytes with misaligned chromosomes at metaphase I in wild type and *paa-1(RNAi)* oocytes was analysed and the percentage is represented ($P<0.0001$, Fisher's exact test).

C. The number of oocytes with an extruded polar body (PB) after meiosis I in wild type and *paa-1(RNAi)* oocytes was analysed and the percentage is represented ($P<0.0001$, Fisher's exact test).

bioRxiv preprint doi: https://doi.org/10.1101/2020.06.12.148254; this version posted November 30, 2020. The copyright holder for this preprint (which was not certified by peer review) is the author/funder, who has granted bioRxiv a license to display the preprint in perpetuity. It is made available under aCC-BY-NC 4.0 International license.

A

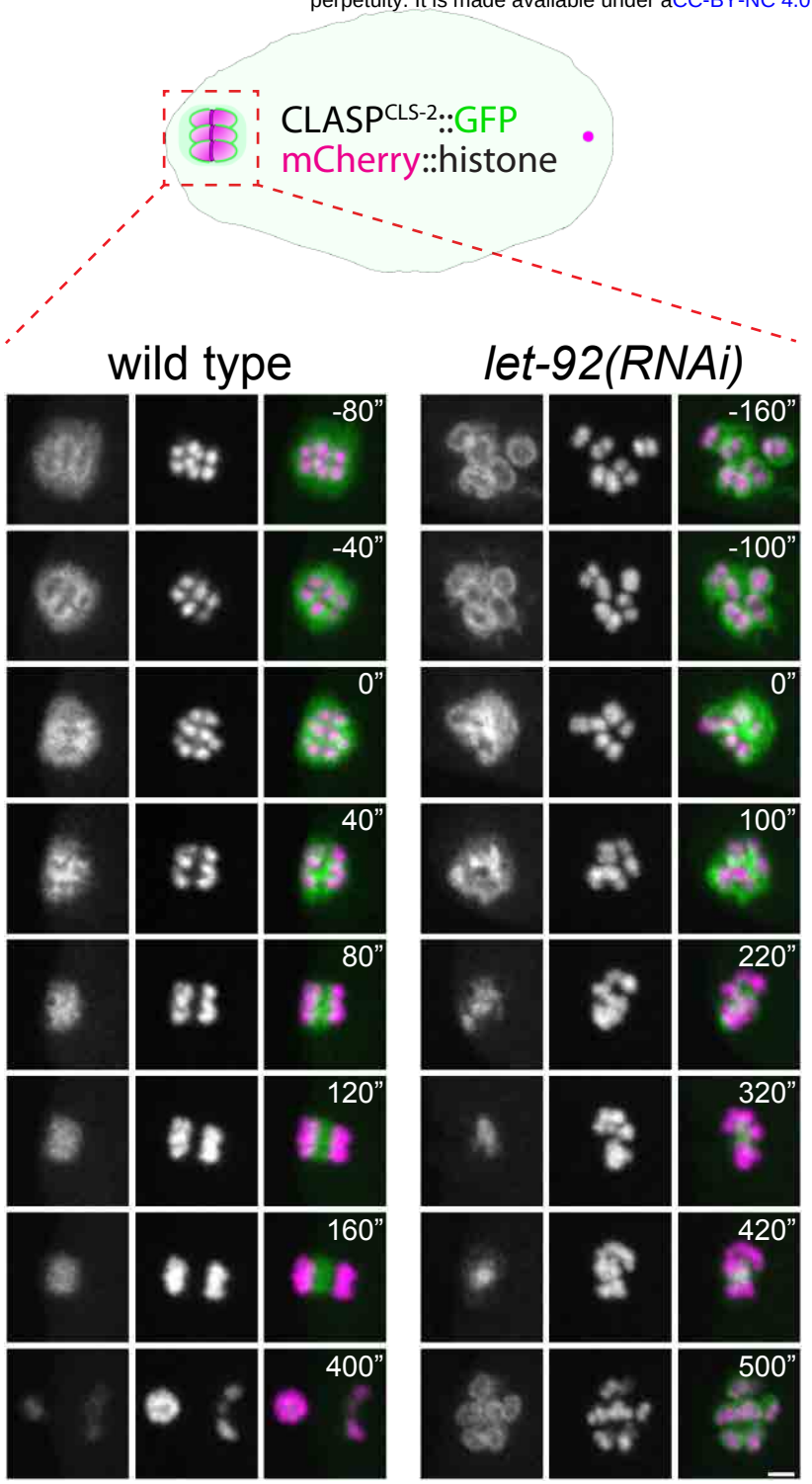

B

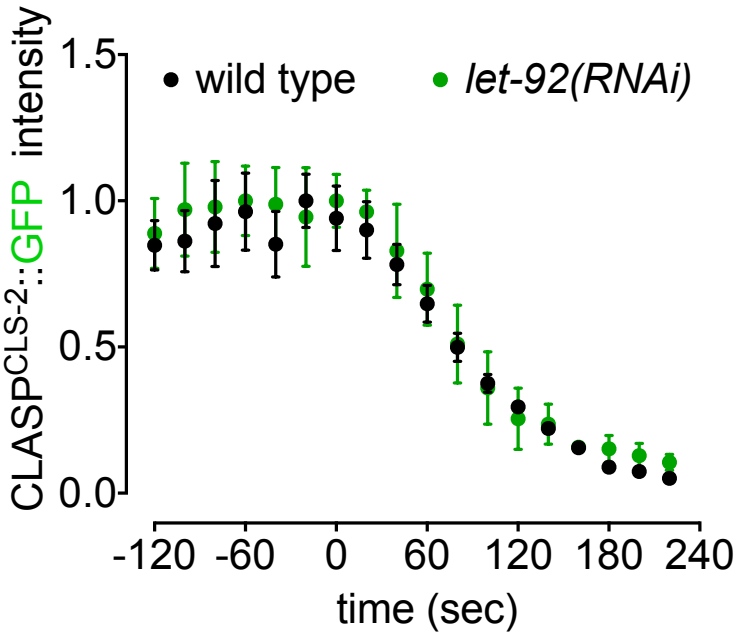

bioRxiv preprint doi: https://doi.org/10.1101/2020.06.12.148254; this version posted November 30, 2020. The copyright holder for this preprint (which was not certified by peer review) is the author/funder, who has granted bioRxiv a license to display the preprint in perpetuity. It is made available under aCC-BY-NC 4.0 International license.

Supplementary Figure 2. CLASP^{CLS-2} intensity and localization is not affected after let-92 depletion.

A. CLASP^{CLS-2} and chromosome dynamics were followed in wild type and *let-92(RNAi)* oocytes expressing CLASP^{CLS-2}::GFP and mCherry::histone. Inset numbers represent the time relative to metaphase I in seconds. Scale bar, 2 µm. See Supp. Movie 4.

B. CLASP^{CLS-2}::GFP levels were measured throughout meiosis I in wild type and *let-92(RNAi)* and the mean ± s.e.m is shown in the graph.

bioRxiv preprint doi: https://doi.org/10.1101/2020.06.12.148254; this version posted November 30, 2020. The copyright holder for this preprint (which was not certified by peer review) is the author/funder, who has granted bioRxiv a license to display the preprint in perpetuity. It is made available under aCC-BY-NC 4.0 International license.

Bel Borja et al. Supp Figure 3

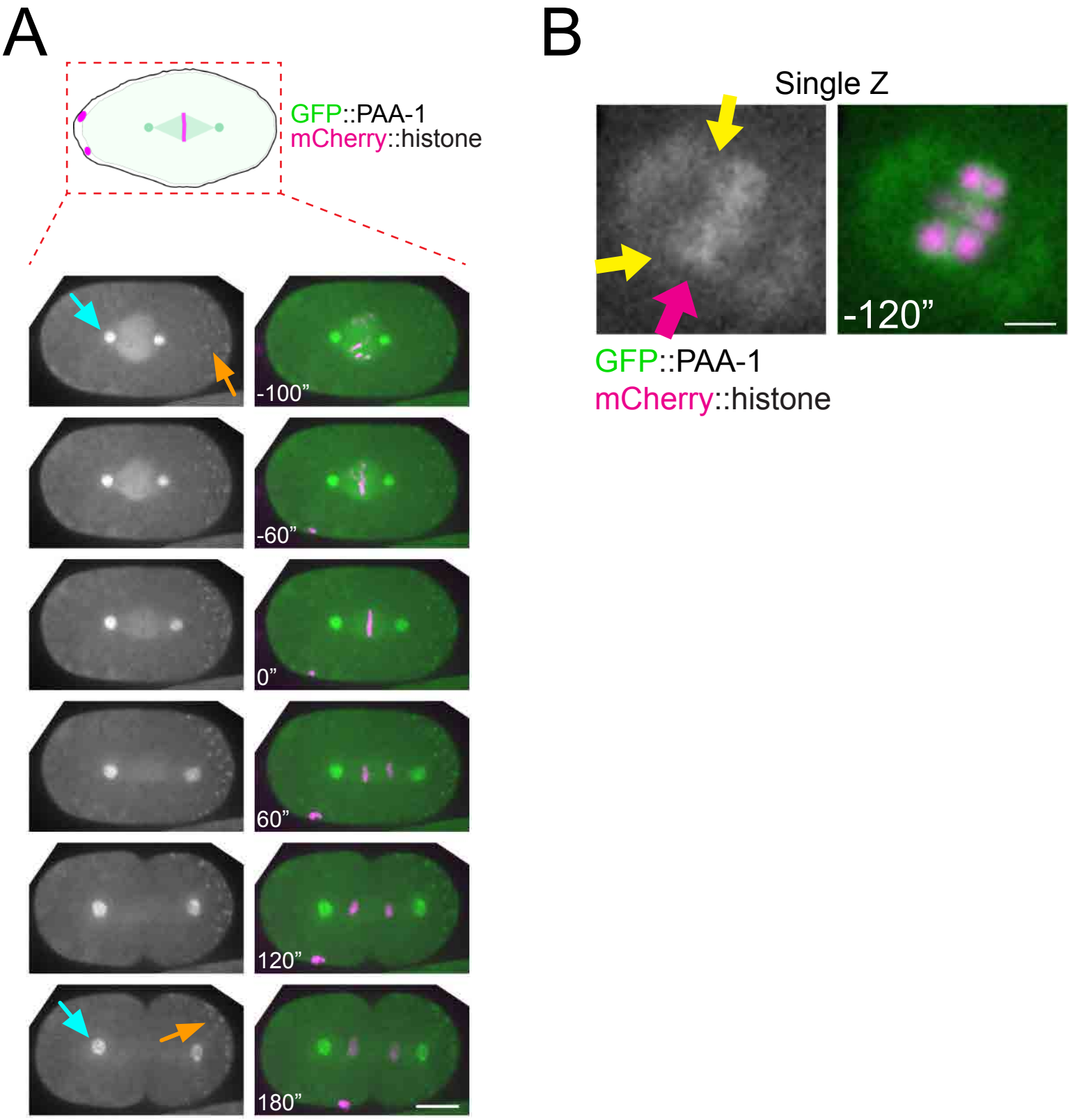

bioRxiv preprint doi: https://doi.org/10.1101/2020.06.12.148254; this version posted November 30, 2020. The copyright holder for this preprint (which was not certified by peer review) is the author/funder, who has granted bioRxiv a license to display the preprint in perpetuity. It is made available under aCC-BY-NC 4.0 International license.

Supplementary Figure 3. Localisation of GFP::PAA-1 during mitosis.

A. PAA-1 localisation was followed during the first mitotic division using endogenously tagged GFP::PAA-1. Cyan arrows point to centrosomes and orange arrows point to P-bodies. Inset numbers represent the time relative to metaphase in seconds. Scale bar, 10 µm.

B. A single Z plane from one time-point (-120") from the same movie as in Figure 2A is shown to highlight that the chromosomal PAA-1 signal is a combination of midbivalent (magenta arrow) and kinetochore (yellow arrows).

bioRxiv preprint doi: https://doi.org/10.1101/2020.06.12.148254; this version posted November 30, 2020. The copyright holder for this preprint (which was not certified by peer review) is the author/funder, who has granted bioRxiv a license to display the preprint in perpetuity. It is made available under aCC-BY-NC 4.0 International license.

Bel Borja et al. Supp. Figure 4

A

Regulatory (B) Subunit	
human	*C. elegans*
PPP2R2A / B55α	SUR-6
PPP2R2B / B55β	
PPP2R2C / B55γ	
PPP2R2D / B55δ	
PPP2R5C / B56γ	PPTR-2
PPP2R5D / B56δ	
PPP2R5A / B56α	PPTR-1
PPP2R5E / B56ε	
PPP2R5B / B56β	

B

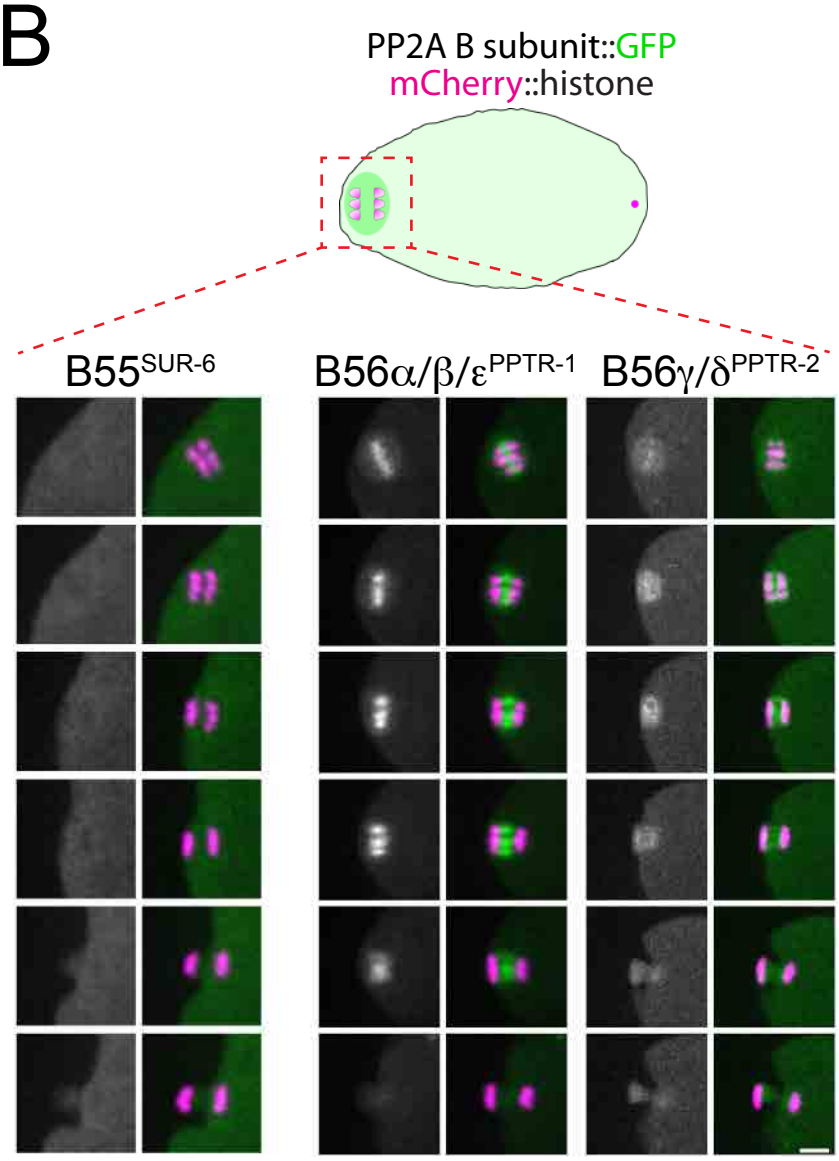

C

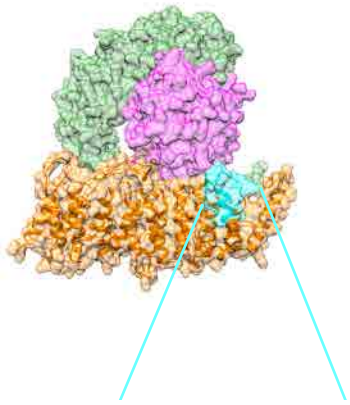

```
B56γ     378- SKTHWNKTIHGLIYNA -393
B56δ     454- SKSHWNKTIHGLIYNA -469
PPTR-2   449- SKSHWNKTIHGLIYNA -464
B56β     409- SKEHWNQTIVSLIYNV -424
PPTR-1   420- SKEHWNQTIVALVYNV -435
B56α     403- SKEHWNPTIVALVYNV -418
B56ε     395- SKEHWNPAIVALVYNV -410
              ** *** :* .*:**.
```

bioRxiv preprint doi: https://doi.org/10.1101/2020.06.12.148254; this version posted November 30, 2020. The copyright holder for this preprint (which was not certified by peer review) is the author/funder, who has granted bioRxiv a license to display the preprint in perpetuity. It is made available under aCC-BY-NC 4.0 International license.

Supplementary Figure 4. Localisation of *C. elegans* B55 and B56 subunits.

A. Chart showing the *C. elegans* orthologues of the human B55 and B56 regulatory B subunits. The chart is based on the alignment provided in Table 1 and Supplementary Table 1.

B. The respective B subunit was endogenously tagged with GFP and their localisation was followed by imaging of dissected oocytes. Scale bar, 2 µm.

C. Alignment of the human and *C. elegans* B56 subunits in the C-terminal stretch shown to be important for kinetochore vs centromere localisation of B56 in human cells during mitosis (Vallardi et al. 2019).

bioRxiv preprint doi: https://doi.org/10.1101/2020.06.12.148254; this version posted December 30, 2020. The copyright holder for this preprint (which was not certified by peer review) is the author/funder, who has granted bioRxiv a license to display the preprint in perpetuity. It is made available under aCC-BY-NC 4.0 International license.

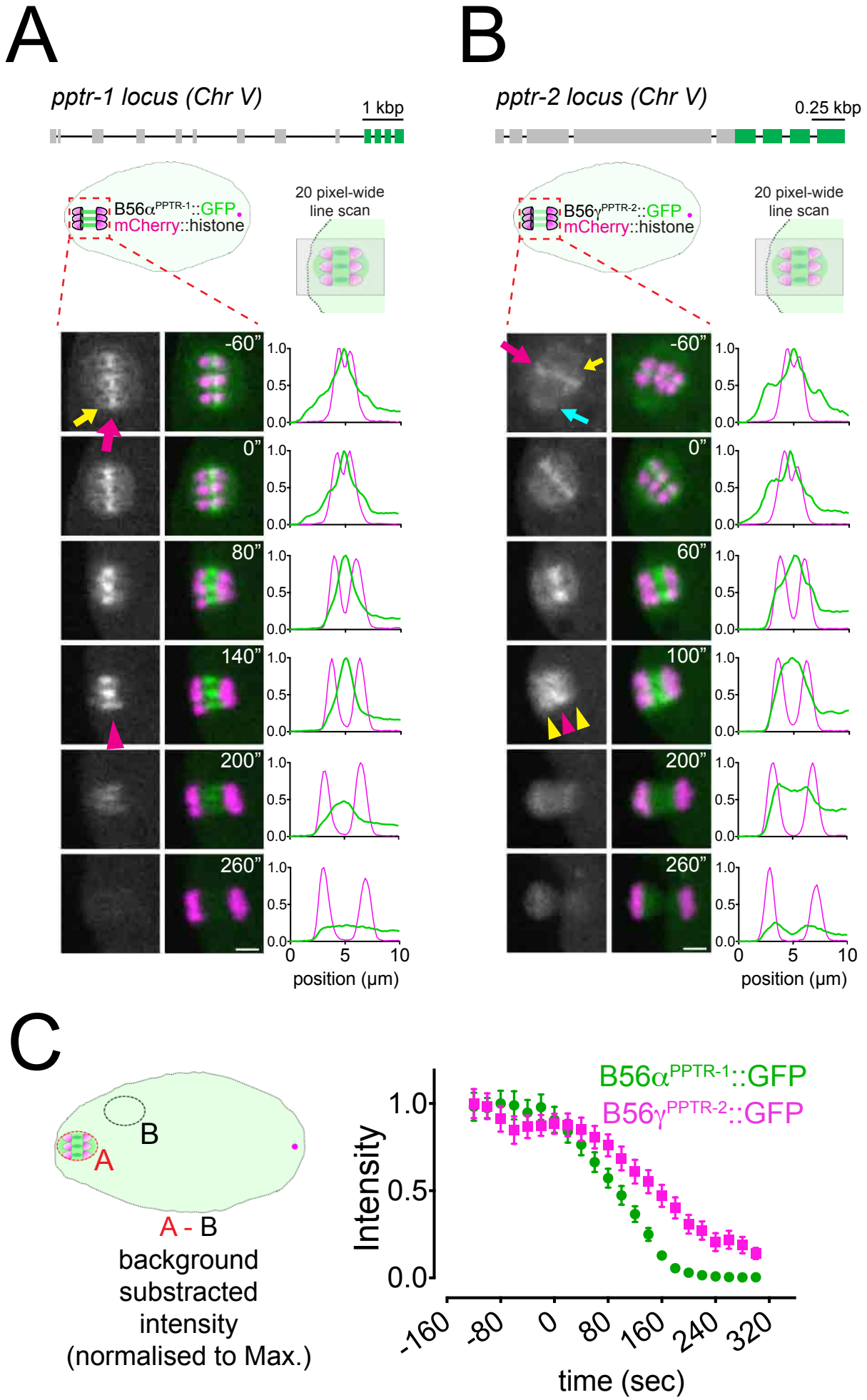

bioRxiv preprint doi: https://doi.org/10.1101/2020.06.12.148254; this version posted November 30, 2020. The copyright holder for this preprint (which was not certified by peer review) is the author/funder, who has granted bioRxiv a license to display the preprint in perpetuity. It is made available under aCC-BY-NC 4.0 International license.

Supplementary Figure 5. Localisation of *C. elegans* B55 and B56 subunits.

A. Top, Schematic of the *pptr-1* gene structure and its tagging with *gfp*. Bottom, PPTR-1 and chromosome dynamics were followed in oocytes expressing PPTR-1::GFP and mCherry::histone. The magenta arrow points to the midbivalent and the yellow arrow points to the kinetochore. Magenta arrowhead highlights the central-spindle localisation. Inset numbers represent the time relative to metaphaseI in seconds. Scale bar, 2 µm. Representative, spindle-wide (20 pixels) line profiles are shown on the right of each time point. See Supp. Movie 6.

B. Top, Schematic of the *pptr-2* gene structure and its tagging with *gfp*. Bottom, PPTR-2 and chromosome dynamics were followed in oocytes expressing PPTR-2::GFP and mCherry::histone. The magenta arrow points to the midbivalent, the yellow arrow points to the kinetochore, and the cyan arrow to the spindle pole. Inset numbers represent the time relative to metaphaseI in seconds. Scale bar, 2 µm. Magenta arrowhead highlights the central-spindle localisation and yellow arrowhead highlights the chromosome-associated signal. Representative, spindle-wide (20 pixels) line profiles are shown on the right of each time point. See Supp. Movie 7.

C. PPTR-1::GFP and PPTR-2::GFP levels were measured throughout meiosis I and the mean ± s.e.m is shown in the graph.

bioRxiv preprint doi: https://doi.org/10.1101/2020.06.12.148254; this version posted November 30, 2020. The copyright holder for this preprint (which was not certified by peer review) is the author/funder, who has granted bioRxiv a license to display the preprint in perpetuity. It is made available under aCC-BY-NC 4.0 International license.

Bel Borja et al. Supp Figure 6

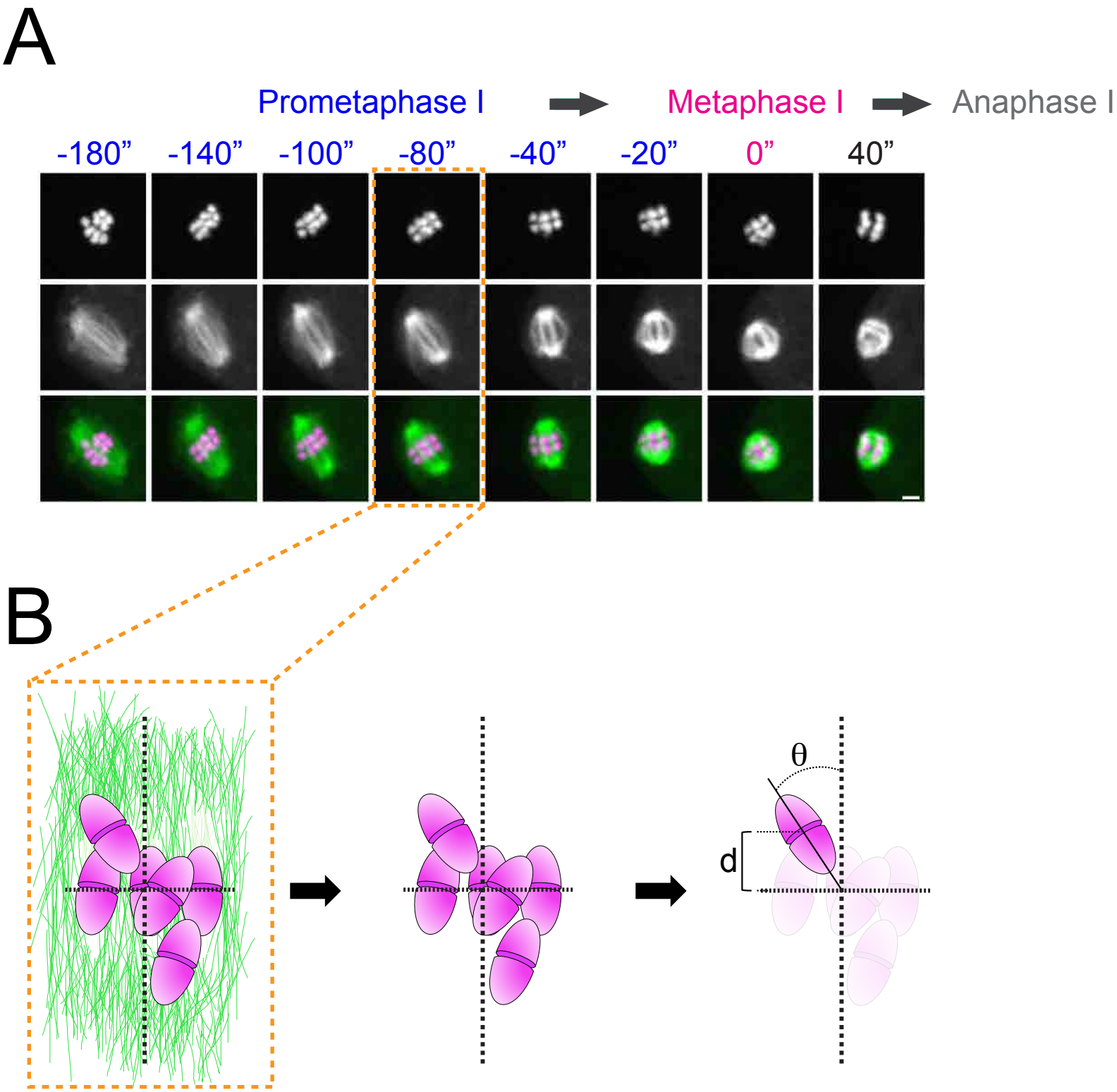

bioRxiv preprint doi: https://doi.org/10.1101/2020.06.12.148254; this version posted November 30, 2020. The copyright holder for this preprint (which was not certified by peer review) is the author/funder, who has granted bioRxiv a license to display the preprint in perpetuity. It is made available under aCC-BY-NC 4.0 International license.

Supplementary Figure 6. Schematics of how congression and alignment were anotated in this study.

A. Microtubules and chromosomes of a wild type oocyte are shown in the panel. For the congression/alignment analysissuring prometaphase I, we chose to analyse 80 seconds before metaphase I, as chromosome are readily aligned in most wild type oocytes.

B. Schematic of a prometaphase I spindle indicating how the angle and the distance of each bivalent was measured.

bioRxiv preprint doi: https://doi.org/10.1101/2020.06.12.148254; this version posted November 30, 2020. The copyright holder for this preprint (which was not certified by peer review) is the author/funder, who has granted bioRxiv a license to display the preprint in perpetuity. It is made available under aCC-BY-NC 4.0 International license.

Bel Borja et al. Supp. Figure 7

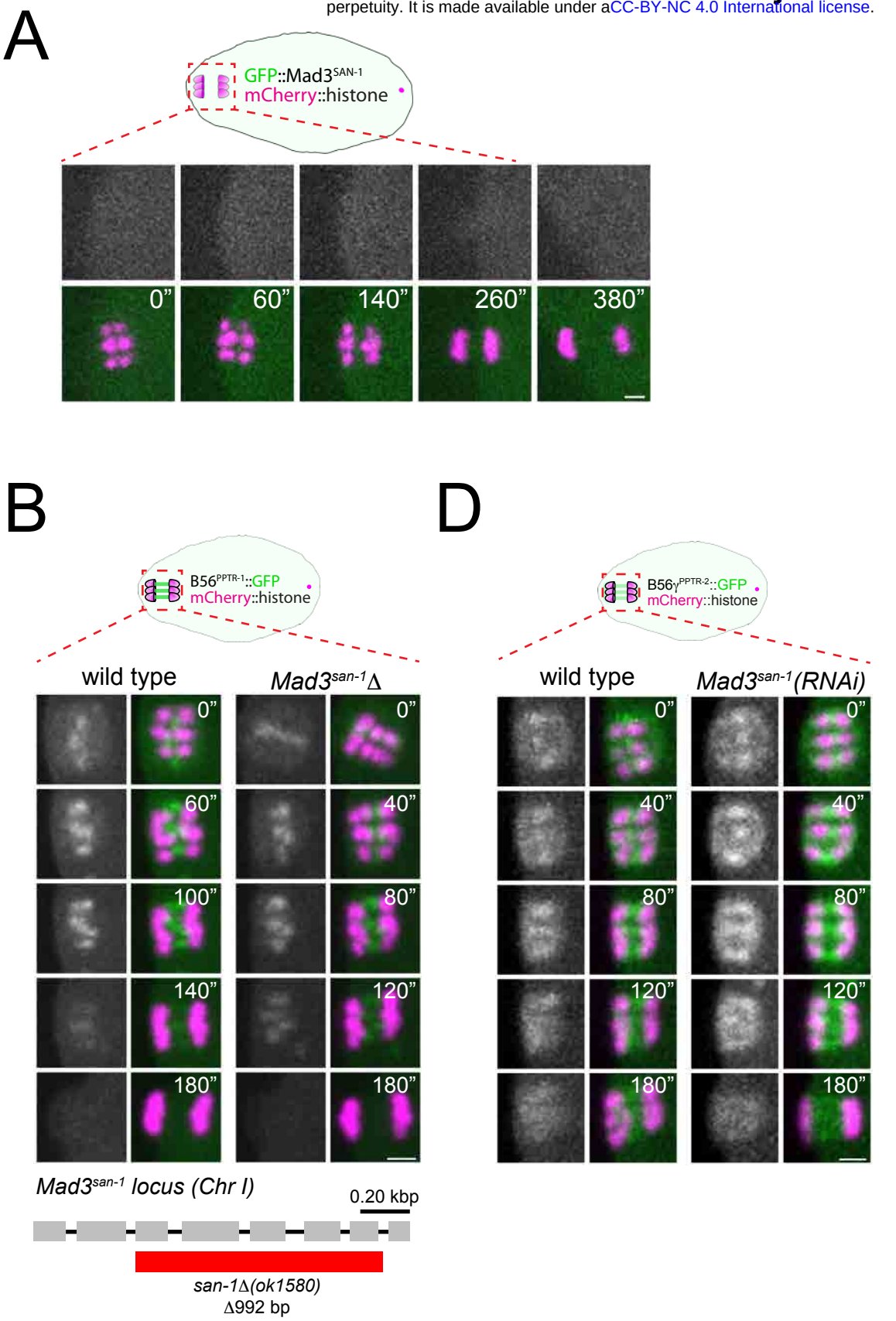

bioRxiv preprint doi: https://doi.org/10.1101/2020.06.12.148254; this version posted November 30, 2020. The copyright holder for this preprint (which was not certified by peer review) is the author/funder, who has granted bioRxiv a license to display the preprint in perpetuity. It is made available under aCC-BY-NC 4.0 International license.

Supplementary Figure 7. Mad3^{SAN-1} does not play a major role in B56α^{PPTR-1} and B56γ^{PPTR-2} targeting.

A. GFP::Mad3^{SAN-1} was imaged during oocyte meiosis along with mCherry::histone to follow chromosomes. Time insets are relative to metaphase I ('t=0'). Scale bar, 2 µm.

B. B56α^{PPTR-1} and chromosome dynamics were followed in wild type and in *Mad3^{SAN-1}Δ* oocytes expressing PPTR-1::GFP and mCherry::histone. Scale bar, 2 µm. The bottom panel shows a schematic of the *san-1Δ* allele.

C. B56γ^{PPTR-2} and chromosome dynamics were followed in wild type and in *Mad3^{san-1}(RNAi)* oocytes expressing PPTR-2::GFP and mCherry::histone. Scale bar, 2 µm.

bioRxiv preprint doi: https://doi.org/10.1101/2020.06.12.148254; this version posted November 30, 2020. The copyright holder for this preprint (which was not certified by peer review) is the author/funder, who has granted bioRxiv a license to display the preprint in perpetuity. It is made available under aCC-BY-NC 4.0 International license.

Bel Borja et al. Supp Figure 8

A

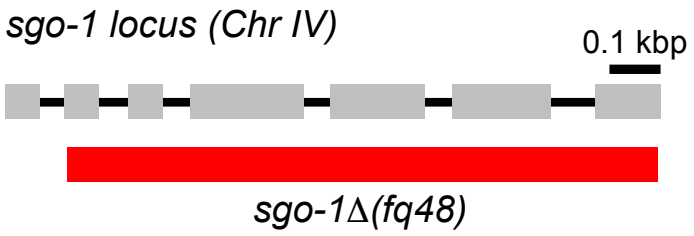

B

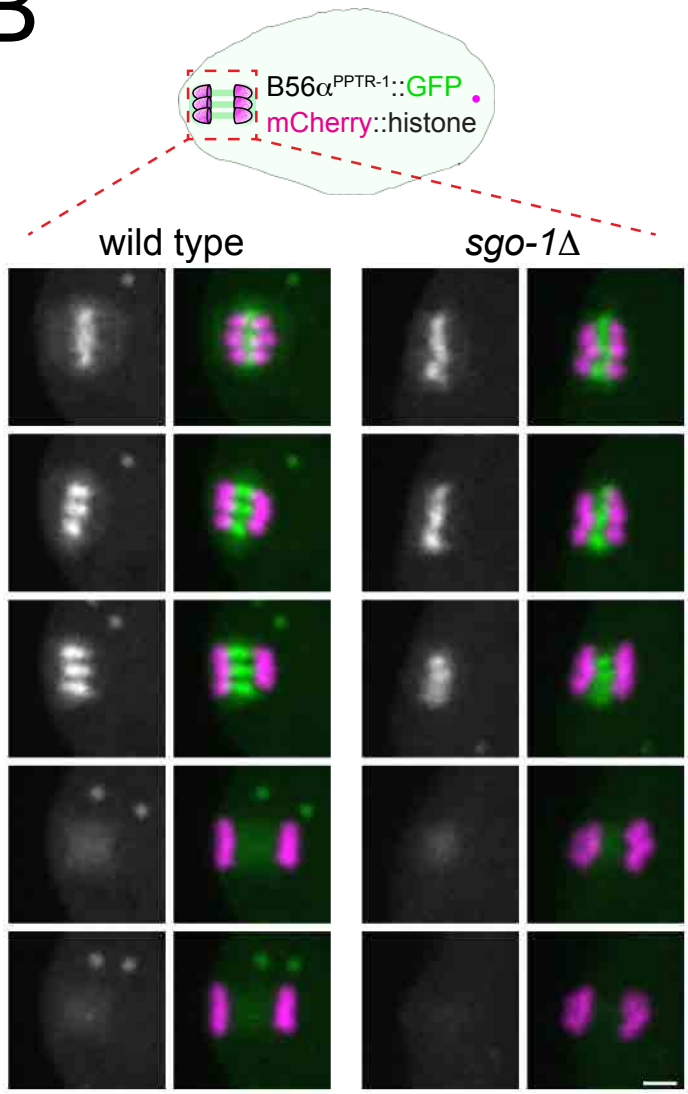

D

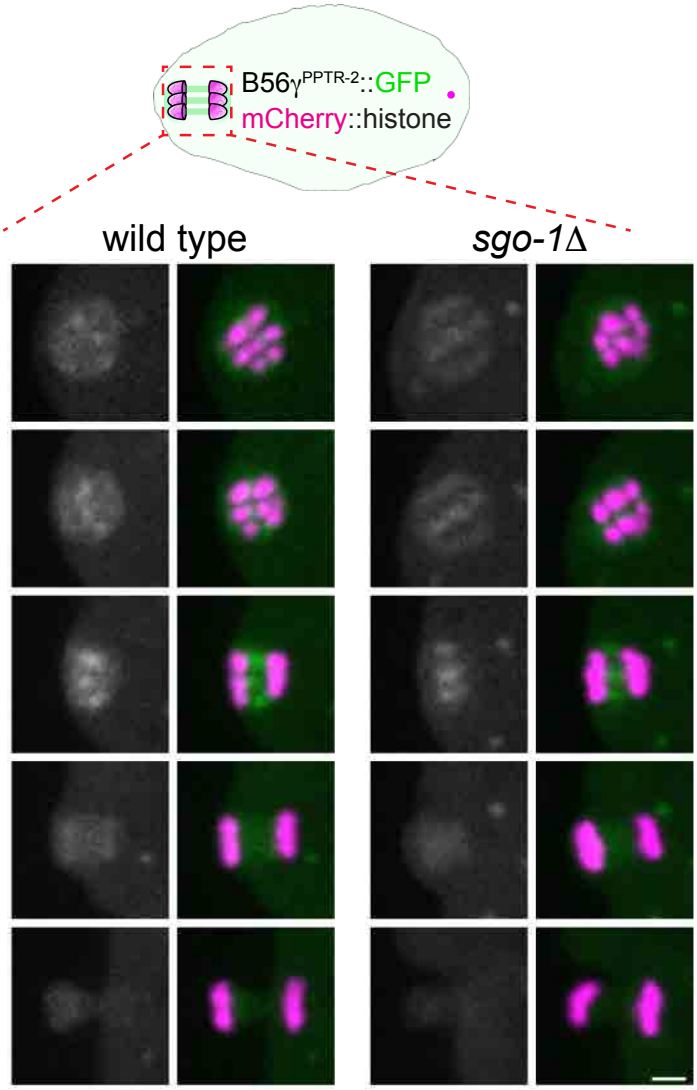

C

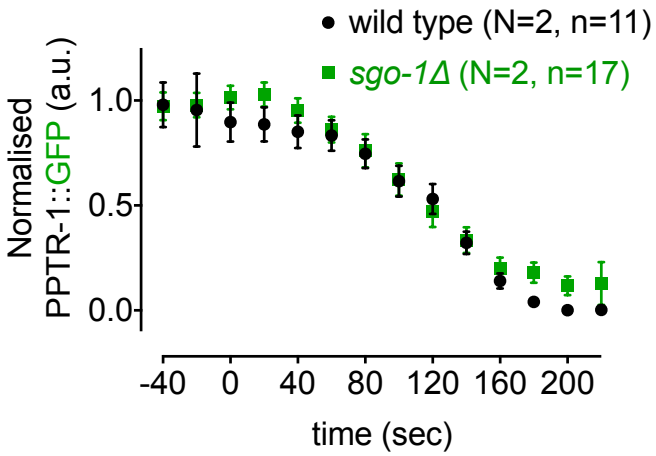

E

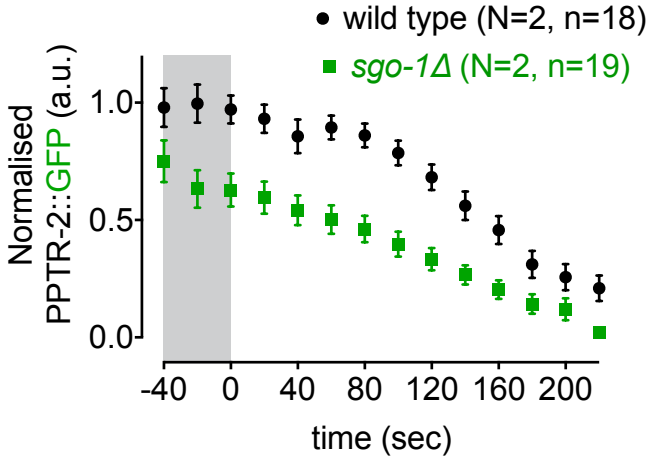

bioRxiv preprint doi: https://doi.org/10.1101/2020.06.12.148254; this version posted November 30, 2020. The copyright holder for this preprint (which was not certified by peer review) is the author/funder, who has granted bioRxiv a license to display the preprint in perpetuity. It is made available under aCC-BY-NC 4.0 International license.

Supplementary Figure 8. Shugoshin^{SGO-1} does not play a major role in B56α^{PPTR-1} and B56γ^{PPTR-2} targeting.

A. Schematic of the *sgo-1Δ* allele.

B. B56α^{PPTR-1} and chromosome dynamics were followed in wild type and in *Shugoshin*$^{sgo-1}$oocytes expressing PPTR-1::GFP and mCherry::histone. Scale bar, 2 µm.

C. PPTR-1::GFP levels were measured in wild type and in *Shugoshin*$^{sgo-1}$oocytes throughout meiosis I and the mean ± s.e.m is shown in the graph. N represents number of experiments and n number of oocytes quantified.

D. B56γ^{PPTR-2} and chromosome dynamics were followed in wild type and *Shugoshin*$^{sgo-1}$oocytes expressing PPTR-2::GFP and mCherry::histone. Scale bar, 2 µm.

E. PPTR-1::GFP levels were measured in wild type and in *Shugoshin*$^{sgo-1}$oocytes throughout meiosis I and the mean ± s.e.m is shown in the graph. N represents number of experiments and n number of oocytes quantified.

bioRxiv preprint doi: https://doi.org/10.1101/2020.06.12.148254; this version posted December 30, 2020. The copyright holder for this preprint (which was not certified by peer review) is the author/funder, who has granted bioRxiv a license to display the preprint in perpetuity. It is made available under aCC-BY-NC 4.0 International license.

Bel Borja et al. Supp Figure 9

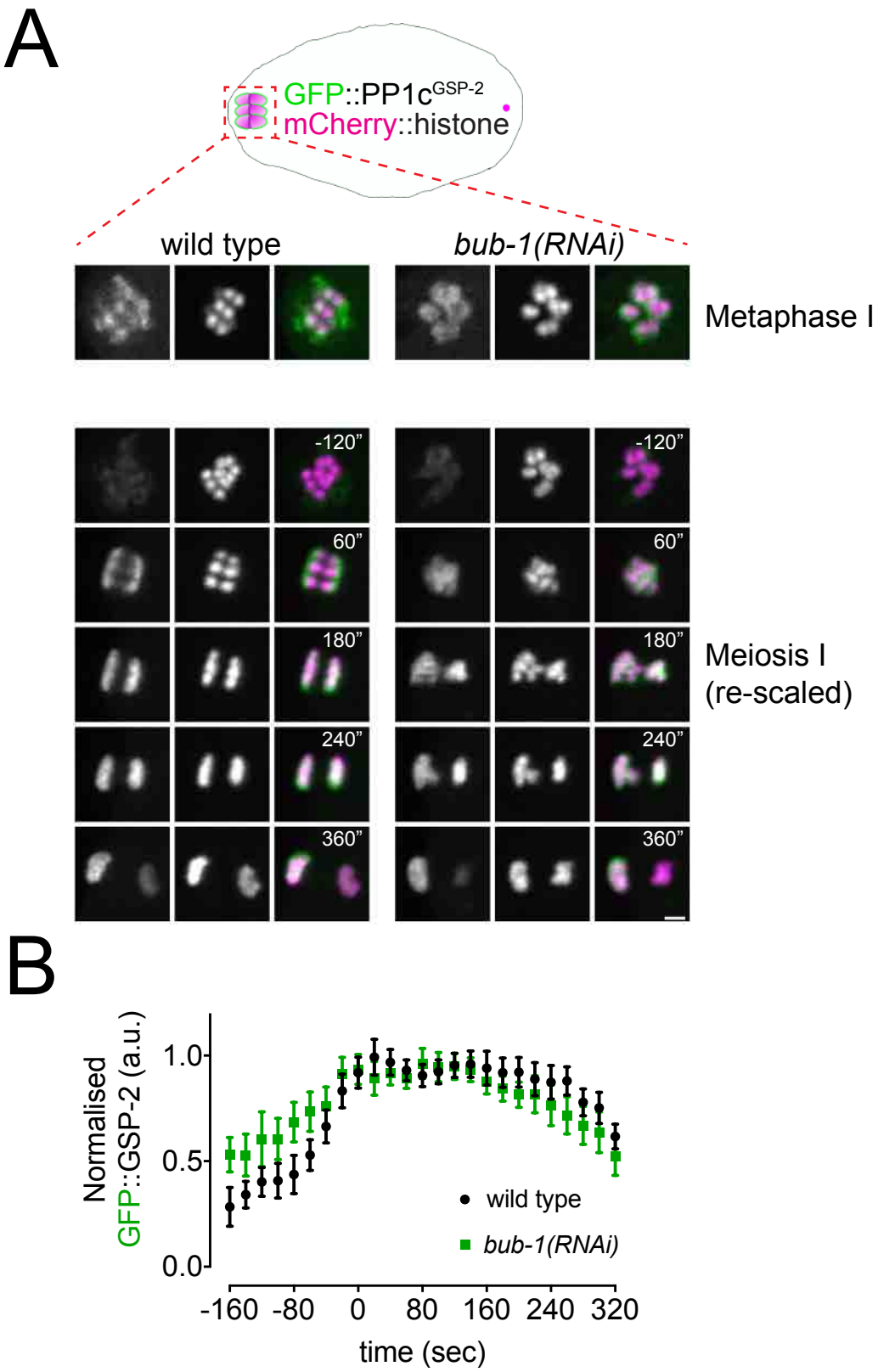

bioRxiv preprint doi: https://doi.org/10.1101/2020.06.12.148254; this version posted November 30, 2020. The copyright holder for this preprint (which was not certified by peer review) is the author/funder, who has granted bioRxiv a license to display the preprint in perpetuity. It is made available under aCC-BY-NC 4.0 International license.

Supplementary Figure 9. PP1 catalytic subunit localisation is not regulated by BUB-1.

A. GFP::PP1c^{GSP-2} and chromosome dynamics were followed in wild type and *bub-1(RNAi)* oocytes. Since the GFP signal increases during anaphase, one scale was chosen to show kinetochore localisation during metaphase I (top) and another for the composite panel (bottom). Scale bar, 2 µm. See Supp. Movie 12.

B. GFP::PP1c^{GSP-2} levels were measured in wild type and *bub-1(RNAi)* oocytes throughout meiosis I and the mean ± s.e.m is shown in the graph.

Bel Borja et al. Supp. Figure 10

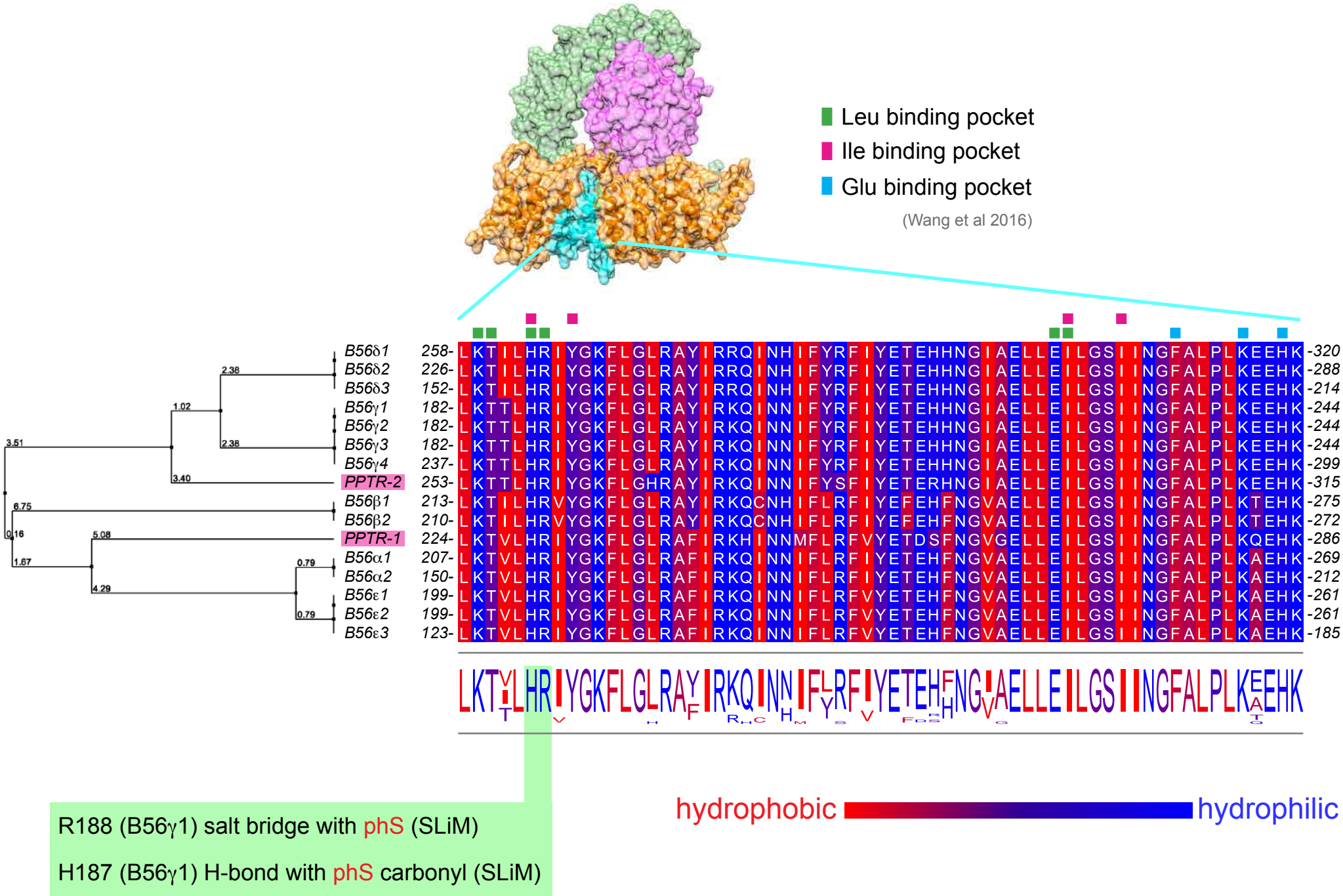

bioRxiv preprint doi: https://doi.org/10.1101/2020.06.12.148254; this version posted November 30, 2020. The copyright holder for this preprint (which was not certified by peer review) is the author/funder, who has granted bioRxiv a license to display the preprint in perpetuity. It is made available under aCC-BY-NC 4.0 International license.

Supplementary Figure 10. Alignment of the B56 subunits LxxIxE motif binding pocket. *C. elegans* and human B56 subunits LxxIxE motif binding pocket were aligned using Clustal Omega and Jalview. The scale from blue to red represents increasing hydrophobicity. Key residues as reported in Wang et al. (2016) are highlighted. Additionally, residues making contact with the phospho-serine are highlighted with green background. The tree on the left was calculated from the distance matrix generated from sequence pairwise scores and confirms the relationship between *C. elegans* and human B56s.

Bel Borja et al. Supp. Figure 11

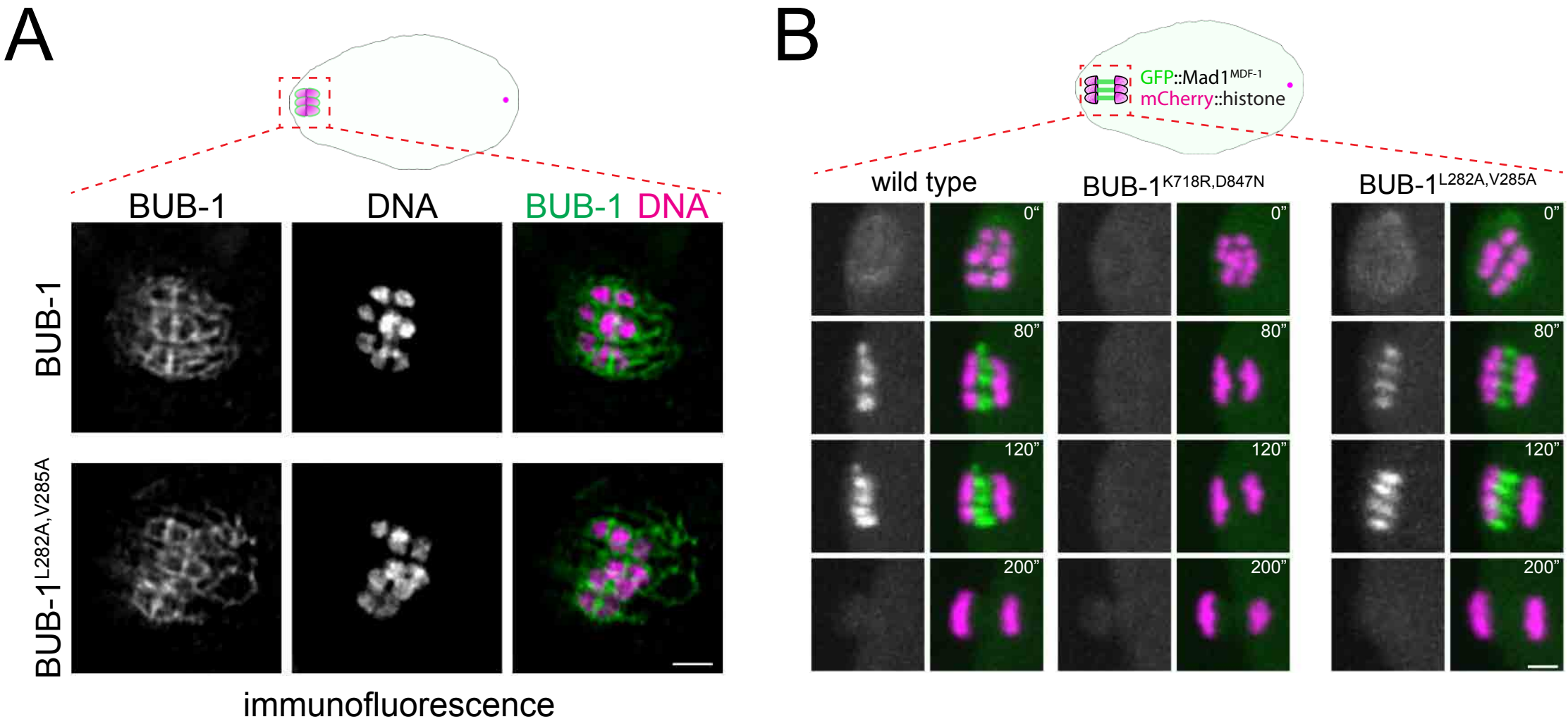

bioRxiv preprint doi: https://doi.org/10.1101/2020.06.12.148254; this version posted November 30, 2020. The copyright holder for this preprint (which was not certified by peer review) is the author/funder, who has granted bioRxiv a license to display the preprint in perpetuity. It is made available under aCC-BY-NC 4.0 International license.

Supplementary Figure 11. Mad1^{MDF-1} localisation is not affected by a LxxIxE motif mutation in BUB-1.

A. BUB-1 localisation was analysed in fixed wild type and BUB-1^{L282A,V285A} mutant oocytes by immunofluorescence using BUB-1 specific antibodies. Scale bar, 2 µm.

B. GFP::Mad1^{MDF-1} was imaged during oocyte meiosis along with mCherry::histone to follow chromosomes. Time insets are relative to metaphase I (t=0”). The BUB-1^{K718R,D847N} mutation completely abolishes Mad1^{MDF-1} localisation. On the other hand, GFP::Mad1^{MDF-1} remained unaltered in the the BUB-1^{L282A,V285A} mutant. Scale bar, 2 µm.

A

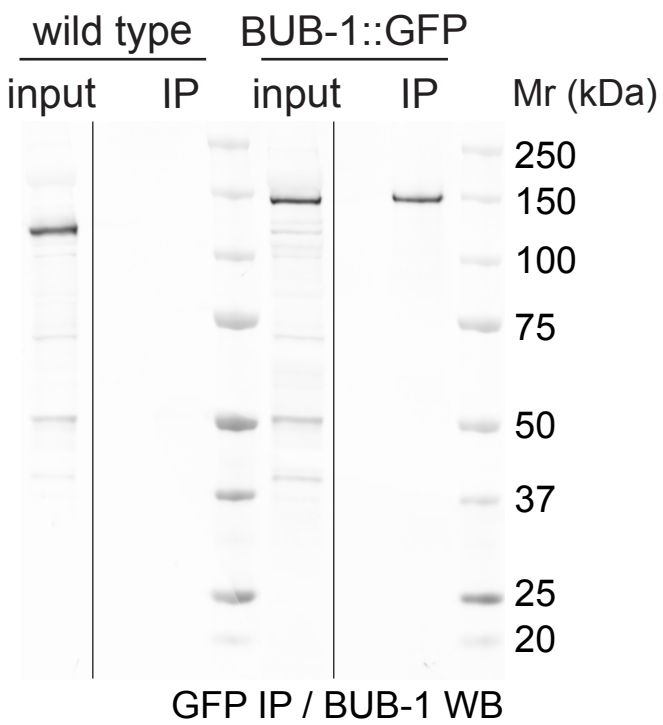

B

R.HLphSPVSEK.T

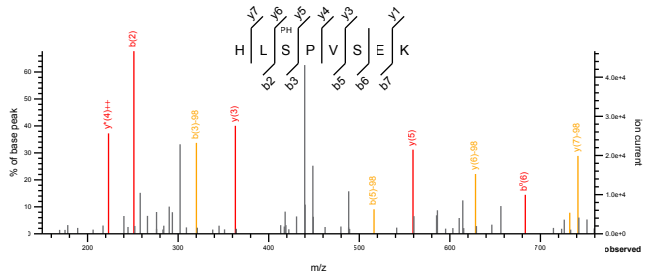

R.RHLphSPVSEK.T

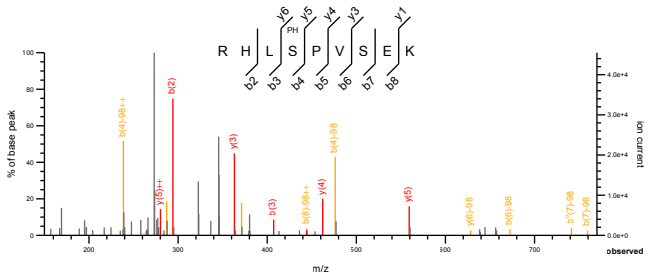

R.RRHLphSPVSEK.T

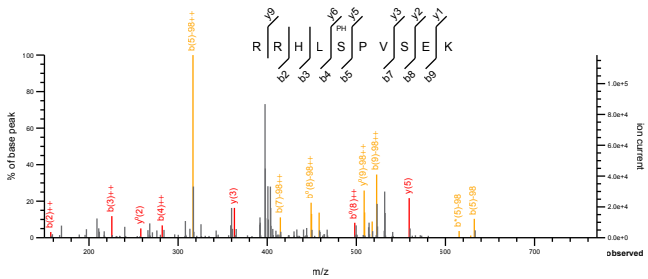

bioRxiv preprint doi: https://doi.org/10.1101/2020.06.12.148254; this version posted November 30, 2020. The copyright holder for this preprint (which was not certified by peer review) is the author/funder, who has granted bioRxiv a license to display the preprint in perpetuity. It is made available under aCC-BY-NC 4.0 International license.

Supplementary Figure 12. BUB-1::GFP immunoprecipitation and selected MS spectra of peptides containing phospho serine 283.

A. Embryo extracts from wild type (N2) and BUB-1::GFP worms were immunoprecipitated using a GFP nanobody coupled to magnetic beads. The inputs and immunoprecipitates were resolved on SDS-PAGE and subject to BUB-1 western blot. BUB-1::GFP is readily pulled down form the extracts, whereas untagged BUB-1 is not. Note the size difference due to the GFP tag. MW marker is shown on the right side.

B. Seleted MS spectra without (top), with one (middle), or with two (bottom) trypsin miscleavages are shown.

bioRxiv preprint doi: https://doi.org/10.1101/2020.06.12.148254; this version posted November 20, 2020. The copyright holder for this preprint (which was not certified by peer review) is the author/funder, who has granted bioRxiv a license to display the preprint in perpetuity. It is made available under aCC-BY-NC 4.0 International license.

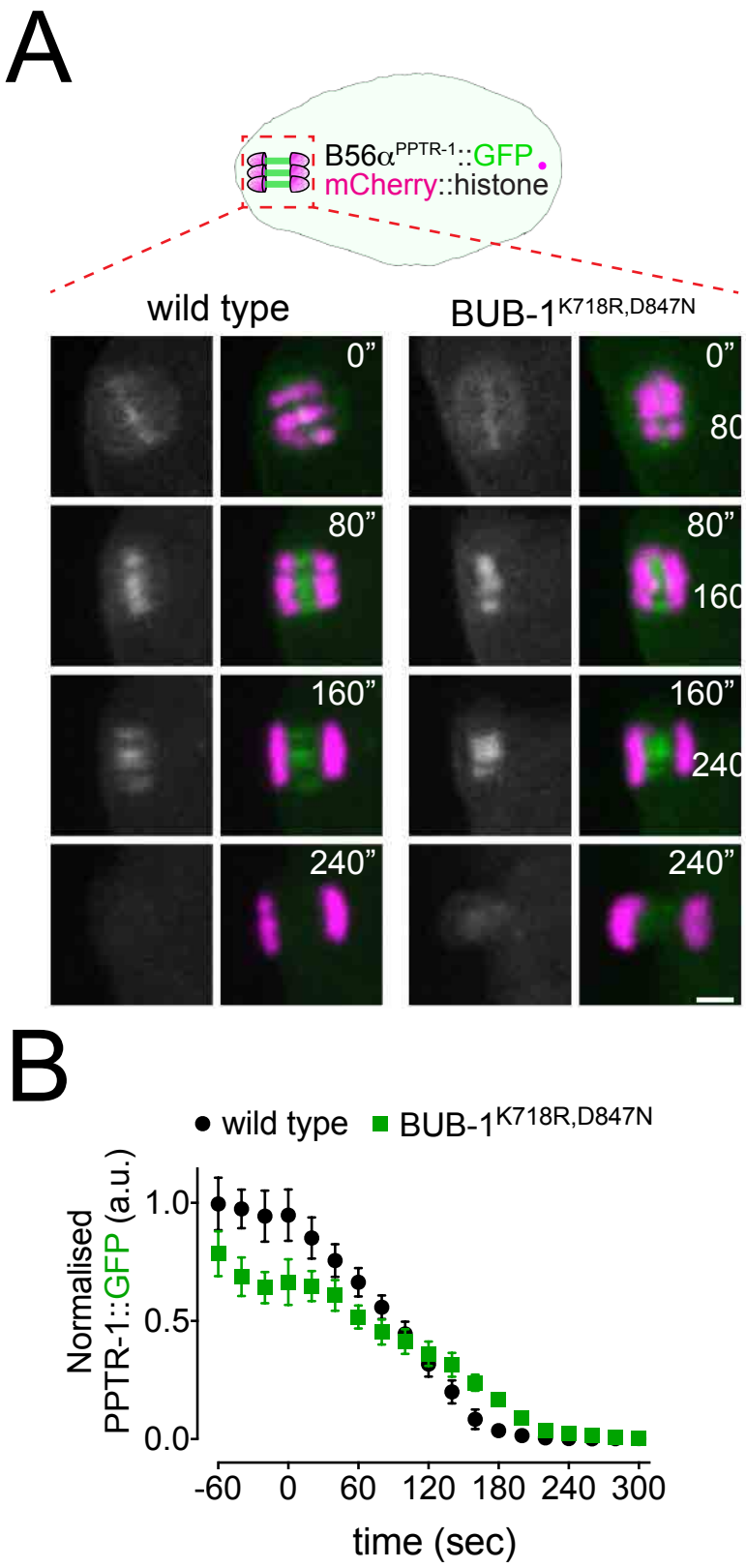

bioRxiv preprint doi: https://doi.org/10.1101/2020.06.12.148254; this version posted November 30, 2020. The copyright holder for this preprint (which was not certified by peer review) is the author/funder, who has granted bioRxiv a license to display the preprint in perpetuity. It is made available under aCC-BY-NC 4.0 International license.

Supplementary Figure 13. Kinase domain in BUB-1 does not regulate targeting of B56α^{PPTR-1} regulatory subunit in meiosis I.

A. PPTR-1 and chromosome dynamics were followed in wild type and BUB-1^{K718R,D847N} oocytes expressing PPTR-1::GFP and mCherry::histone. Inset numbers represent the time relative to metaphaseI in seconds. Scale bar, 2 µm. See Supp. Movie 19.

B. PPTR-1::GFP levels were measured throughout meiosis I in wild type and BUB-1^{K718R,D847N} oocytes and the mean ± s.e.m is shown in the graph.

	PPTR-1	B56β1	B56β2	B56ε2	B56ε3	B56ε1	B56α2	B56α1	PPTR-2	B56δ1	B56δ2	B56δ3	B56γ4	B56γ5	B56γ1	B56γ2	B56γ3
PPTR-1		60.12	60.08	66.67	71.87	66.59	68.30	63.35	52.26	54.81	56.10	60.17	60.42	57.75	64.48	63.27	59.27
B56β1	60.12		97.56	72.17	73.66	71.83	71.79	69.77	56.36	62.75	63.85	67.13	65.28	64.47	66.21	67.13	64.44
B56β2	60.08	97.56		71.86	73.66	71.52	71.79	69.28	56.59	62.53	63.62	67.13	64.78	63.97	65.68	66.59	63.94
B56ε2	66.67	72.17	71.86		99.74	99.78	78.21	77.49	59.87	66.16	67.60	70.49	67.62	67.81	69.14	69.88	68.75
B56ε3	71.87	73.66	73.66	99.74			79.80	79.80	63.94	71.36	71.36	71.36	73.70	72.38	72.82	73.70	72.38
B56ε1	66.59	71.83	71.52	99.78			78.23	77.52	59.66	65.88	67.28	70.12	67.10	67.27	68.58	69.30	68.19
B56α2	68.30	71.79	71.79	78.21	79.80	78.23		99.07	60.84	67.92	69.14	69.14	71.53	69.56	70.74	71.78	69.79
B56α1	63.35	69.77	69.28	77.49	79.80	77.52	99.07		56.49	63.35	64.97	68.00	66.74	66.37	68.35	69.30	67.49
PPTR-2	52.26	56.36	56.59	59.87	63.94	59.66	60.84	56.49		62.31	61.76	66.19	63.55	60.66	68.97	66.25	62.74
B56δ1	54.81	62.75	62.53	66.16	71.36	65.88	67.92	63.35	62.31		99.65	98.19	79.07	75.68	81.29	80.00	76.72
B56δ2	56.10	63.85	63.62	67.60	71.36	67.28	69.14	64.97	61.76	99.65		98.39	79.72	77.37	82.46	81.05	77.63
B56δ3	60.17	67.13	67.13	70.49	71.36	70.12	69.14	68.00	66.19	98.19	98.39		84.40	81.72	87.62	85.71	81.72
B56γ4	60.42	65.28	64.78	67.62	73.70	67.10	71.53	66.74	63.55	79.07	79.72	84.40		94.57	93.00	93.81	93.61
B56γ5	57.75	64.47	63.97	67.81	72.38	67.27	69.56	66.37	60.66	75.68	77.37	81.72	94.57		92.87	94.64	95.23
B56γ1	64.48	66.21	65.68	69.14	72.82	68.58	70.74	68.35	68.97	81.29	82.46	87.62	93.00	92.87		99.77	98.44
B56γ2	63.27	67.13	66.59	69.88	73.70	69.30	71.78	69.30	66.25	80.00	81.05	85.71	93.81	94.64	99.77		99.79
B56γ3	59.27	64.44	63.94	68.75	72.38	68.19	69.79	67.49	62.74	76.72	77.63	81.72	93.61	95.23	98.44	99.79	

Supplementary Table 1. Percent Identity (%) Matrix of the full length sequence alignment of mammalian B56 isoforms and *C.elegans* orthologues PPTR-1 and PPTR-2 .Created with Clustal Omega version 2.1.

bioRxiv preprint doi: https://doi.org/10.1101/2020.06.12.148254; this version posted November 30, 2020. The copyright holder for this preprint (which was not certified by peer review) is the author/funder, who has granted bioRxiv a license to display the preprint in perpetuity. It is made available under aCC-BY-NC 4.0 International license.

Markers / *mutants*	Strain Number	Genotype	Source
SUR-6::GFP	OD4579	*sur-6(ltl183[GFP::loxP::3xFlag::sur-6]) I*	this study
SUR-6::GFP; mCherry::histone	FGP354	*sur-6(ltl183[GFP::loxP::3xFlag::sur-6])I; ltIs37[pAA64; pie-1p::mCherry::his-58; unc-119 (+)]IV*	this study
GFP::tubulin; mCherry::histone	OD868	*ltSi220[pOD1249/pSW077; Pmex-5::GFP::tbb-2::operon_linker::mCHerry::his-11; cb-unc-119(+)]I*	Wang et al, 2015 (PMID: 24217623)
GFP::tubulin; mCherry::histone; *bub-1(L282A;V285A)*	FGP339	*ltSi220[pOD1249/pSW077; Pmex-5::GFP::tbb-2::operon_linker::mCHerry::his-11; cb-unc-119(+)]I; bub-1(syb1936[bub-1((L282A;V285A)])I*	this study
GFP::tubulin; mCherry::histone; *pptr-2 Δ*	FGP369	*pptr-2(ok1467)V; ltSi220[pOD1249/pSW077; Pmex-5::GFP::tbb-2::operon_linker::mCHerry::his-11; cb-unc-119(+)]I*	this study
GFP::tubulin; mCherry::histone; *bub-1(K718R;D847N)*	FGP337	*ltSi220[pOD1249/pSW077; Pmex-5::GFP::tbb-2::operon_linker::mCHerry::his-11; cb-unc-119(+)]I; bub-1(syb1746[bub-1((K718R;D847N)])*	this study
GFP::tubulin; mCherry::histone; bub-1(L282A;V285A;K718R;D847N)	FGP402	*ltSi220[pOD1249/pSW077; Pmex-5::GFP::tbb-2::operon_linker::mCHerry::his-11; cb-unc-119(+)]I; bub-1(syb1936,syb2383[bub-1(L282A;V285A,K718R;D847N)])I*	this study
bub-1(S283A); GFP::tubulin; mCherry::histone	FGP500	*bub-1(syb2396[bub-1((S283A)])I;ltSi220[pOD1249/pSW077; Pmex-5::GFP::tbb-2::operon_linker::mCHerry::his-11; cb-unc-119(+)]I*	this study
IFY-1::GFP; mCherry::histone	JAB222	*ify-1(erb-82[ify-1::linker::GFP])II;ltIs37[pAA64; pie-1p::mCherry::his-58; unc-119 (+)]IV; unc-119(ed3)???*	this study
IFY-1::GFP; mCherry::histone; *bub-1(L282A;V285A)*	FGP405	*ify-1(erb-82[ify-1::linker::GFP])II; ltIs37 [pAA64; pie-1p::mCherry::his-58; unc-119 (+)]IV; unc-119(ed3)???; bub-1(syb1936[bub-1(L282A;V285A)])I*	this study
GFP::MDF-1; mCherry::histone	OD2920	*unc-119(ed3)?III; ltIs37[pAA64; pie-1p::mCherry::his-58; unc-119 (+)]IV; mdf-1(lt39[gfp::tev::loxP::3xFlag::mdf-1])V*	Kim et al, 2017 (PMID: 28698300)
GFP::MDF-1; mCherry::histone; *bub-1(K718R;D847N)*	FGP434	*unc-119(ed3)?III; ltIs37[pAA64; pie-1p::mCherry::his-58; unc-119 (+)]IV; mdf-1(lt39[gfp::tev::loxP::3xFlag::mdf-1])V; bub-1(syb1746[bub-1((K718R;D847N)])I*	this study
GFP::MDF-1; mCherry::histone; *bub-1(L282A;V285A)*	FGP426	*unc-119(ed3)?III; ltIs37[pAA64; pie-1p::mCherry::his-58; unc-119 (+)]IV; mdf-1(lt39[gfp::tev::loxP::3xFlag::mdf-1])V; bub-1(syb1936[bub-1(L282A;V285A)])I*	this study
GFP::PAA-1; mCherry::histone	FGP438	*paa-1(syb2267[GFP::linker::paa-1]III; ltIs37[pAA64; pie-1p::mCherry::his-58; unc-119 (+)]IV*	this study
GFP::PAA-1; mCherry::histone; *bub-1(L282A;V285A)*	FGP388	*paa-1(syb2267[GFP::linker::paa-1]III; ltIs37 [pAA64; pie-1p::mCherry::his-58; unc-119 (+)]IV; bub-1(syb1936[bub-1((L282A;V285A)])I*	this study
GFP::PAA-1; mCherry::histone; bub-1(*K718R;D847N*)	FGP413	*paa-1(syb2267[GFP::linker::paa-1]III; ltIs37 [pAA64; pie-1/mCHERRY::his-58; unc-119 (+)]IV; bub-1(syb1746[bub-1((K718R;D847N)])I*	this study
GFP::PAA-1; mCherry::histone; bub-1(*L282A;V285A;K718R;D847N*)	FGP443	*paa-1(syb2267[GFP::linker::paa-1]III; ltIs37 [pAA64; pie-1/mCHERRY::his-58; unc-119 (+)]IV; bub-1(syb1936,syb2383[bub-1(L282A;V285A,K718R;D847N)])I*	this study
GFP::PAA-1; mCherry::histone; bub-1(*S283A*)	FGP445	*paa-1(syb2267[GFP::linker::paa-1]III; ltIs37 [pAA64; pie-1/mCHERRY::his-58; unc-119 (+)]IV; bub-1(syb1936,syb2383[bub-1(bub-1(syb2396[bub-1((S283A)])I)])I*	this study
GFP::PAA-1; mCherry::histone; *pptr-2Δ*	FGP387	*paa-1(syb2267[GFP::linker::paa-1]III; ltIs37 [pAA64; pie-1/mCHERRY::his-58; unc-119 (+)]IV; pptr-2(ok1467)V*	this study
PPTR-1::GFP	OD3600	*pptr-1(lt89[pptr-1::gfp])V*	Kim et al, 2017 (PMID: 28698300)
PPTR-1::GFP; mCherry::histone	FGP344	*pptr-1(lt89[pptr-1::gfp])V; ltIs37 [pAA64; pie-1p::mCherry::his-58; unc-119 (+)]IV*	this study
PPTR-1::GFP; mCherry::histone; *bub-1(K718R;D847N)*	FGP349	*pptr-1(lt89[pptr-1::gfp])V; ltIs37 [pAA64; pie-1p::mCherry::his-58; unc-119 (+)]IV; bub-1(syb1746[bub-1((K718R;D847N)])I*	this study
PPTR-1::GFP; mCherry::histone; *bub-1(L282A;V285A)*	FGP350	*pptr-1(lt89[pptr-1::gfp])V; ltIs37 [pAA64; pie-1p::mCherry::his-58; unc-119 (+)]IV; bub-1(syb1936[bub-1((L282A;V285A)])I*	this study
PPTR-1::GFP; mCherry::histone; *san-1Δ*	FGP379	*pptr-1(lt89[pptr-1::gfp])V;ltIs37 [pAA64; pie-1p::mCherry::his-58; unc-119 (+)]IV; san-1(ok1580) I*	this study
PPTR-1::GFP; mCherry::histone; bub-1(*L282A;V285A;K718R;D847N*)	FGP400	*pptr-1(lt89[pptr-1::gfp])V; bub-1(syb1936,syb2383[bub-1(L282A;V285A,K718R;D847N)]I*	this study
PPTR-1::GFP; mCherry::histone; bub-1(*S283A*)	FGP441	*pptr-1(lt89[pptr-1::gfp])V; ltIs37 [pAA64; pie-1/mCHERRY::his-58; unc-119 (+)]IV; bub-1(syb2396[bub-1((S283A)])I*	this study
PPTR-2::GFP	OD3424	*pptr-2(lt91[pptr-2::gfp])V*	Kim et al, 2017 (PMID: 28698300)
PPTR-2::GFP; mCherry::histone	FGP317	*pptr-2(lt91[pptr-2::gfp])V; ltIs37[pAA64; pie-1p::mCherry::his-58; unc-119 (+)]IV*	this study
PPTR-2::GFP; mCherry::histone; *bub-1(K718R;D847N)*	FGP323	*pptr-2(lt91[pptr-2::gfp])V; ltIs37[pAA64; pie-1p::mCherry::his-58; unc-119 (+)]IV; bub-1(syb1746[bub-1((K718R;D847N)])I*	this study
PPTR-2::GFP; mCherry::histone; *bub-1(L282A;V285A)*	FGP324	*pptr-2(lt91[pptr-2::gfp])V; ltIs37[pAA64; pie-1p::mCherry::his-58; unc-119 (+)]IV; bub-1(syb1936[bub-1((L282A;V285A)])I*	this study
PPTR-2::GFP; mCherry::histone; *san-1Δ*	FGP380	*pptr-2(lt91[pptr-2::gfp])V; ltIs37[pAA64; pie-1p::mCherry::his-58; unc-119 (+)]IV; san-1(ok1580) I*	this study
PPTR-2::GFP; mCherry::histone; bub-1(*L282A;V285A;K718R;D847N*)	FGP398	*pptr-2(lt91[pptr-2::gfp])V; bub-1(syb1936,syb2383[bub-1(L282A;V285A,K718R;D847N)]I*	this study
PPTR-2::GFP; mCherry::histone; bub-1(*S283A*)	FGP447	*pptr-2(lt91[pptr-2::gfp])V; ltIs37 [pAA64; pie-1/mCHERRY::his-58; unc-119 (+)]IV; bub-1(syb2396[bub-1((S283A)])I*	this study
GFP::ASPM-1; mCherry::histone	EU2876	*or1935[GFP::aspm-1] I; itIs37[pie-1p::mCherry::H2B::pie-1 3'UTR + unc-119(+)] IV*	Connolly AA, et al. J (PMID: 26370499)
PPTR-2::GFP; mCherry::histone	FGP477	*pptr-2(lt91[pptr-2::gfp])V; bqSi189[lmn-1p::mCherry::his-58 + unc-119(+)]II*	this study
PPTR-2::GFP; mCherry::histone; *sgo-1Δ*	FGP478	*pptr-2(lt91[pptr-2::gfp])V; bqSi189[lmn-1p::mCherry::his-58 + unc-119(+)]II; sgo-1(fq48)IV*	this study
PPTR-1::GFP; mCherry::histone	FGP479	*pptr-1(lt89[pptr-1::gfp])V; bqSi189[lmn-1p::mCherry::his-58 + unc-119(+)]II*	this study
PPTR-1::GFP; mCherry::histone; *sgo-1Δ*	FGP480	*pptr-1(lt89[pptr-1::gfp])V; bqSi189[lmn-1p::mCherry::his-58 + unc-119(+)]II; sgo-1(fq48)IV*	this study

Markers / *mutants*	Alelle	Primers (5'-3')	primer name	Restriction enzyme
bub-1(L282A;V285A); bub-1(L282A;V285A);(K718R;D847N)	*bub-1(syb1936[bub-1((L282A;V285A)])I; bub-1(syb1936,syb2383[bub-1 (L282A;V285A,K718R;D847N)]I*	ATGGAATATCGATTGAGGAGTTTC	fgp_153	*NsiI*
		CAATTTCGGGTTGTACTTCAGA	fgp_154	
bub-1(S283A)	*bub-1(syb2396[bub-1((S283A)])I*	ATGGAATATCGATTGAGGAGTTTC	fgp_153	*HhaI*
		CAATTTCGGGTTGTACTTCAGA	fgp_154	
bub-1(K718R;D847N)	*bub-1(syb1746[bub-1((K718R;D847N)])I*	GATGTGTCTTGTGCGTCCTC	fgp_125	*BmrI*
		CCAGTCCGGAAGTGAATCA	fgp_126	
pptr-2Δ	*pptr-2(ok1467)V*	ATCCTTGCTAAGCACAGTTGAAGT	fgp_137	
		CGTGAACGTGACTTTCTGAAGA	fgp_138	
san-1Δ	*san-1(ok1580) I*	GAAACTGCACGCTTAAAGCTTG	fgp_139	
		CTTTCCACGTTTCCCGTATC	fgp_140	
		GGGTGATTCGGCAGAAGA	fgp_141	
PPTR-1::GFP	*pptr-1(lt89[pptr-1::gfp])V*	CCTCGGAGAGTACACAAGACC	fgp_158	
		TGGAGTTGTCCCAATTCTTGTT	fgp_2	
		AGCAGCAGAAGACGAGAGAGT	fgp_159	
PPTR-2::GFP	*pptr-2(lt91[pptr-2::gfp])V*	ACGCCCTCAAGATGTTCAT	fgp_160	
		TGGAGTTGTCCCAATTCTTGTT	fgp_2	
		ACTGGGTAAGGAAGTCGAATCA	fgp_161	
AID::GFP::GSP-2	*gsp-2(syb545[AID::gfp::gsp-2])III*	TCTAATTGGGTTGTTTGAGCG	fgp_53	
		TGGAGTTGTCCCAATTCTTGTT	fgp_2	
		TTTTCCCTGGTTTGGATCC	fgp_54	

Supplementary Table 3. List of primers used for genotyping.